DJI Zenmuse L3 Accuracy Analysis and Use Case Exploration

VERTICAL ASPECT

DJI

www.verticalaspect.com

Contents

OVERVIEW AND TESTING OBJECTIVES

DJI Enterprise requested that Vertical Aspect, LLC provide feedback on their DJI Zenmuse L3 Lidar system for the DJI M400 enterprise drone. This analysis aims to provide an unbiased look at the L3 Lidar system, DJI Enterprise's latest Lidar offering. DJI chose Vertical Aspect to provide this review and analysis due to the company's extensive subject-matter expertise in the enterprise UAS Lidar domain.

For Vertical Aspect, LLC, it was important that the L3 system be analyzed using a rigorous testing methodology that provides both qualitative and quantitative analysis and utilizes industry-accepted standard testing methods. The aim of this review is to provide both the type of thorough investigation that Vertical Aspect's customers expect and comprehensive guidance and documentation of the testing results, so that others may replicate the analysis and findings utilizing the data sources provided in this report.

All data used in this analysis has been provided, along with relevant metadata, to ensure others can validate the results. All resource links are available for download: www.verticalaspect.com/products-dji-zenmuse-l3.

For the following testing, Vertical Aspect was provided with a pre-production engineering unit of the DJI Zenmuse L3 system and the M400 UAS airframe. While firmware and software updates may occur between testing and system release, the underlying hardware has remained the same, to Vertical Aspect's knowledge.

System Specifications and Key Improvements

Technical Specifications

- Laser Wavelength: 1535 nm
- Effective Range: 300-500 meters
- Pulse Repetition Frequency:
  - 100 kHz
  - 350 kHz
  - 1,000 kHz
  - 2,000 kHz
- Beam Divergence: 0.25 mrad x 0.25 mrad ($1/e^2$)
- Returns: 16 returns max. *1,000 kHz (up to 8 returns), 2,000 kHz (up to 4 returns)
- Intensities: 16-bit depth
- Scanner type: Risley Prism Scanner
- Scan patterns:
  - Linear Scan
  - Non-repetitive Scan
  - Star Pattern Scan
- Scanner Field of View: 80 deg x 80 deg
- IMU Accuracy:
  - 0.02 deg (heading)
  - 0.01 deg (roll, pitch)
- Camera: 2 x Micro 4/3 RGB (up to 100 MP per camera)
- Camera Field of View: 106 degrees
- Shutter Type: Mechanical
- Shutter Lifetime: 300,000 shutters
- Flight Platform: DJI Enterprise M400
- Flight Time: 37 Minutes

Laser System Advancements

Given these specifications, the L3 represents a clear step forward from previous generation systems. The most significant upgrade lies in the laser architecture itself. The L2, which was already a major improvement over the L1, used a 905 nm silicon-based pulsed diode laser that was cost-effective but limited in precision. In contrast, the L3 incorporates a 1535 nm Indium Gallium Arsenide (InGaAs) based eye-safe laser. This class of emitter, commonly used in high-end time-of-flight (ToF) topographic mapping systems, is more expensive to manufacture but offers substantial advantages over silicon-based diodes typically found in automotive Lidar units.

InGaAs technology is approximately 40 times safer for the human eye at the same power levels , allowing 10 to 20 times higher output power, which results in a significantly longer detection range. It also provides narrower beam divergence, improved atmospheric performance, and enhanced precision in complex environments.

In addition to the laser type, the L3 introduces a major improvement in pulse repetition frequency (PRF). The DJI L2 operated at a maximum pulse frequency of 240 kHz, while the L3 supports up to 2 MHz (2,000 kHz) with selectable rates of 100, 350, 1,000, and 2,000 kHz. In testing, Vertical Aspect evaluated how different PRFs affected system performance and data quality. While higher pulse rates increase point density and coverage efficiency, they also introduce potential trade-offs, including multiple-pulse-in-air (MPiA) interference, reduced energy per pulse, and diminished precision at long ranges.

Other notable improvements in the L3's laser system include smaller beam divergence, a higher number of detectable returns per pulse, and expanded intensity bit depth.

The reduction in beam divergence means the laser energy remains more tightly focused over distance, producing a smaller footprint on the ground. This results in improved laser precision and sharper edge definition when mapping fine features such as building edges, powerlines, curbs and gutters. Smaller divergence also increases the signal-to-noise ratio of each return, as more of the emitted energy is concentrated on the target rather than dispersed across a wider area.

The L3 can record up to 16 discrete returns per emitted pulse, compared to only 5 with the L2. This increase allows for more detailed vertical profiling of trees, powerline utilities, or mixed terrain with vegetation.

Additionally, the L3 records 16-bit intensity values, an upgrade from the L2's 8-bit dynamic range. The 16-bit digitization allows for 65,536 possible intensity levels, compared to only 256 in 8-bit systems, representing a 256× increase in reflectance resolution. This expanded range enhances the system's ability to distinguish subtle differences in surface reflectivity.

Scanning Mechanism and IMU Improvements

The L3 retains the same Risley-prism scanning mechanism used in the L1 and L2, offering three selectable scan patterns. The familiar repetitive and non-repetitive modes remain, and a new star pattern has been introduced to balance noise and look angle, especially for utility features. The scanner's field of view has been expanded to 80 × 80 degrees, providing broader area coverage per flight line.

Beyond the laser system, the inertial navigation system (INS) has also been upgraded. The stated accuracies are 0.02 degrees in heading and 0.01 degrees in roll and pitch, representing an improvement over the L2 (0.05 degrees in heading and 0.03 degrees in roll and pitch).

Imaging System Enhancements

The imaging subsystem now includes two Micro Four Thirds RGB cameras, each with a native resolution of 100 megapixels. Both cameras feature mechanical shutters rated for 300,000 cycles. Their combined field of view of 106 degrees slightly exceeds the Lidar scan area, ensuring complete color coverage of the scanned area.

Overall, the L3's design reflects incremental advancements in scanning efficiency, navigation accuracy, and imaging resolution. To determine how these specifications influence real-world data quality and operational performance, the next section details the procedures and testing conditions used in the evaluation.

FIELD TESTING THE ZENMUSE L3: PERFORMANCE INSIGHTS

Vertical Aspect developed a structured series of tests to evaluate the performance of the Zenmuse L3 compared to the previous-generation Zenmuse L2. The objective was to determine how the stated hardware and specification improvements, including changes in ranging capability, pulse repetition frequency, number of returns, laser wavelength, and intensity bit depth, perform in real-world conditions. To ensure consistency and repeatability, all testing followed recognized industry standards.

Testing Standards Framework

For this analysis, the ASPRS Positional Accuracy Standards for Digital Geospatial Data were used as the evaluation framework. These standards provide a technology-independent method for measuring positional accuracy and have been used in prior analyses of DJI's L1 and L2 Lidar systems. Since the release of the L2, the American Society for Photogrammetry and Remote Sensing (ASPRS) has issued an updated standard titled Edition 2, Version 2 (2024). This revision reflects both user feedback and advances in sensor technology.

Key ASPRS updates include:

- Relaxation of accuracy requirements for ground control points
- Inclusion of survey checkpoint accuracy in the final computed product accuracy
- An increase in the minimum number of checkpoints required from 20 to 30
- Introduction of a new metric called three-dimensional positional accuracy

While several other revisions were made, these are the most relevant to this analysis. The ASPRS framework is designed to be broadly applicable, brand-neutral, and platform-independent, focusing on the accuracy, precision, and quality of the final geospatial data products.

Site Selection and Testing Methodology

A total of two separate sites were selected. Each site served a different purpose.

- Site A: Utility and Linear Feature Testing
- Site B: Precision and Accuracy Testing

Site A: Utility and Linear Feature Testing

Site A was located just outside Kansas City, Missouri, east of Highway 435 and north of Highway 210. The area covered approximately 100 acres and included an electric utility substation, multiple transmission and distribution corridors, and an adjoining section of rail line. Conductors at the site ranged from 12 kV distribution lines to 161 kV transmission structures mounted on both wood and steel poles.

The site was selected to evaluate the Lidar 's ability to capture thin linear features and high-voltage infrastructure under realistic field conditions. The adjacent rail corridor provided a consistent, high-reflectivity surface that allowed assessment of the system's capability to resolve small, discrete linear objects near ground level. Terrain across the site was generally level with limited low vegetation from surrounding agricultural fields. Flights over this area were configured to test the system's precision in mapping utilities of varying diameters, materials, and elevations within a controlled geometric environment.

Site B: Precision and Accuracy Testing

Site B was used for precision and accuracy testing and was located in Kansas City, Kansas, at the Legends Shopping Center, which provided an ideal controlled environment for Lidar accuracy assessment. The test site consisted of approximately 5 hectares of open parking area with extensive paint striping that offered numerous photo-identifiable features. The presence of multiple parking islands oriented in various directions allowed for qualitative evaluation of curb and gutter detail, while the site's flat and planar surface made it well-suited for assessing interswath precision.

All data for this site were collected on a single day, September 30, 2025, between 9:00 a.m. and approximately 2:00 p.m. Weather conditions were clear with temperatures ranging from 16°C to 28°C, maximum wind speeds of 13 kph, and visibility of 16 km. These conditions provided stable lighting and minimal atmospheric disturbance, ensuring consistent data acquisition across all flights and scan configurations.

Survey Control Network Establishment

A total of 32 photo-identifiable checkpoints were established at the ends of parking stripes. Mag nails were placed at each surveyed location and sequentially numbered. The primary control point was established using eight hours of static GNSS observations processed through the NOAA Online Positioning User Service (OPUS). A secondary 120-epoch observation was collected using the Leica SmartNet network on a separate day for verification. The horizontal delta between the two observations was 0.32 cm.

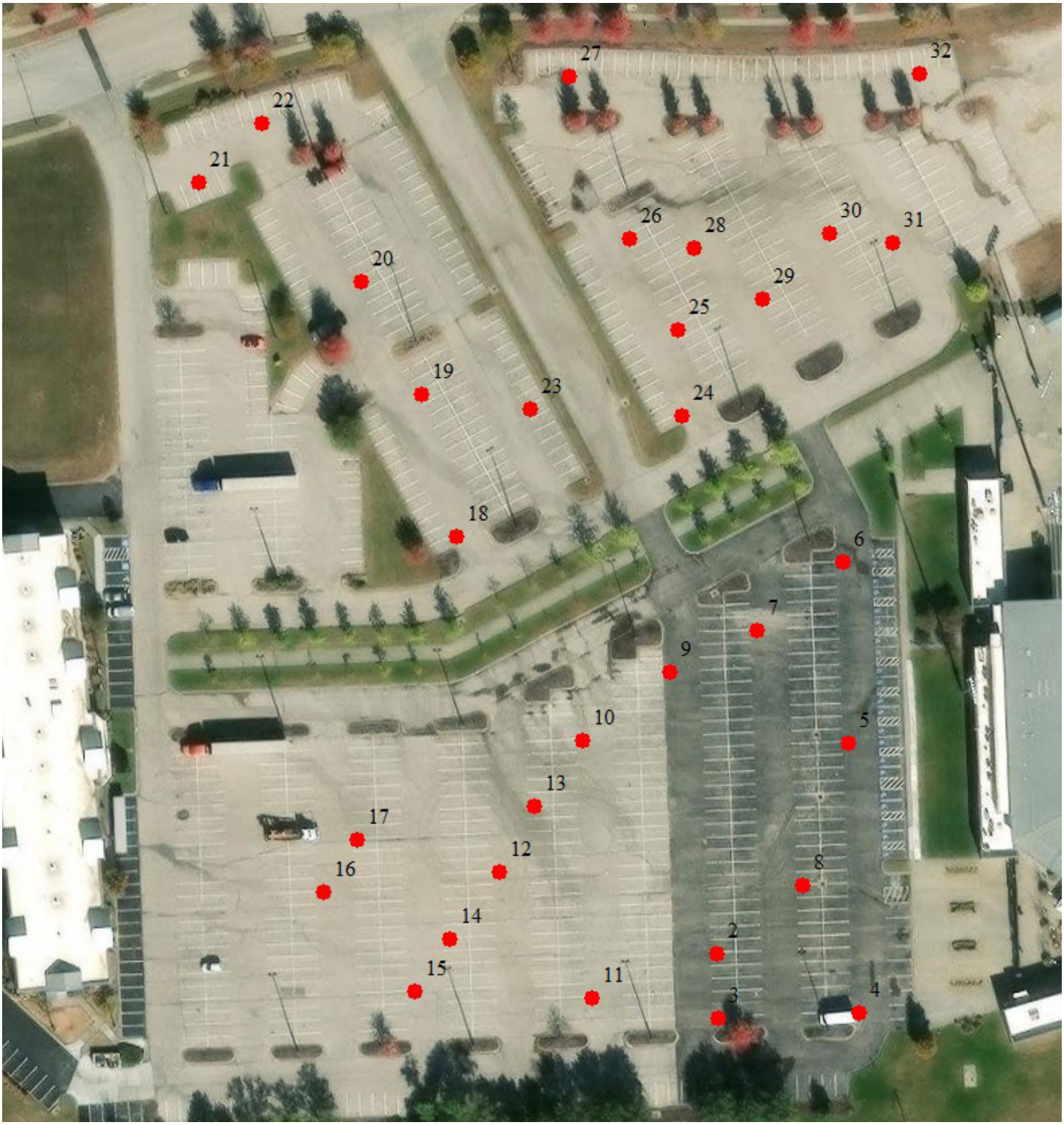

Thirty-one additional checkpoints were collected using two 30-epoch GNSS observations at each location with a Carlson BRx7 GNSS receiver connected to the Leica SmartNet VRS network. The reference station used for these observations was located approximately five miles from the test site. The combined horizontal root mean square error (RMSE) across all observations was 0.85cm, with an average horizontal delta between observations of 0.13cm.

Once the horizontal control network was verified, Checkpoint 1 was held as the vertical benchmark for the project. Using a Nikon AC-2s 24x automatic optical level, dual closed loops were run through the entire project area to establish vertical control. Each control point was double-measured and averaged. Each loop closed flat <0.00cm> and met the requirements Federal Geodetic Control Subcommittee (FGCS) Second-Order, Class II.

Testing Matrix

Test Number	Sampling Rate	Altitude (m)	Speed m/s	Return Mode	Scan Mode	GSD (CM/pix)	Side Overlap	Forward Overlap	Point Density PPSM
101	100 KHz	120	15 m/s	Sixteen Returns	Star-Shaped	1.22	50.00%	70.00%	79
102	350 KHz	120	15 m/s	Sixteen Returns	Star-Shaped	1.22	50.00%	70.00%	79
103	1MHz	120	15 m/s	Eight Returns	Star-Shaped	1.22	50.00%	70.00%	79
104	2 MHz	120	15 m/s	Sixteen Returns	Star-Shaped	1.22	50.00%	70.00%	79
105	350 KHz	120	15 m/s	Quad Return	Non-Repetitive	1.22	50.00%	70.00%	1.25
106	350 KHz	120	15 m/s	Quad Return	Linear	1.22	50.00%	70.00%	79
107	350 KHz	120	15 m/s	Sixteen Returns	Linear	1.23	30.00%	70.00%	117
108	350 KHz	90	15 m/s	Sixteen Returns	Linear	0.92	30.00%	70.00%	192
109	350 KHz	60	15 m/s	Sixteen Returns	Linear	0.61	30.00%	70.00%	436
111	100 KHz	120	15 m/s	Sixteen Returns	Linear	1.22	30.00%	70.00%	30
112	1MHz	120	15 m/s	Eight Returns	Linear	1.22	30.00%	70.00%	326
113	2 MHz	120	15 m/s	Quad Return	Linear	1.22	30.00%	70.00%	664
114	100 KHz	90	15 m/s	Sixteen Returns	Linear	0.92	30.00%	70.00%	60
115	1MHz	90	15 m/s	Eight Returns	Linear	0.92	30.00%	70.00%	596
116	2 MHz	90	15 m/s	Quad Return	Linear	0.92	30.00%	70.00%	1,378
117	100 KHz	60	15 m/s	Sixteen Returns	Linear	0.61	30.00%	70.00%	134
118	1MHz	60	15 m/s	Eight Returns	Linear	0.61	30.00%	70.00%	1,350
119	2 MHz	60	15 m/s	Quad Return	Linear	0.61	30.00%	70.00%	2,830

**Flights at 30m AGL were not flown due to aerial obstructions.*
***Flight 110 was removed due to altitude*

All data collected during this testing were processed using PPK, with a Robota RoboDot GNSS base station. DJI Terra was used for the initial processing of the point cloud data. The Lidar point cloud was generated with a density of 100% and the optimized accuracy setting. The smoothing algorithm in DJI Terra was not used in any of the processing. Flights 107-122 and 128 were processed in NAD83 (2011) Kansas North (ftUS) NAVD88 (Geoid18 ftUS). Flights 101-106 and 123-127 were processed in NAD83 (2011) UTM Zone 15N (m) NAVD88 (Geoid18 m).

ACCURACY TESTING STANDARDS AND PROCEDURES

To evaluate the positional accuracy of the DJI Zenmuse L3, all data were tested following the ASPRS Positional Accuracy Standards for Digital Geospatial Data, Edition 2, Version 2 (2024). These procedures define a standardized, technology-independent approach for quantifying accuracy using both the dataset's measured error (first component) and the independent ground survey accuracy (second component).

Point Cloud Processing Methodology

All accuracy testing was performed in Terrasolid TerraScan, using point cloud data and trajectories exported from DJI Terra. Each mission's .LAS point cloud and corresponding .SBET trajectory file were imported using the TerraScan Drone Wizard, where flight trajectories were segmented into individual flight lines. Point sorting and deducing by time were applied to assign correct flightline identifiers to each strip and to improve processing efficiency. These preparatory steps were repeated for each mission. For the absolute accuracy assessment, no ground classification was applied at this stage.

Control Point Measurement Procedures

Once loaded, ground control points (GCPs) were imported, and all control locations were measured directly within the unclassified point cloud (atmospheric and MPiA errors were classified as noise). Measurements were performed manually using the Output Control Report tool in TerraScan configured as shown in Figure 1. Each control point was identified visually in both horizontal and vertical dimensions using the intensity display mode in TerraScan.

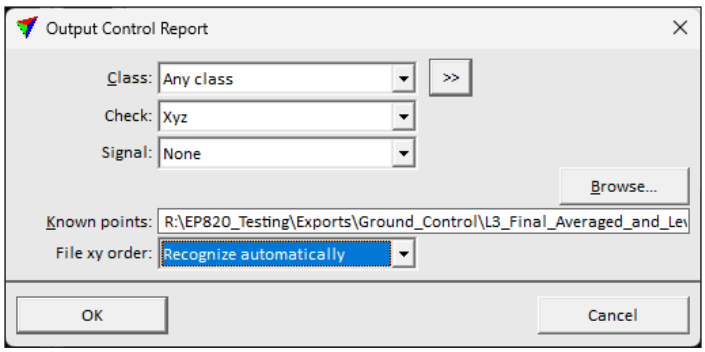

Horizontal positioning was guided by the visible paint stripe edges, typically approximately 10 cm (4 in) wide. While this method offers excellent visual reference, minor human error, combined with point density variations, introduces small uncertainties in the measured positions.

After all GCPs were measured, TerraScan's Output Control Report generated a control report summary including the mean offset, standard deviation, and RMSE for both horizontal and vertical components. To remove systematic GNSS bias from each mission, an XYZ translation debias was applied. This step translates the entire point cloud as a single body based on the mean error in X, Y, and Z. Each mission was debiased independently, as recommended in the ASPRS Positional Accuracy Standards for Digital Geospatial Data.

The resulting horizontal and vertical RMSE values represent the first component positional accuracy. These were combined with the surveyed ground control network accuracy (the second component positional error) to compute the final horizontal, vertical, and three-dimensional positional accuracy.

Accuracy Calculation Methods

All accuracy values were computed following the ASPRS Edition 2, Version 2 standard formulas:

$$\mathrm{RMSE}_V = \sqrt{(\mathrm{RMSE}_{v1})^2 + (\mathrm{RMSE}_{v2})^2}$$

$$\mathrm{RMSE}_h = \sqrt{(\mathrm{RMSE}_{h1})^2 + (\mathrm{RMSE}_{h2})^2}$$

$$\mathrm{RMSE}_{3D} = \sqrt{(\mathrm{RMSE}_H)^2 + (\mathrm{RMSE}_V)^2}$$

This methodology ensures a rigorous, standardized comparison of the L3's absolute positional accuracy across all tested missions.

ABSOLUTE POSITIONAL ACCURACY

Initial Testing Results

The DJI Zenmuse L3 exhibited outstanding absolute accuracy performance across all tested missions. Even under higher-altitude and maximum pulse repetition frequency (PRF) conditions, the system maintained exceptional consistency between the derived LiDAR surface and surveyed ground control.

Across the full test matrix, the maximum observed vertical error was 0.007m (0.7cm), and the maximum three-dimensional positional error did not exceed 0.013 m (1.3 cm). These results were consistent across different PRF configurations (100 kHz, 350 kHz, 1 MHz, and 2 MHz) and altitudes ranging from 60–120 meters AGL.

Test Number	Sampling Rate	Altitude (m)	Return Mode	Point Density PPSM	NVA RMSEh debiased (m) all points Total Error	NVA RMSEv debiased (m) all points Total Error	Three-Dimensional Positional Accuracy Debiased (m)
107	350 KHz	120	Sixteen Returns	117	0.009	0.004	0.010
108	350 KHz	90	Sixteen Returns	192	0.009	0.004	0.010
109	350 KHz	60	Sixteen Returns	436	0.009	0.004	0.010
111	100 KHz	120	Sixteen Returns	30	0.011	0.007	0.012
112	1MHz	120	Eight Returns	326	0.010	0.006	0.012
113	2 MHz	120	Quad Return	664	0.009	0.005	0.011
114	100 KHz	90	Sixteen Returns	60	0.010	0.006	0.011
115	1MHz	90	Eight Returns	596	0.010	0.006	0.012
116	2 MHz	90	Quad Return	1,378	0.012	0.005	0.013
117	100 KHz	60	Sixteen Returns	134	0.009	0.004	0.010
118	1MHz	60	Eight Returns	1,350	0.009	0.005	0.010
119	2 MHz	60	Quad Return	2,830	0.009	0.004	0.010

Correlation Analysis: Altitude, PRF, and Point Density

Interestingly, correlation analysis between altitude, PRF, and point density revealed negligible dependence between these parameters and the measured positional accuracy. The highest correlation observed was between altitude and vertical RMSE, at r = 0.051, while the lowest was between point density and 3D accuracy (r = –0.07). This low correlation suggests that the L3's ranging precision and navigation solution maintain stability regardless of scan density or altitude within the tested range.

These findings indicate that the L3's integrated IMU, GNSS, and laser system effectively manage potential geometric drift and timing offsets, even under high data acquisition rates. The system's precision can largely be attributed to the upgraded 1535 nm InGaAs laser, tight beam divergence (0.25 mrad), and the improved INS performance (0.02° heading, 0.01° roll/pitch).

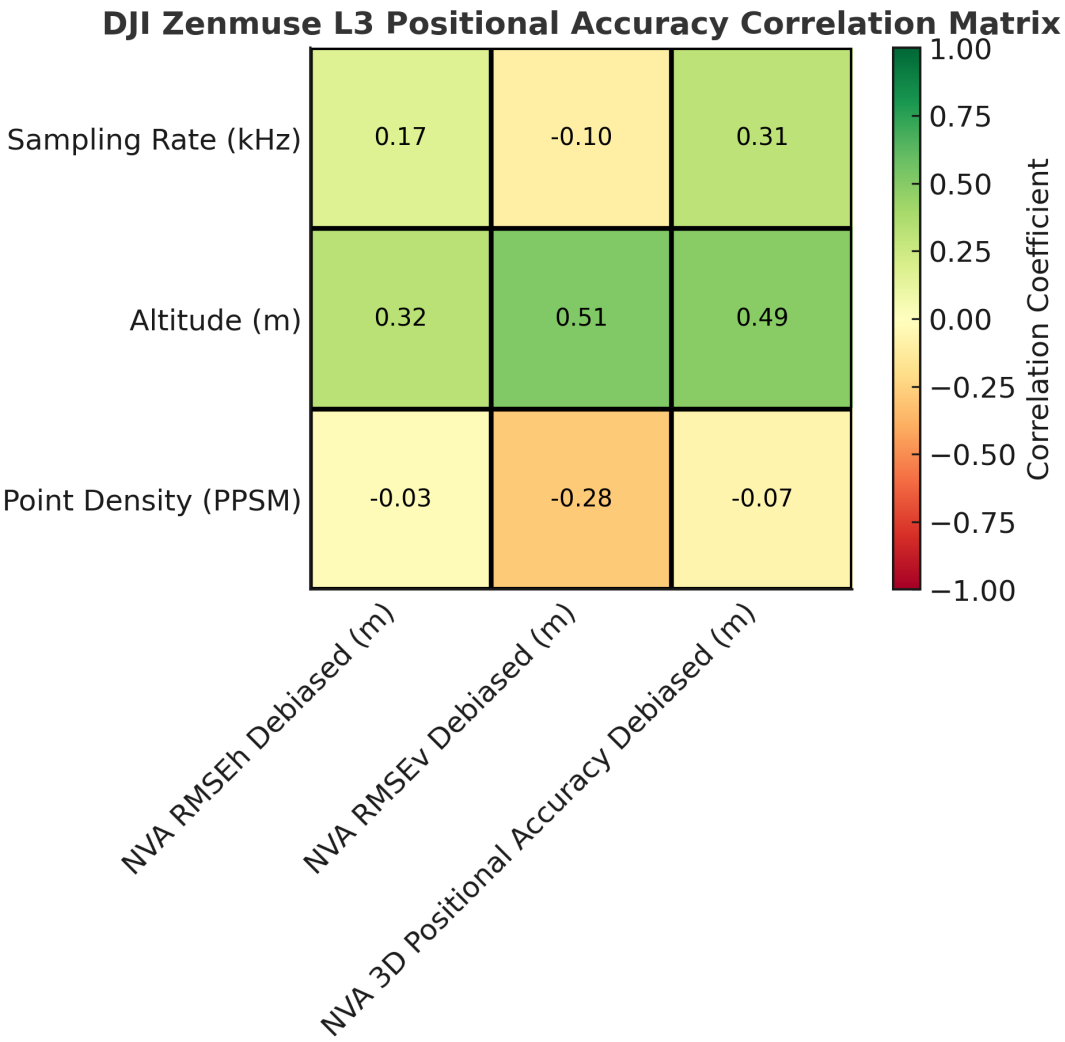

Results Across Multiple Classification Conditions

To further evaluate how post-processing affects absolute accuracy, the vertical positional accuracy of the point cloud was analyzed under three filtering conditions:

- All Points (Unclassified, Full Overlap - shown above)
- Unclassified Points with Overlap Removed
- Ground-Classified Points Only

This step was performed to isolate how point cloud precision and overlap geometry influence the overall positional accuracy metrics. Because relative precision and surface smoothness directly affect derived elevations, it is standard ASPRS practice to perform accuracy testing on ground-classified point clouds. However, the objective was to determine how the data were affected under all three conditions.

Previous studies conducted on the DJI Zenmuse L1 and Zenmuse L2 systems demonstrated that post-processing typically improves absolute accuracy by reducing residual noise, eliminating overlapping edge inconsistencies, and minimizing interpolation artifacts. To maintain consistency with these earlier analyses, identical procedures were followed for the Zenmuse L3 dataset.

Each version of the point cloud was independently assessed against the surveyed control network using the same Output Control Report workflow described previously. The same RMSE formula for vertical positional accuracy was applied.

Test Number	Sampling Rate	Altitude (m)	Return Mode	Point Density PPSM	NVA RMSEv debiased (m) all points Total Error	Measured VRMSE debiased (m) no overlap Total Error	Measured VRMSE debiased (m) ground Total Error
107	350 KHz	120	Sixteen Returns	117	0.004	0.004	0.006
108	350 KHz	90	Sixteen Returns	192	0.004	0.003	0.006
109	350 KHz	60	Sixteen Returns	436	0.004	0.004	0.006
111	100 KHz	120	Sixteen Returns	30	0.007	0.004	0.008
112	1MHz	120	Eight Returns	326	0.006	0.004	0.009
113	2 MHz	120	Quad Return	664	0.005	0.005	0.009
114	100 KHz	90	Sixteen Returns	60	0.006	0.003	0.007
115	1MHz	90	Eight Returns	596	0.006	0.004	0.007
116	2 MHz	90	Quad Return	1,378	0.005	0.004	0.008
117	100 KHz	60	Sixteen Returns	134	0.004	0.003	0.005
118	1MHz	60	Eight Returns	1,350	0.005	0.004	0.006
119	2 MHz	60	Quad Return	2,830	0.004	0.004	0.007

The results across all three filtering levels were nearly identical, confirming that the L3's positional stability is largely unaffected by overlap removal or ground classification. The ground-classified datasets exhibited a slightly higher vertical RMSE, a minor degradation attributed to lower point density and the formation of longer triangles in measured areas.

This small difference is statistically insignificant but informative: it indicates that the L3's precision is uniformly high throughout the point cloud and that classification-based thinning introduces minimal geometric bias. The nearly identical results across all filtering conditions reinforce the overall quality of the L3 data, both in unclassified form and after standard processing steps.

Key Findings: Absolute Accuracy

Across all tests, the DJI Zenmuse L3 consistently achieved sub-centimeter vertical accuracy and sub-1.5-centimeter 3D accuracy, with no meaningful dependency on PRF, altitude, or point density. The absence of correlation between acquisition parameters and measured accuracy demonstrates high system calibration, low boresight error, and robust GNSS/IMU integration.

In practical terms, these results confirm that the Zenmuse L3 delivers high absolute accuracy that will meet most intended use cases. While absolute accuracy is not the only metric that matters when evaluating a system's capability, it establishes a strong foundation for the subsequent Relative Precision Assessment, which examines internal consistency within and between flight lines.

INTERNAL PRECISION ANALYSIS

Relative precision describes the internal consistency of LiDAR measurements within and between flight lines. It is distinct from absolute accuracy in that it evaluates how well individual swaths align with each other and how consistently points fit local surface geometry, independent of control or external references. High relative precision ensures that surfaces appear smooth and continuous without misalignment of artifacts across overlapping areas. For this study, two complementary tests were conducted using Terrasolid software:

- Within-Swath Precision: evaluating point-to-plane consistency within individual flight lines.
- Swath-to-Swath Precision: evaluating vertical alignment consistency between overlapping flight lines.

Within-Swath Precision

Testing Methodology

Within-swath precision was assessed using Terrasolid's Compute Distance tool, which calculates local surface roughness by fitting a best-fit plane to points within a defined area and measuring the vertical distance from each point to that plane. For this test, a 1-square-foot window was selected as the fitting area.

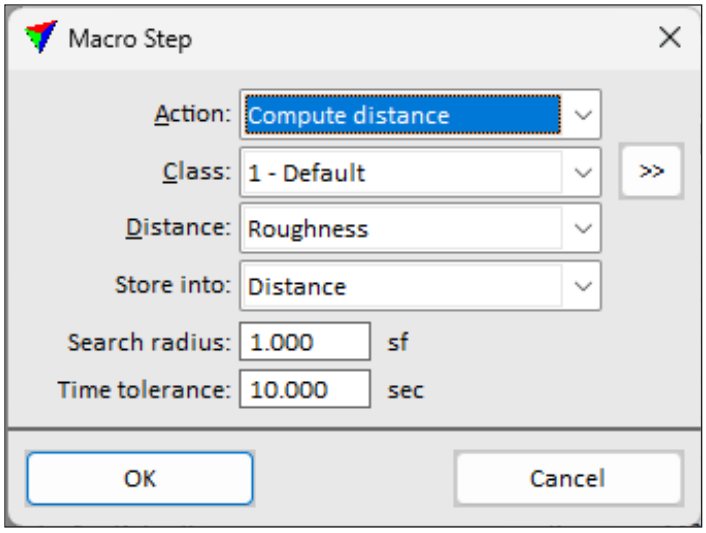

This window size was chosen based on lessons learned from earlier DJI L1 and L2 testing, where larger sample areas often incorporated natural undulations in road surfaces. Given that the lowest point density collected in the L3 dataset was approximately 30 points/m² and the highest exceeded 2,800 points/m², a 1-ft² window provided an optimal balance between local sampling size and statistical robustness.

All points along a smooth east–west road segment within the test site were used for analysis, regardless of return number or classification. The test was restricted to single flight lines (i.e., within-swath) to eliminate any influence from IMU or GNSS drift between lines. Each point within the analyzed section was assigned a residual distance value (distance to local plane), and all distance values were aggregated for statistical analysis.

The resulting data were exported and plotted as histograms to visualize the distribution of surface residuals. Statistical descriptors including mean, standard deviation, and RMSE were computed and reported in the final results to align with ASPRS reporting requirements.

No outlier filtering was applied. While this approach resulted in maximum distance values between 0.20–0.25 m, these were extremely rare (<0.01% of all points) and represent isolated, non-systematic deviations. These outliers were likely associated with small surface imperfections such as deep cracks rather than systematic sensor noise.

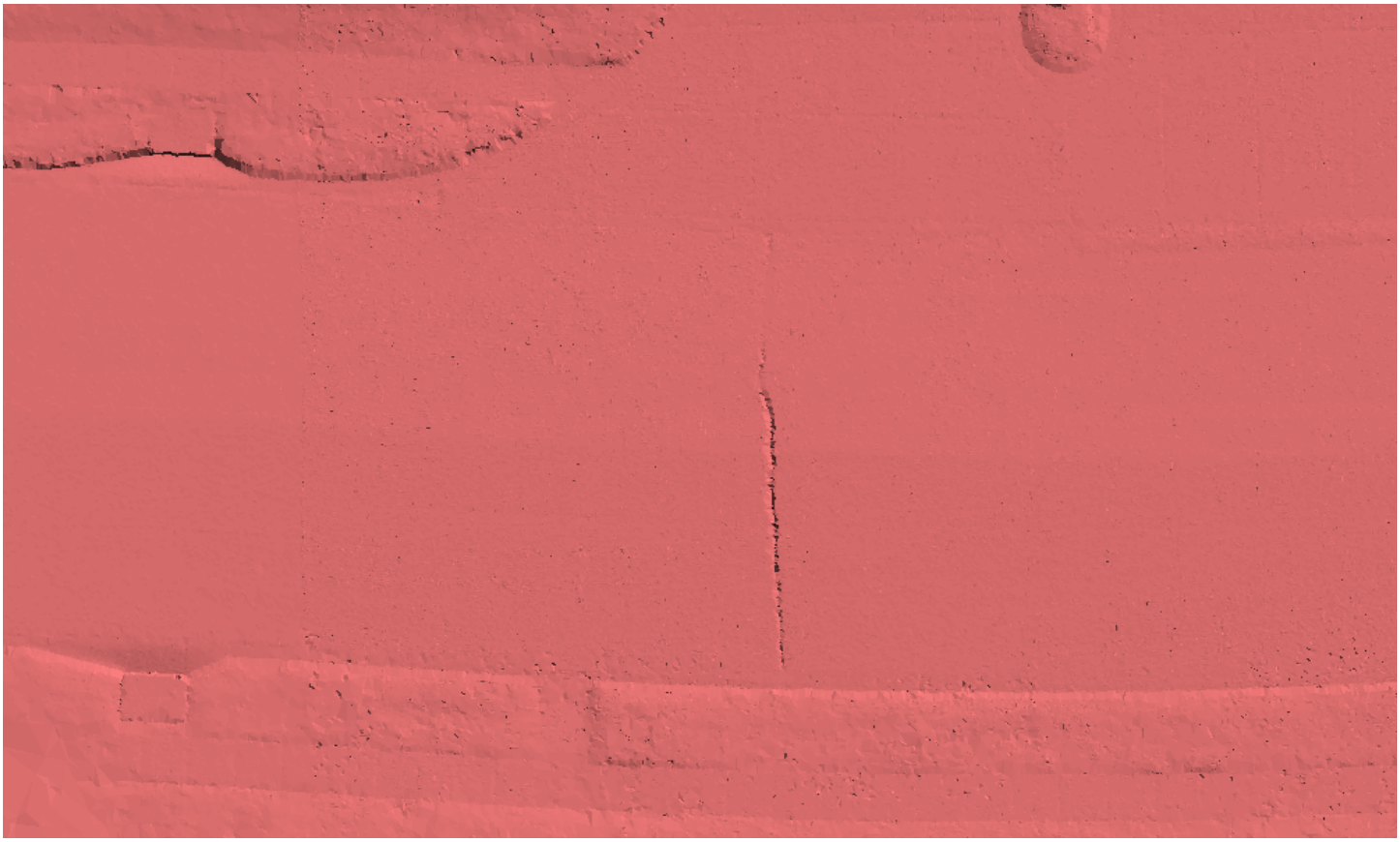

Figure 1: shows road cracking in sample area

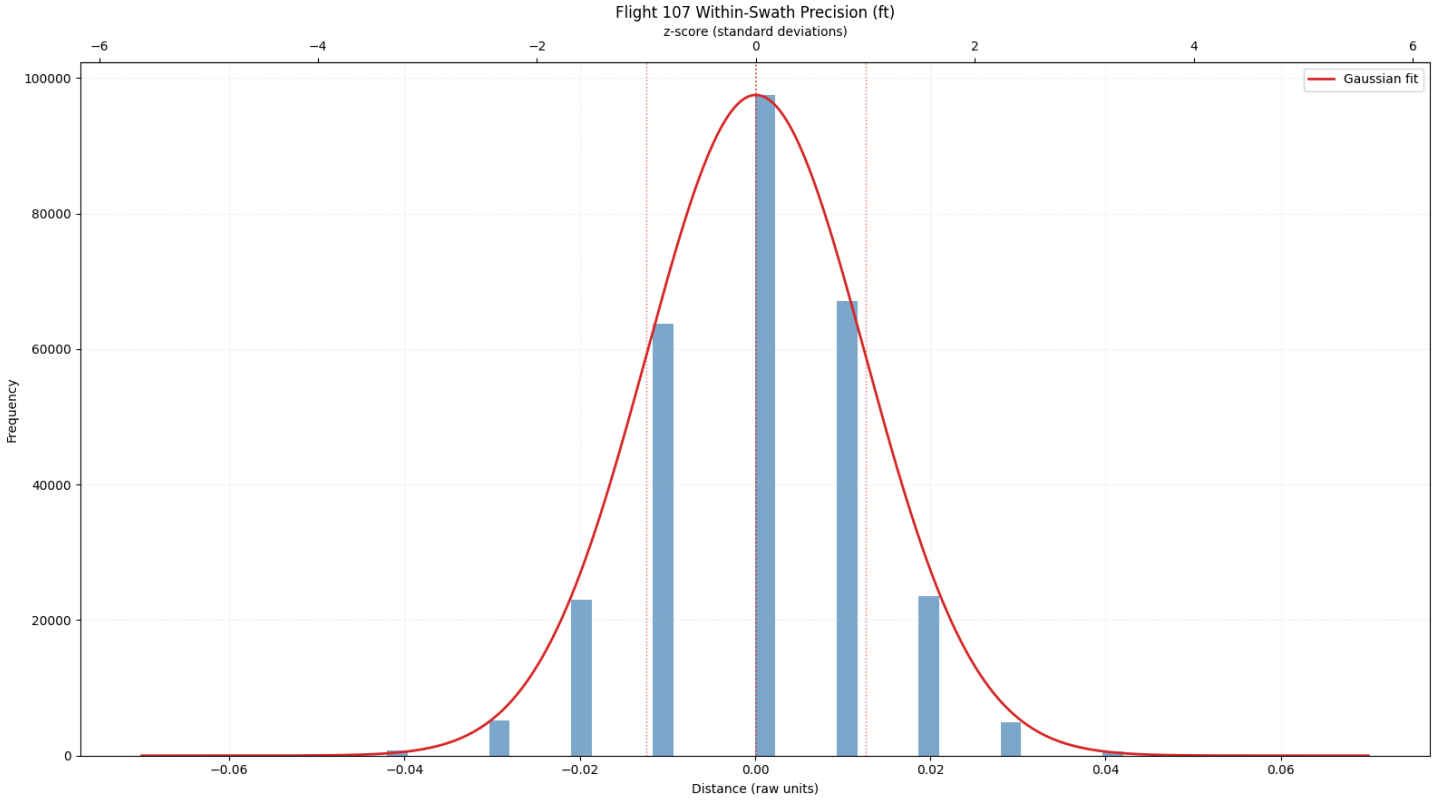

Figure 2: Within-Swath Precision Histogram Example: Distribution of residual point distances relative to best-fit plane.

Within-Swath Results

Across all test configurations, within-swath vertical RMSE values averaged 0.005 m, with standard deviations ranging between 0.001–0.003 m. The tall, narrow Gaussian distribution of residuals observed in all histograms indicates minimal random noise and consistent surface geometry throughout each swath.

Maximum deviation values (0.22–0.25 m) were many times greater than the RMSE, confirming that these represent isolated outliers rather than a spread of data variability. Despite their inclusion, the mean and standard deviation remained stable, illustrating the robustness of the dataset.

Test Number	Sampling Rate	Altitude (m)	Return Mode	Point Density PPSM	Within-Swath Measure Point Noise RMSEv (m)	Within-Swath Measure Point Noise std (m)	Within-Swath Precision Max Diff (m)
107	350 KHz	120	Sixteen Returns	117	0.005	0.002	0.223
108	350 KHz	90	Sixteen Returns	192	0.005	0.001	0.238
109	350 KHz	60	Sixteen Returns	436	0.004	0.002	0.241
111	100 KHz	120	Sixteen Returns	30	0.005	0.003	0.183
112	1MHz	120	Eight Returns	326	0.006	0.003	0.238
113	2 MHz	120	Quad Return	664	0.007	0.004	0.229
114	100 KHz	90	Sixteen Returns	60	0.004	0.002	0.213
115	1MHz	90	Eight Returns	596	0.006	0.002	0.244
116	2 MHz	90	Quad Return	1,378	0.005	0.003	0.241
117	100 KHz	60	Sixteen Returns	134	0.005	0.002	0.241
118	1MHz	60	Eight Returns	1,350	0.005	0.002	0.253
119	2 MHz	60	Quad Return	2,830	0.006	0.002	0.259

The absence of meaningful variation across altitude or pulse repetition frequency (PRF) suggests limited effects on data precision at these test conditions. Surface roughness remained visually smooth, with fine details such as curbs and gutters edges clearly defined even at 120m AGL.

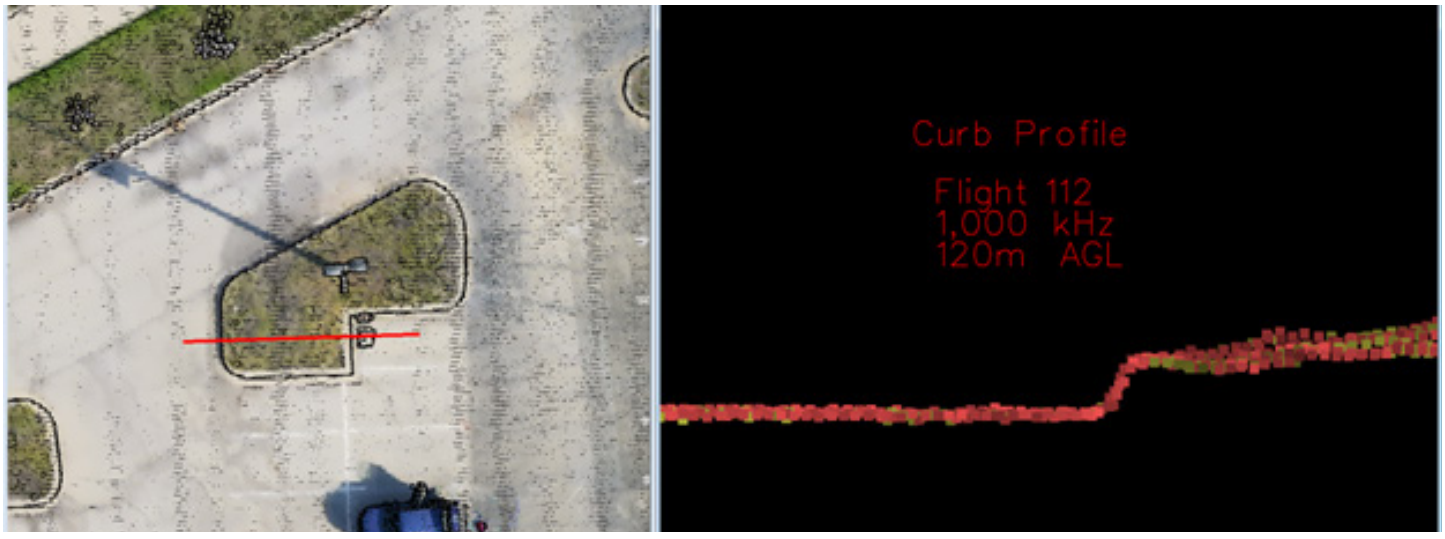

Swath-to-Swath Precision

Testing Methodology

Swath-to-swath precision was evaluated using TerraMatch's Measure Match tool, which calculates the elevation difference between overlapping flight lines relative to a mean surface. This analysis quantifies how well the point clouds from adjacent strips align vertically. Each flightline was individually ground-classified using a "ground per flightline" macro prior to the comparison to ensure consistent surface references.

The Measure Match tool computes elevation differences between corresponding surface areas using triangulation across overlapping regions. The resulting report provides mean, magnitude, and point count per flight line, which collectively describe the quality of inter-swath alignment.

Additionally, using Terrasolid, the Compute Distance tool was run to compute a distance value between overlapping flightlines and a distance value was assigned to each point. Similar to the within-swath analysis, these values were then exported and further analyzed in Python using NumPy and Matplotlib to calculate RMSEdz, standard deviation, and maximum difference across all overlaps combined.

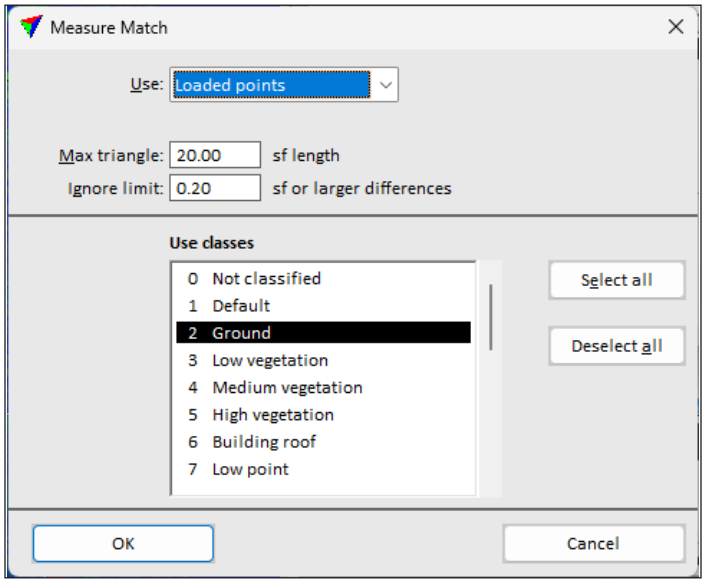

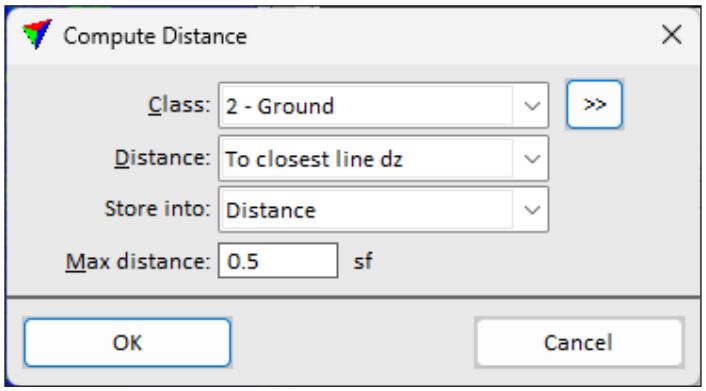

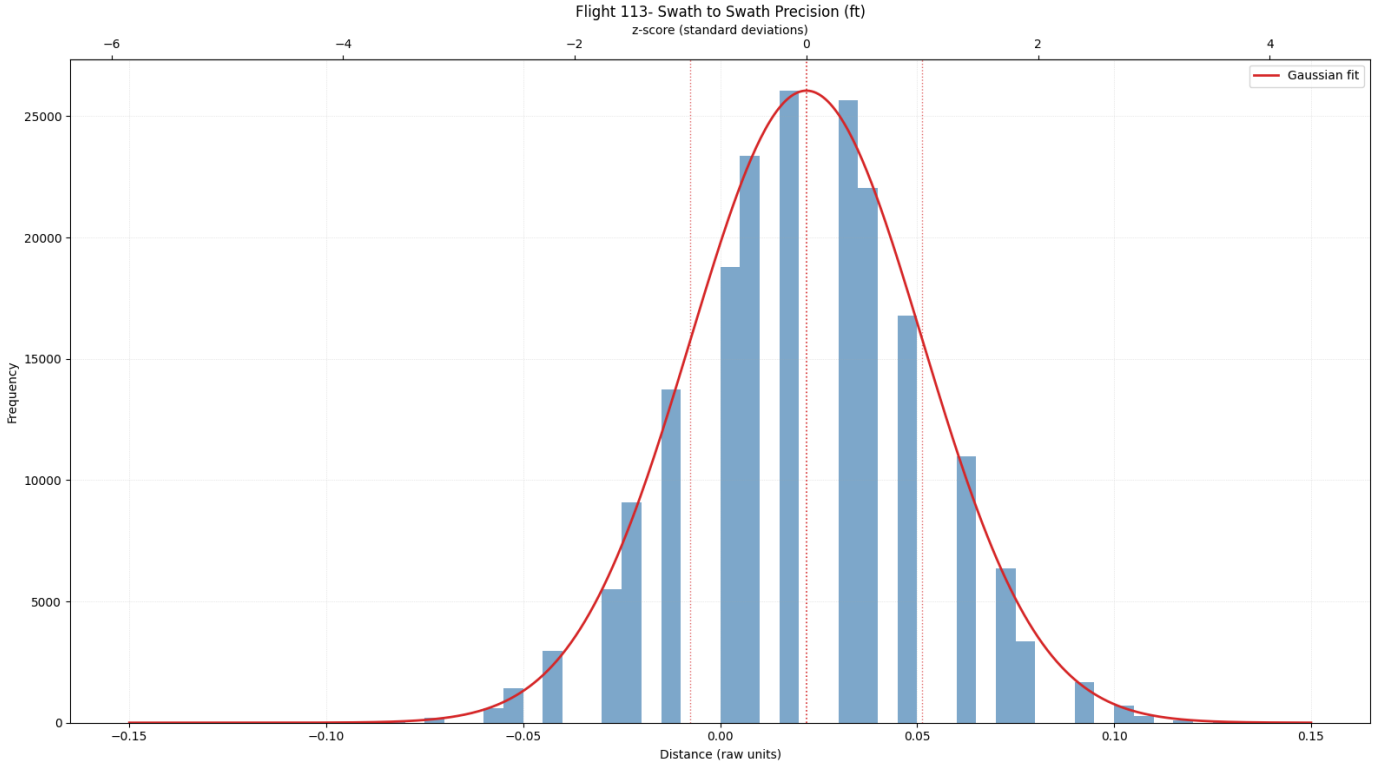

Figure 3: Swath-to-Swath Precision Histogram Example: Distribution of residual point distances relative to nearest overlapping line

Visual Cross-Section Analysis

Cross-sections were also visually reviewed in TerraScan to qualitatively assess horizontal and vertical alignment between strips. In most locations, overlapping swaths were visually indistinguishable, with negligible measurable offset.

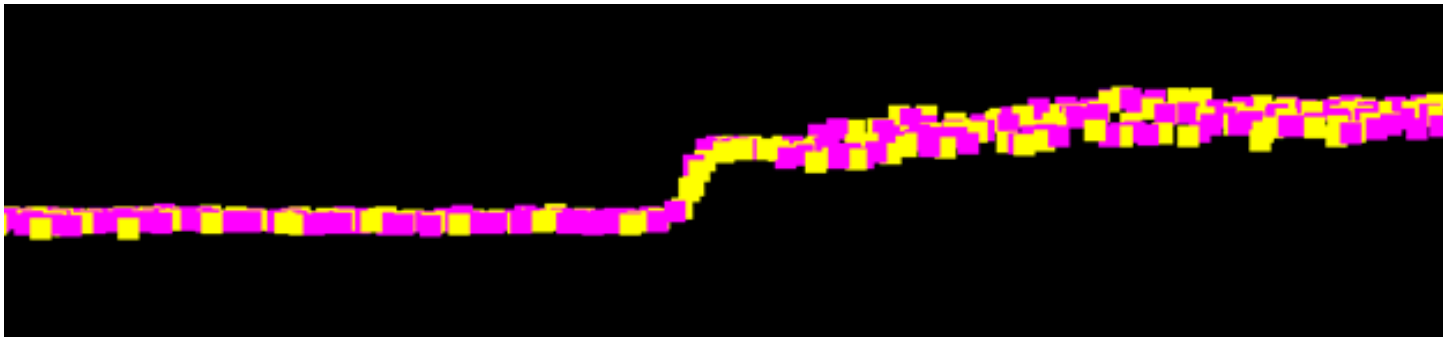

Test Number	Sampling Rate	Altitude (m)	Return Mode	Point Density PPSM	Swath-to-Swath Non-Vegitated RMSEdz (m)	Swath-to-Swath Non-Vegitated std (m)	Swath-to_Swath Non-Vegitated Max Diff (m)
107	350 KHz	120	Sixteen Returns	117	0.005	0.006	0.058
108	350 KHz	90	Sixteen Returns	192	0.005	0.005	0.067
109	350 KHz	60	Sixteen Returns	436	0.006	0.005	0.174
111	100 KHz	120	Sixteen Returns	30	0.010	0.007	0.119
112	1MHz	120	Eight Returns	326	0.009	0.008	0.125
113	2 MHz	120	Quad Return	664	0.011	0.008	0.165
114	100 KHz	90	Sixteen Returns	60	0.009	0.006	0.149
115	1MHz	90	Eight Returns	596	0.008	0.007	0.177
116	2 MHz	90	Quad Return	1,378	0.010	0.007	0.155
117	100 KHz	60	Sixteen Returns	134	0.005	0.004	0.149
118	1MHz	60	Eight Returns	1,350	0.006	0.005	0.152
119	2 MHz	60	Quad Return	2,830	0.007	0.006	0.192

Key Findings: Relative Precision

The combined results of the within-swath and swath-to-swath analyses confirm that the DJI Zenmuse L3 demonstrates exceptionally low internal noise and minimal swath-to-swath misalignment. Both within-swath (~0.005m) and swath-to-swath (~0.006m) RMSE values are quite low and align with the absolute accuracy of observations.

This level of precision represents a substantial improvement over previous-generation DJI LiDAR units, and the consistency among all flight altitudes and PRFs shows that the L3 is a highly stable and reliable sensor for high-density, high-accuracy mapping applications.

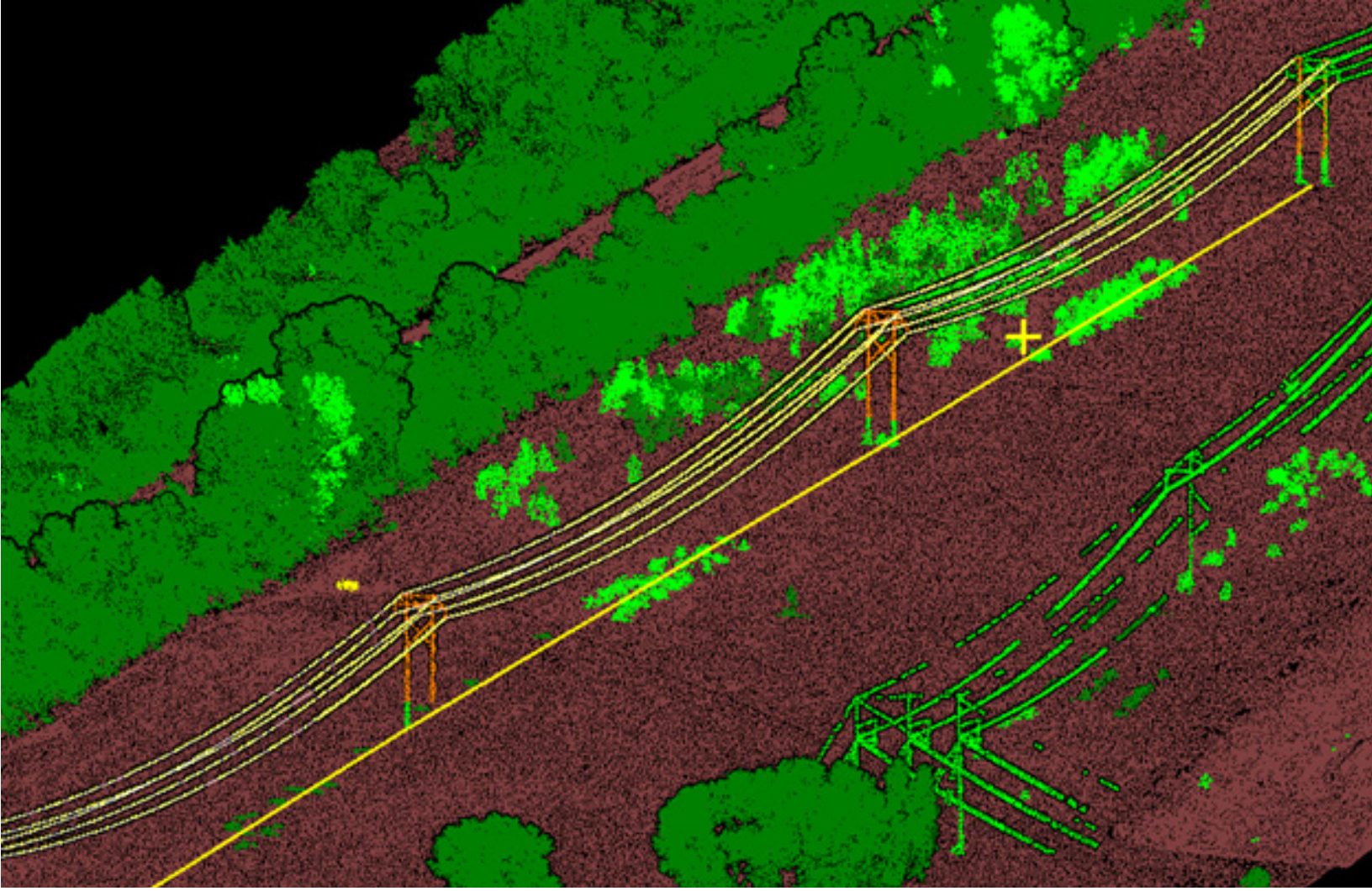

LINEAR FEATURE PERFORMANCE: POWERLINE ANALYSIS

After establishing the Zenmuse L3's positional accuracy and internal precision, additional testing was performed to evaluate how the system captures small, suspended linear features, specifically, electrical transmission and distribution conductors. Powerlines are an especially difficult target for airborne LiDAR due to their small cross-sectional area, variable sag geometry, reflectance characteristics, and continuous movement caused by wind and temperature changes. This section provides both a quantitative assessment of wire measurement precision and qualitative examples of conductor capture under varying pulse repetition frequencies (PRFs) and scan geometries.

Test Objectives and Scope

The purpose of this analysis was to determine how PRF and scan pattern influence the L3's ability to resolve powerline conductors. Specifically, the objective was to observe whether increasing pulse repetition frequency improves

Test Number	Sampling Rate	Altitude (m)	Speed m/s	Return Mode	Scan Mode
101	100 KHz	120	15 m/s	Sixteen Returns	Star-Shaped
102	350 KHz	120	15 m/s	Sixteen Returns	Star-Shaped
103	1MHz	120	15 m/s	Eight Returns	Star-Shaped
104	2 MHz	120	15 m/s	Sixteen Returns	Star-Shaped
105	350 KHz	120	15 m/s	Quad Return	Non-Repetitive
106	350 KHz	120	15 m/s	Quad Return	Linear

continuity and hit density or, conversely, reduces measurement precision due to lower per-pulse energy. Two independent variables were tested:

(1) pulse repetition frequency and

(2) scan mode (star, linear, and non-repetitive).

All flights were conducted at 120 m AGL and 15 m/s over the same corridor at Site A, which contained a mixture of transmission and distribution structures adjacent to an electrical substation.

Test Limitations and Constraints

It is important to note that this test is not intended to establish absolute accuracy of the wire geometries themselves. There was no access to verified conductor diameters, exact tension values, or thermal states during acquisition. Each of these parameters directly affects the true sag and position of a span. Additionally, since wire positions vary throughout the day due to loading and wind, the analysis represents a best fit in time rather than a static model.

The results should therefore be interpreted as a measure of internal consistency and return behavior, not as a definitive geometric truth of the actual wire location. Similarly, because all analysis was limited to single-swath datasets, potential effects from multi-swath alignment were intentionally excluded.

Powerline Analysis Methodology

Wire features were extracted using Terrasolid's Detect Wires tool to generate modeled catenaries based on LiDAR hits. These modeled catenaries served as assumed centerlines for each span. Points associated with insulators, towers, and other non-conductor features were excluded from the analysis to avoid introducing geometric bias or noise.

For each dataset, Terrasolid's Compute Distance tool was used to calculate the distance between each LiDAR point and its corresponding modeled catenary. The residual distances from this operation represent a three-dimensional deviation of individual returns relative to the assumed wire location.

To account for temporal movement, each dataset was processed independently. A new catenary was fitted to each span per dataset to avoid cross-referencing wire positions collected under differing environmental conditions. The same three spans were analyzed in each dataset.

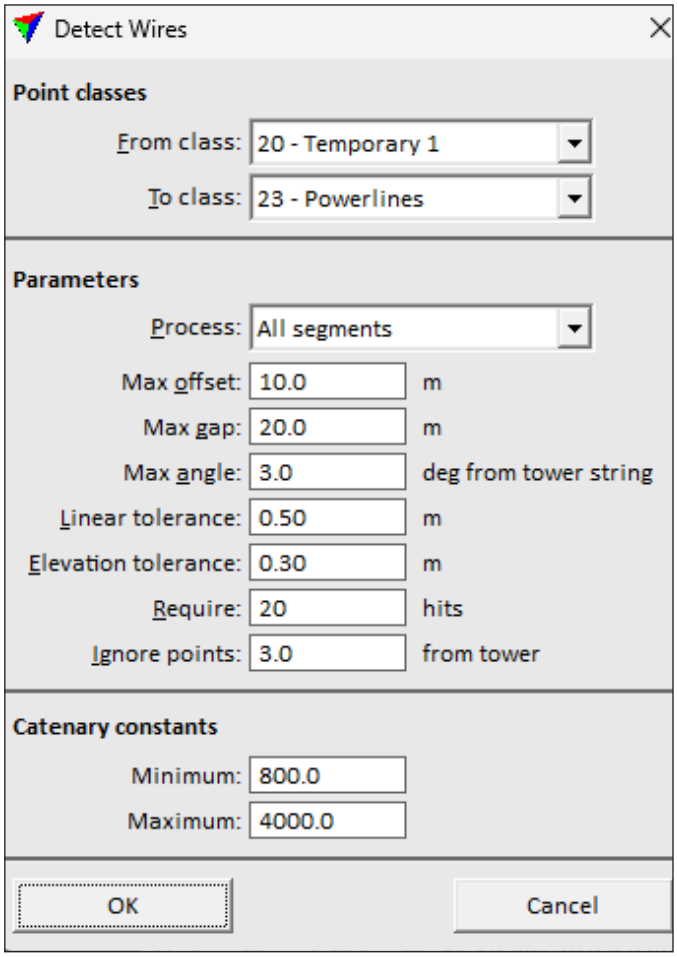

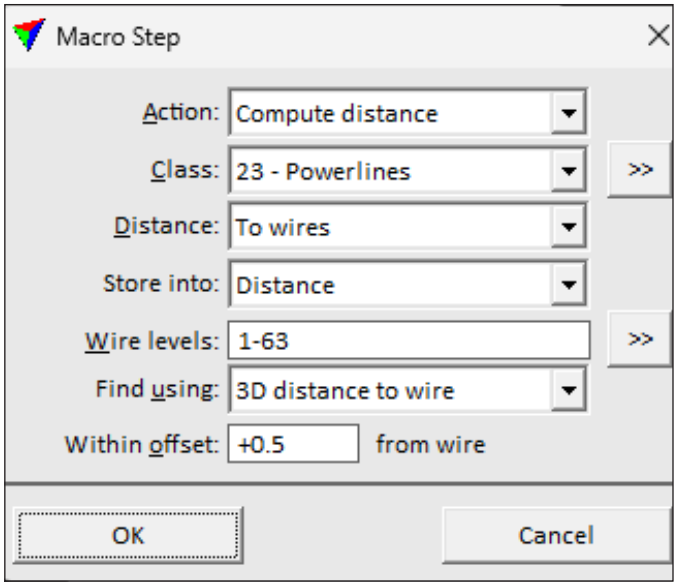

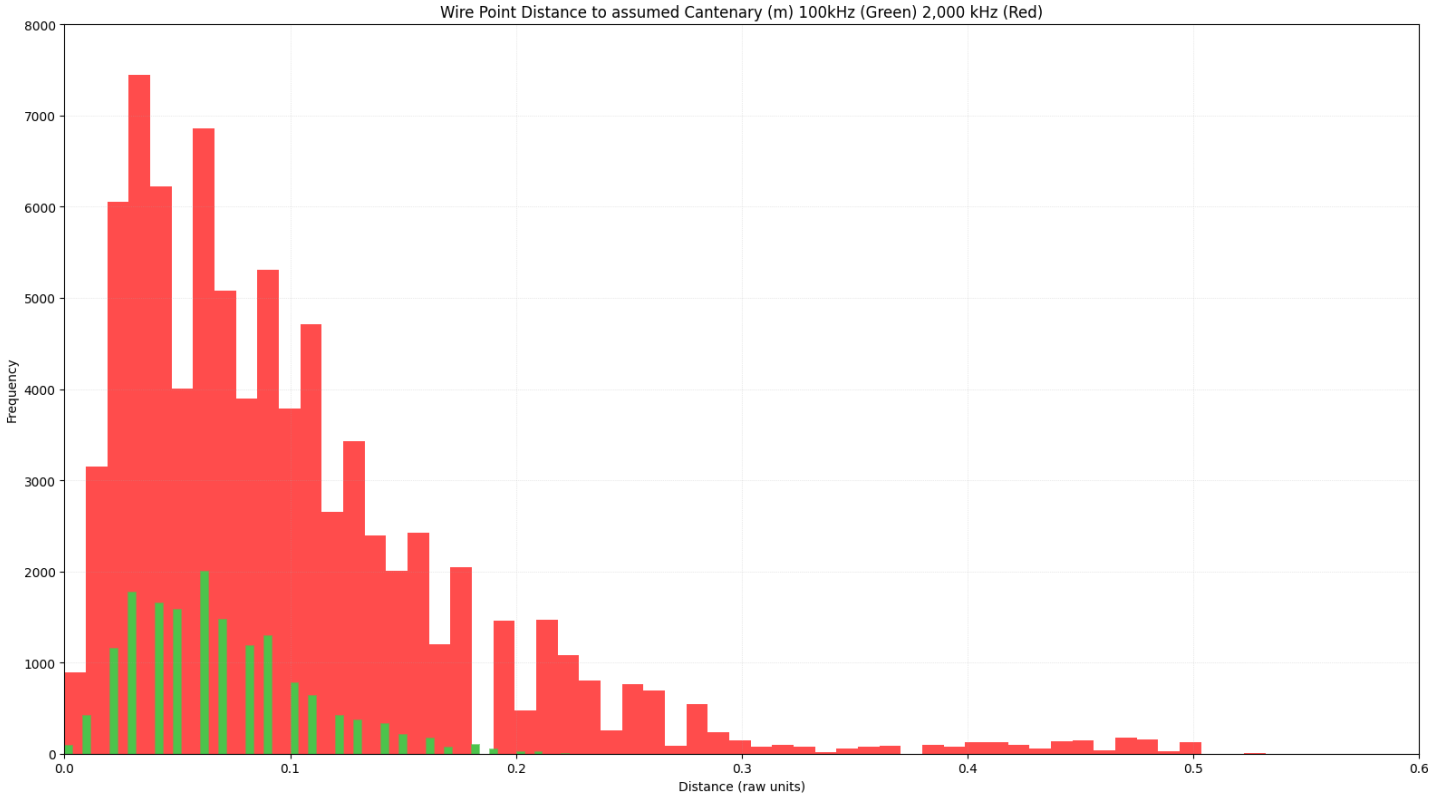

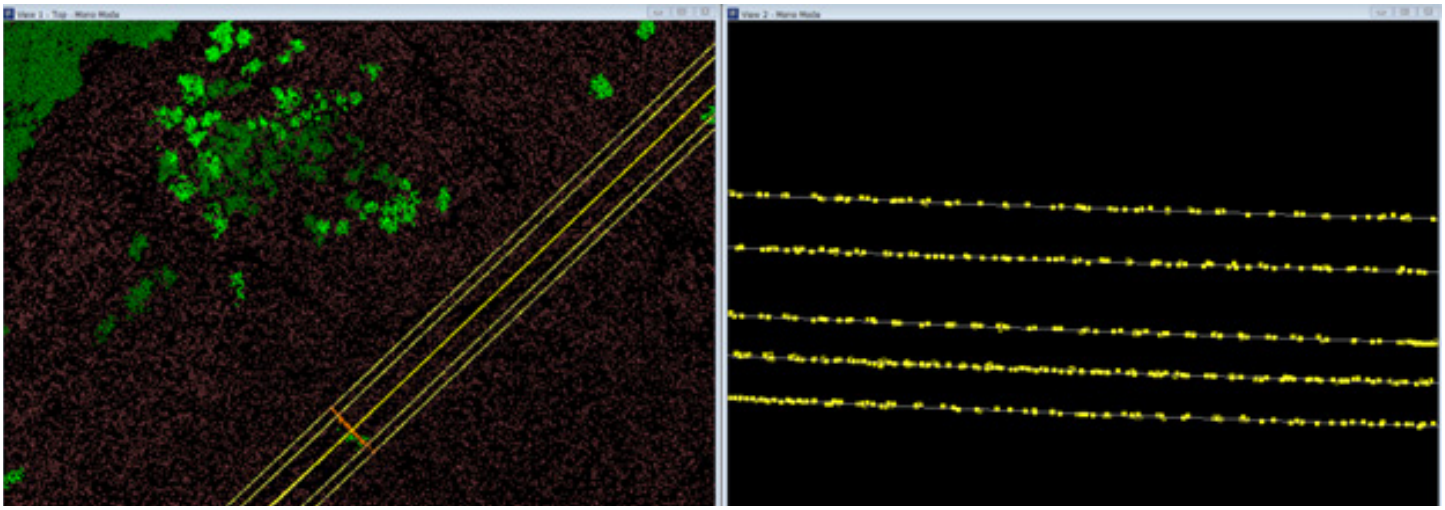

Test Number	Sampling Rate	Return Mode	Scan Mode	Powerline error (std dev) (m)	Powerline Mean distance (m)	Powerline Max distance (m)	Powerline Sampling point count
101	100 KHz	Sixteen Returns	Star-Shaped	0.0382	0.0674	0.24	15,921
102	350 KHz	Sixteen Returns	Star-Shaped	0.0304	0.0453	0.26	39,445
103	1MHz	Eight Returns	Star-Shaped	0.0567	0.0884	0.36	88,438
104	2 MHz	Sixteen Returns	Star-Shaped	0.0798	0.0988	0.57	84,340
105	350 KHz	Quad Return	Non-Repetitive	0.0487	0.0746	0.33	37,094
106	350 KHz	Quad Return	Linear	0.0362	0.0573	0.48	80,018

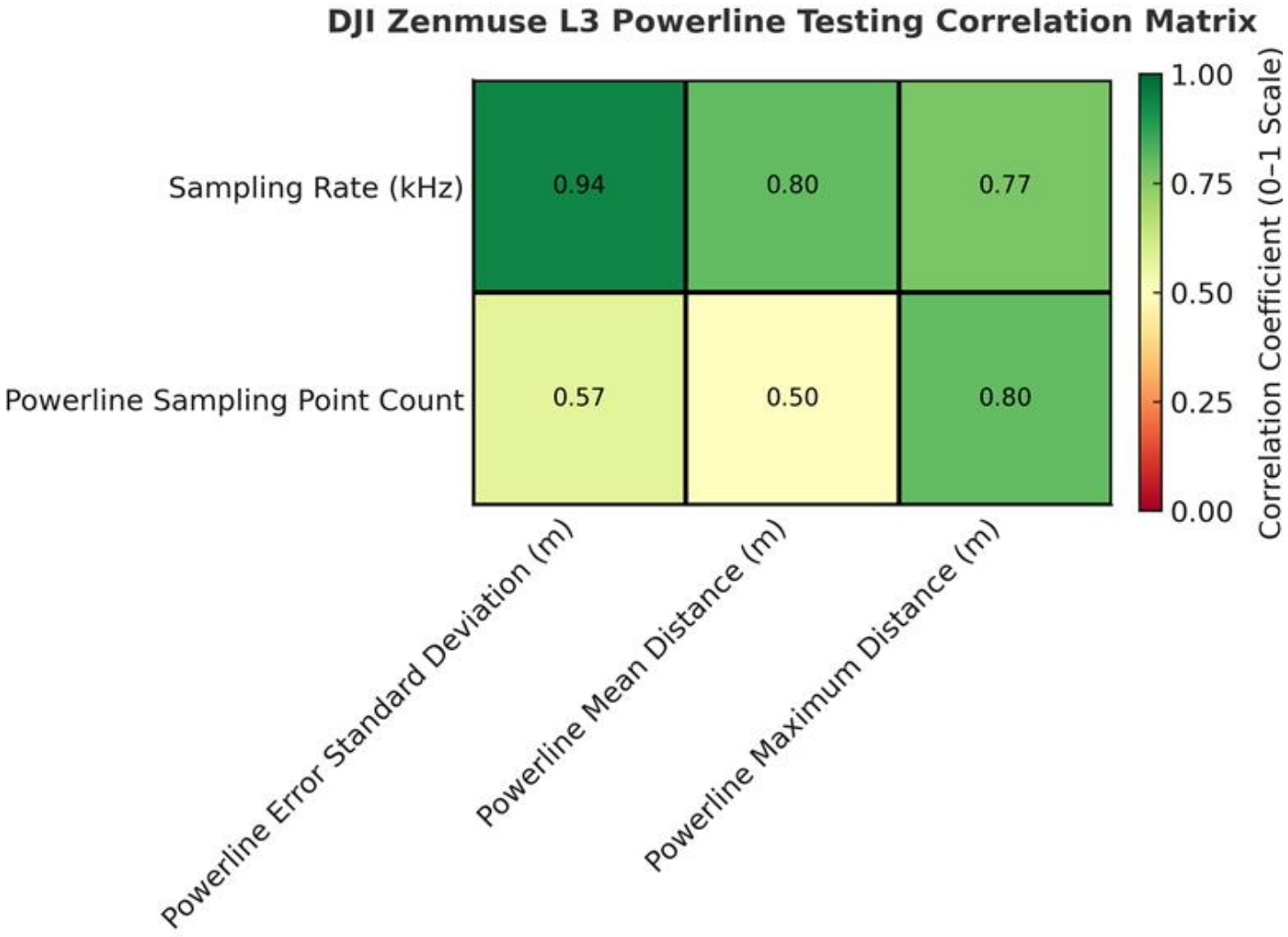

PRF Impact on Wire Detection

At 100 kHz, per-pulse energy was highest, but wire continuity suffered; smaller distribution and telecommunication conductors often exhibited gaps. The mean residual was lowest, as expected, but total wire hits were minimal.

At 350 kHz, returns became markedly more complete while maintaining relatively low noise, representing the best balance of energy and sampling density in this dataset.

At 1 MHz, total wire hits peaked; however, residuals widened modestly, indicating slightly higher dispersion about the modeled catenary. Visually, this flight had the best balance of powerline returns and noise.

At 2 MHz, a distinct decline in wire continuity was visible, along with higher mean and maximum distances. This reduction in data density corresponds to decreased pulse energy per shot, a common trade-off in high-PRF LiDAR systems.

Statistical comparison yielded a correlation coefficient of r = 0.94 between PRF and measured mean distance, confirming that higher sampling rates were directly associated with increased residual error.

Scan-Pattern Evaluation

Three 350 kHz flights were analyzed using the linear, star, and non-repetitive scan patterns. The expectation was that the non-repetitive pattern would yield the greatest diversity of look angles, the linear pattern the highest repeatability, and the star pattern a compromise between both.

Empirical results showed that while standard deviation values remained largely unchanged, mean distance, maximum distance, and wire hit density varied significantly between scan patterns. These differences likely result from variations in incidence angle distribution rather than from sensor noise. Additional repetitions would be required to determine whether the trend is systematic or partly driven by limited sampling.

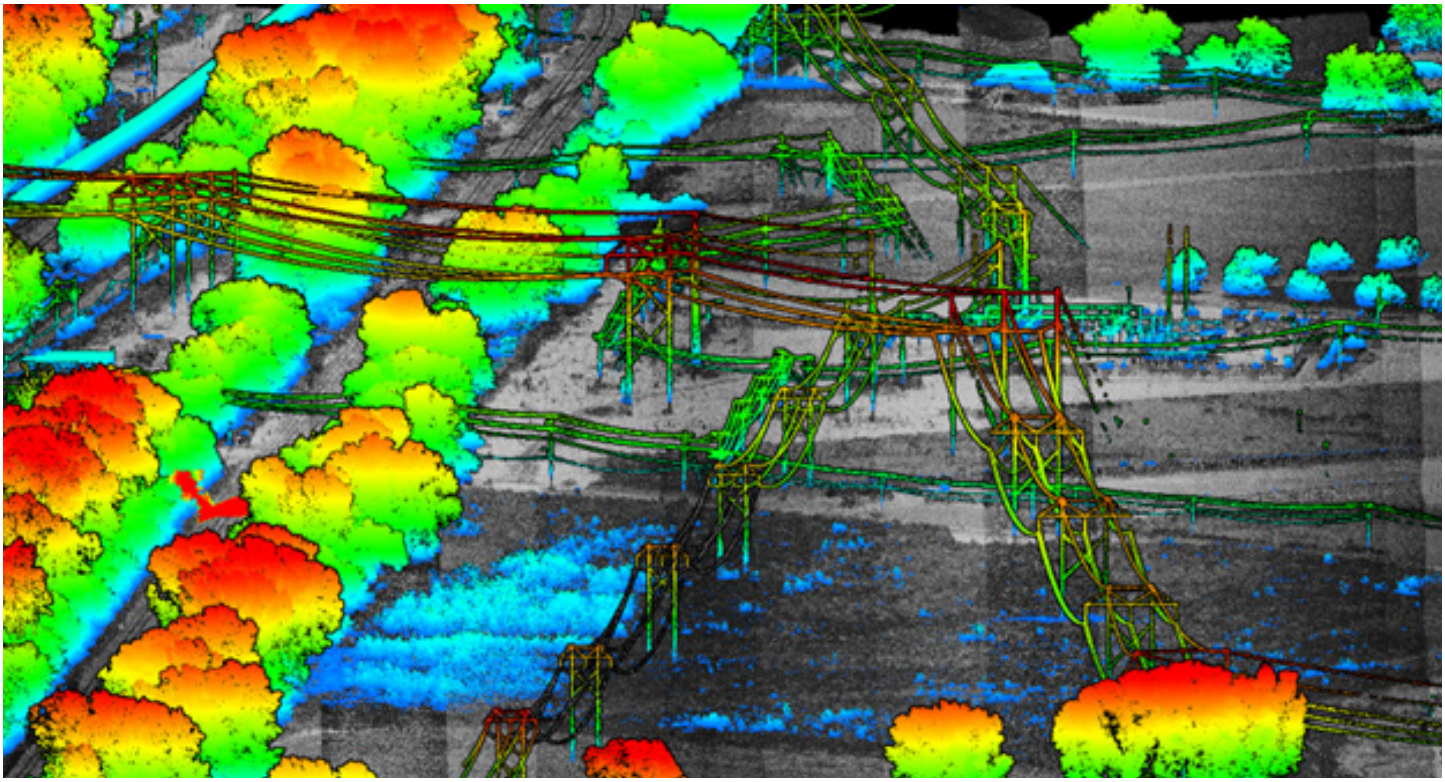

Example of 1,000 kHz displayed as elevation distance above ground.

Powerline Testing Conclusions

Taken collectively, these results demonstrate that the Zenmuse L3 maintains consistent and predictable behavior when mapping small suspended conductors. Performance scales logically with PRF. Importantly, this experiment highlights both the capability and the limitations of the Zenmuse L3 for powerline analysis. While quantitative residuals provide valuable insight into sensor ability to collect powerlines with minimal noise, the dynamic nature of the target prevents direct translation into true precision or accuracy statements.

The subsequent figures visualize these findings through cross-sectional profiles and residual histograms, illustrating continuity differences across transmission and distribution spans under identical conditions.

Other Sensor Observations

Across all tests performed, the Zenmuse L3 demonstrated substantial improvement over previous DJI LiDAR generations. However, as this evaluation was conducted on a pre-production engineering unit using a beta release of DJI Terra, several software-related behaviors were observed that may be addressed prior to the product's official release. These observations are included for completeness and should not be interpreted as indicators of hardware limitations but as software issues identified during testing.

Multiple Pulses in Air (MPiA)

At very high pulse repetition frequencies (PRF), LiDAR systems must manage multiple pulses in the air simultaneously. When the travel time of one pulse exceeds the interval before the next is emitted, the system must accurately associate each return with its originating pulse. If the processing algorithm misidentifies these associations, geometric stacking artifacts can appear, typically as vertically displaced layers within the point cloud. This phenomenon is well documented across many high-PRF LiDAR platforms and is normally mitigated through signal-tracking algorithms.

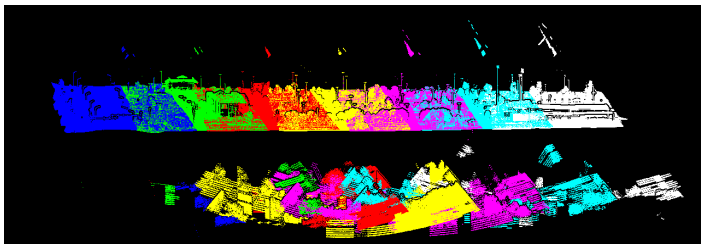

MPiA effects were observed only in datasets collected at 1 MHz and 2 MHz PRF.

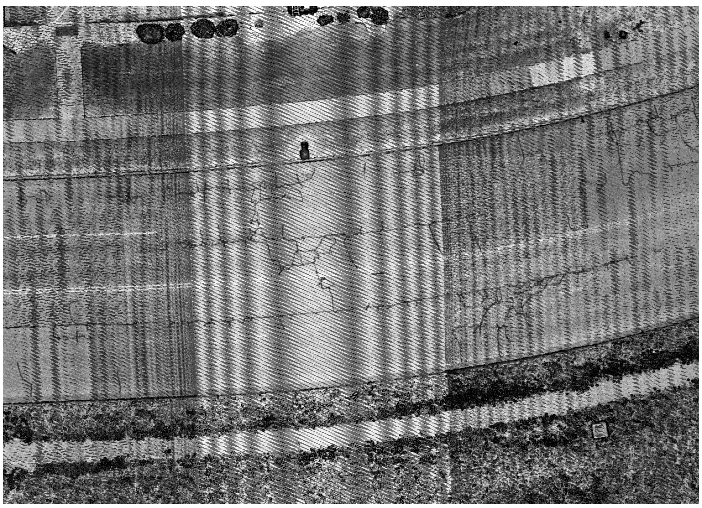

The magnitude of these artifacts varied by altitude and pulse rate, as summarized below:

Flight	PRF	Altitude (m)	Total Points	Points with MPiA Artifacts	Percent of Points
112	1 MHz	120	43,563,843	435,638	1.0 %
113	2 MHz	120	174,345,130	7,649,620	4.4 %
115	1 MHz	90	189,842,721	1,578	<0.01 %
116	2 MHz	90	366,505,707	24,903,573	6.8 %
118	1 MHz	60	468,711,447	7,453	<0.01 %
119	2 MHz	60	832,540,478	16,172,298	1.9 %

Artifacts were not observed in any 100 kHz and 350 kHz datasets.
During processing, affected points were assigned to the Noise class for exclusion from subsequent accuracy analyses. After filtering, the remaining data exhibited no measurable degradation in positional accuracy or internal precision beyond what was reported above.

DJI has acknowledged this behavior in early software builds and is actively refining its signal-matching algorithms. Because MPiA mitigation is handled algorithmically rather than optically, it is expected that this will be resolved through future firmware and software updates prior to commercial release.

Intensity Scaling

The second observation relates to intensity normalization across the swath.

Although the L3's 16-bit dynamic range provides a significantly greater reflectance resolution than prior DJI Lidar systems, the test data showed a gradual darkening of intensity values toward the edges of the scan field.
This effect appeared consistently across all altitudes, PRFs, and scan modes and manifested as a linear decrease in relative brightness with increasing scan angle.

In practice, this radiometric gradient is minimal when overlaps are clipped or colorization is applied, but it

becomes noticeable when comparing adjacent swaths by intensity alone. The result is a variation in apparent reflectance between flight lines, which can make visual interpretation of uniform surfaces slightly inconsistent.

Based on the observed behavior, this appears to be related to incident-angle corrections and scaling table calibration within the software rather than to a hardware characteristic of the sensor. Refining the intensity normalization and vignetting compensation algorithms within DJI Terra should address this behavior in future releases.

OVERALL CONCLUSIONS AND RECOMMENDATIONS

The testing conducted across multiple configurations demonstrates that the DJI Zenmuse L3 represents a substantial improvement in performance over previous generation DJI Lidar sensors. Throughout all evaluations, absolute accuracy, precision, and feature-specific testing, the system consistently produced results indicative of high geometric stability and repeatability.

At flight altitudes ranging from 60 to 120 meters AGL, vertical and horizontal accuracy remained within a few millimeters of variation between test configurations. Changes in PRF, altitude, and scan geometry produced minimal changes, supporting the conclusion that the system's ranging and INS integration are both stable and internally consistent.

Feature-specific analyses, including powerline conductor profiling and planar precision studies, reinforced these findings. The L3 demonstrated the ability to detect and model fine linear features such as powerline conductors. Observed limitations, specifically, multiple-pulse-in-air artifacts and minor edge-of-swath intensity scaling, were isolated to higher PRF settings and are more than likely characteristic of software limitations identified during testing rather than hardware constraints.

Overall, results indicate that the L3 achieves reliable, high-density LiDAR data suitable for many engineering, topographic, and infrastructure mapping applications where geometric accuracy and repeatability are critical. Additional testing is planned to further characterize the system's performance under expanded conditions and to evaluate additional sensor metrics.

Vertical Aspect welcomes questions, collaboration, and feedback related to this study and ongoing sensor evaluations. Inquiries can be directed to support@verticalaspect.com

ACKNOWLEDGMENTS

This study was made possible through the support and collaboration of several key partners.

The authors would like to acknowledge DJI Enterprise North America for providing early access to pre-production hardware and technical coordination throughout the evaluation period.

Special thanks are extended to Terrasolid Ltd. for their continued software support and for enabling advanced analysis workflows that made this testing possible utilizing TerraScan, TerraModeler, and TerraMatch.

We would also like to thank Eric Wischropp with Laser Specialist for his assistance in check point data collection, equipment setup, and field validation. Their technical expertise and commitment to methodological consistency contributed greatly to the quality and completeness of this study.

APPENDIX A

About Vertical Aspect

Vertical Aspect specializes in geospatial technology solutions that solve complex challenges across multiple industries. We take a consultative approach, working alongside clients to identify opportunities, select the right tools, and implement systems that deliver results. Our team adapts to each client's unique situation, whether you need strategic guidance, technical implementation, or comprehensive project support from start to finish.

Our team works closely with clients to clarify objectives, build effective strategies, and extract actionable insights that fuel measurable growth. Through hands-on expertise and data-driven problem-solving, we deliver solutions across diverse industries, from precision agriculture and construction to surveying and environmental monitoring.

As trusted partners with leading technology providers, we connect clients with the right hardware and software for their specific needs. Vertical Aspect provides complete solutions: industry-leading equipment, powerful software platforms, responsive technical support, and hands-on training that empowers your team to succeed.

Learn more at www.verticalaspect.com

APPENDIX B

References

The American Society of Photogrammetry and Remote Sensing

The ASPRS Positional Accuracy Standards for Digital Geospatial Data Edition 2, Version 2.0.

Terrasolid TerraScan User Guide

Terrasolid TerraMatch User Guide

APPENDIX C

Within-Swath Histograms

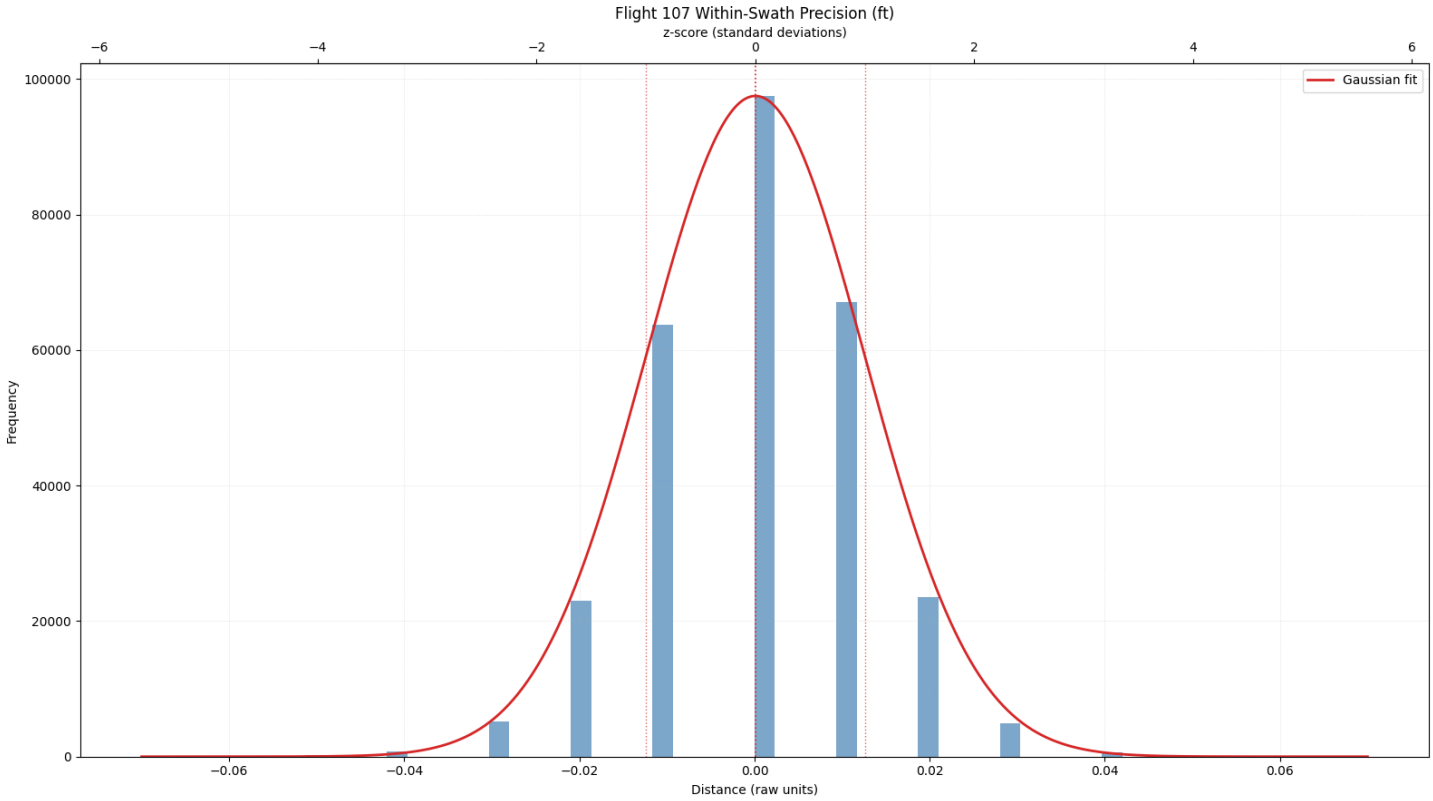
Flight 107 Within-Swath Precision (ft)
z-score (standard deviations)
−6
−4
−2
0
2
4
6
Gaussian fit
100000
80000
60000
40000
20000
0
Frequency
−0.06
−0.04
−0.02
0.00
0.02
0.04
0.06
Distance (raw units)

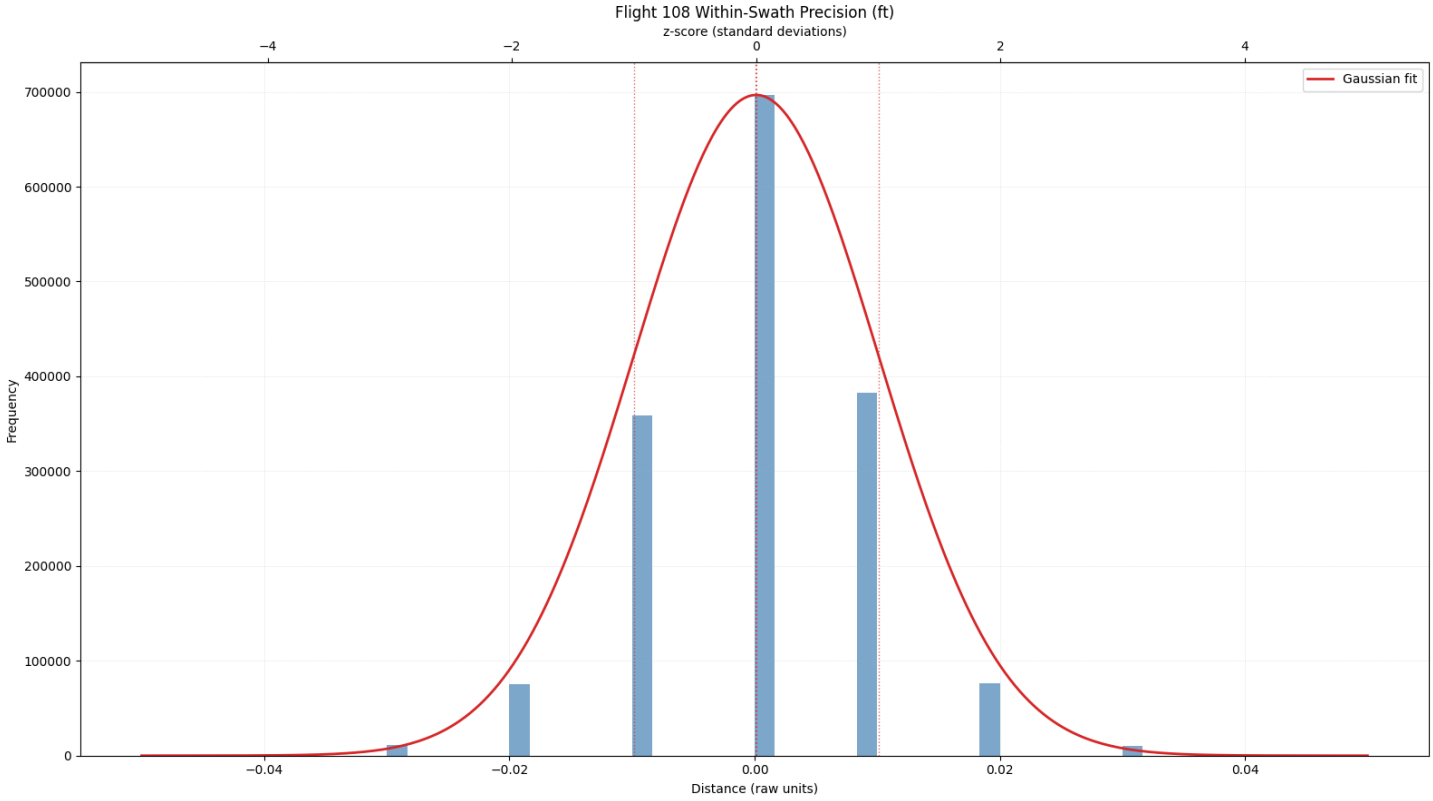
Flight 108 Within-Swath Precision (ft)
z-score (standard deviations)
−4
−2
0
2
4
Gaussian fit
700000
600000
500000
400000
300000
200000
100000
0
Frequency
−0.04
−0.02
0.00
0.02
0.04
Distance (raw units)

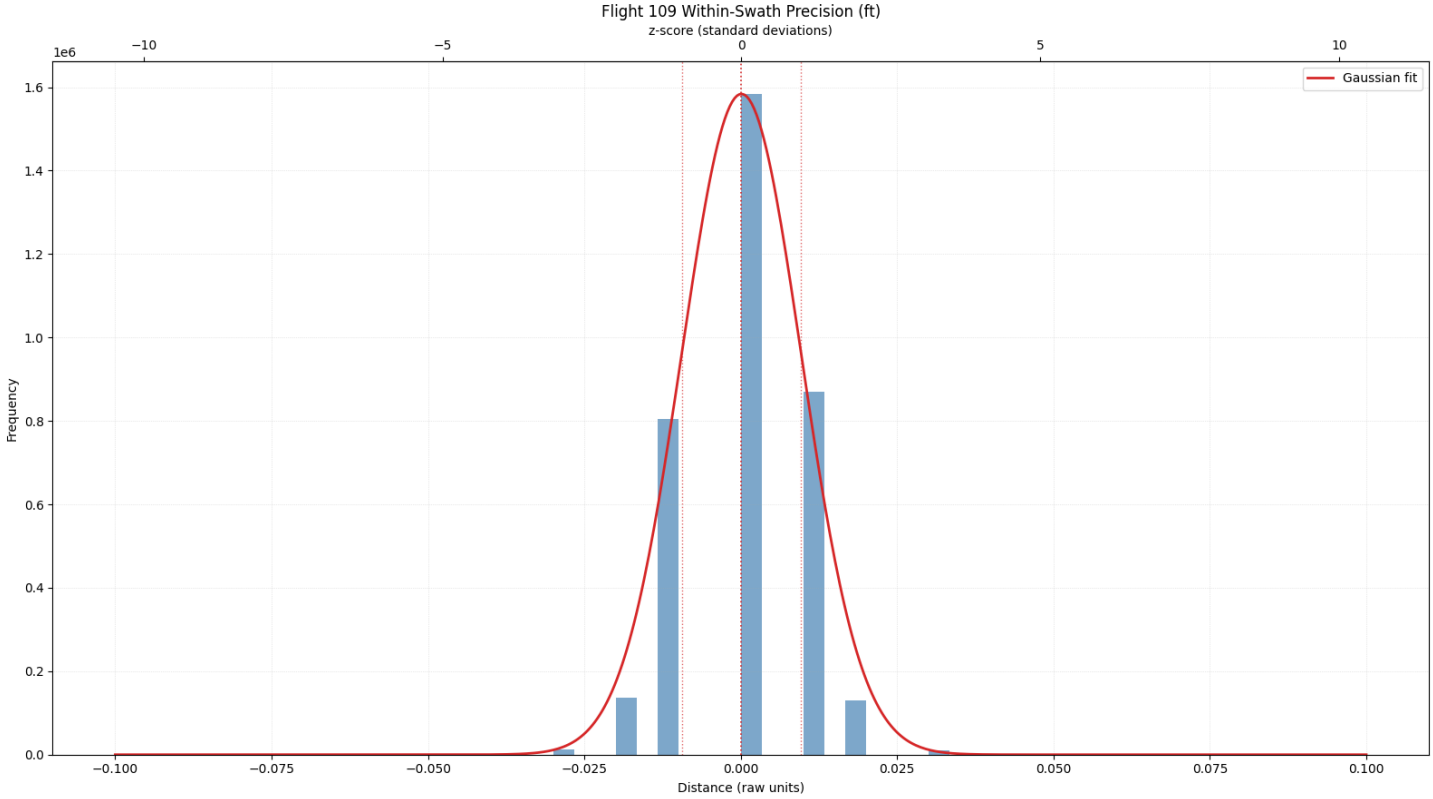
Flight 109 Within-Swath Precision (ft)
z-score (standard deviations)
−10
−5
0
5
10
1e6
1.6
1.4
1.2
1.0
0.8
0.6
0.4
0.2
0.0
Frequency
Gaussian fit
−0.100
−0.075
−0.050
−0.025
0.000
0.025
0.050
0.075
0.100
Distance (raw units)

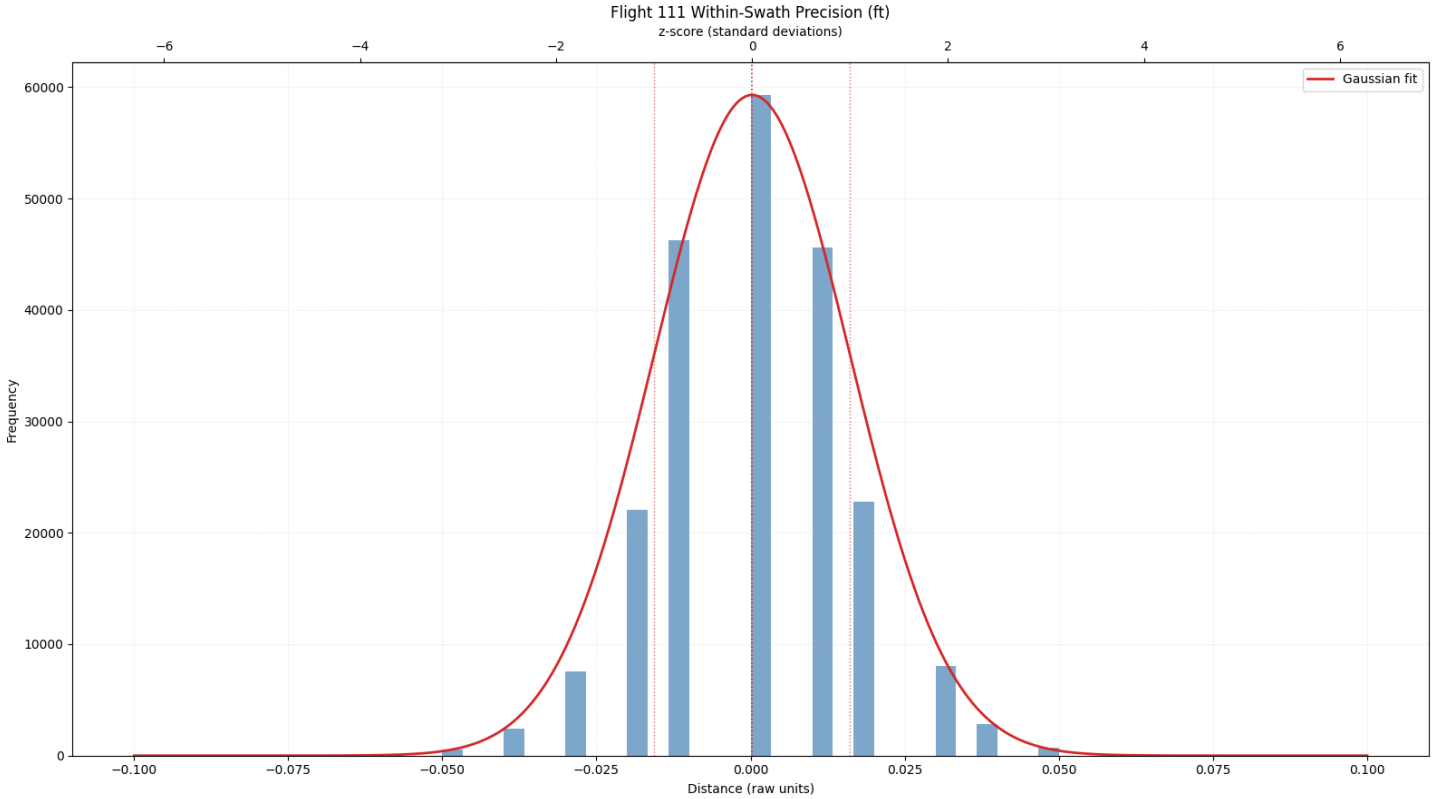
Flight 111 Within-Swath Precision (ft)
z-score (standard deviations)
−6
−4
−2
0
2
4
6
60000
50000
40000
30000
20000
10000
0
Frequency
Gaussian fit
−0.100
−0.075
−0.050
−0.025
0.000
0.025
0.050
0.075
0.100
Distance (raw units)

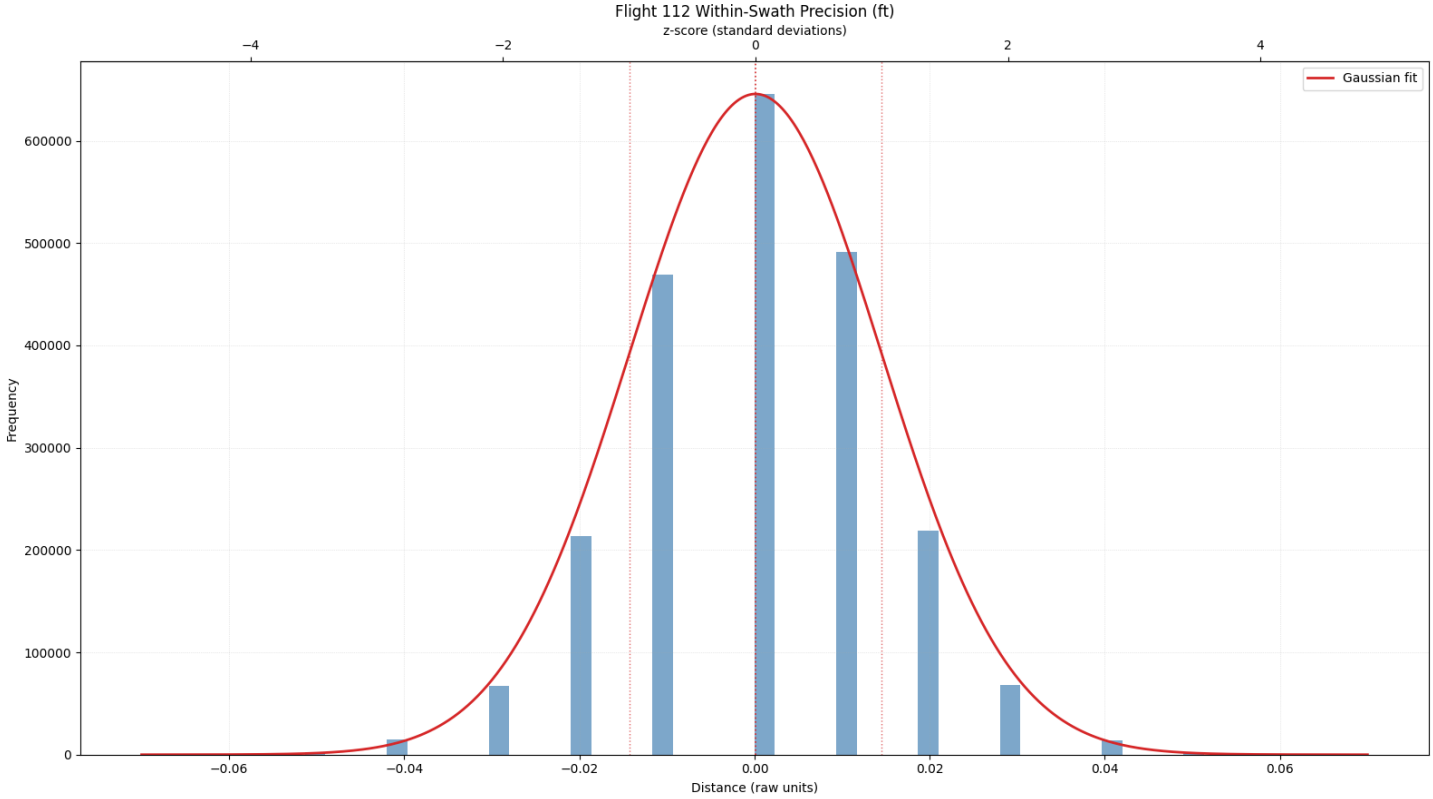
Flight 112 Within-Swath Precision (ft)
z-score (standard deviations)
−4
−2
0
2
4
Gaussian fit
600000
500000
400000
300000
200000
100000
0
Frequency
−0.06
−0.04
−0.02
0.00
0.02
0.04
0.06
Distance (raw units)

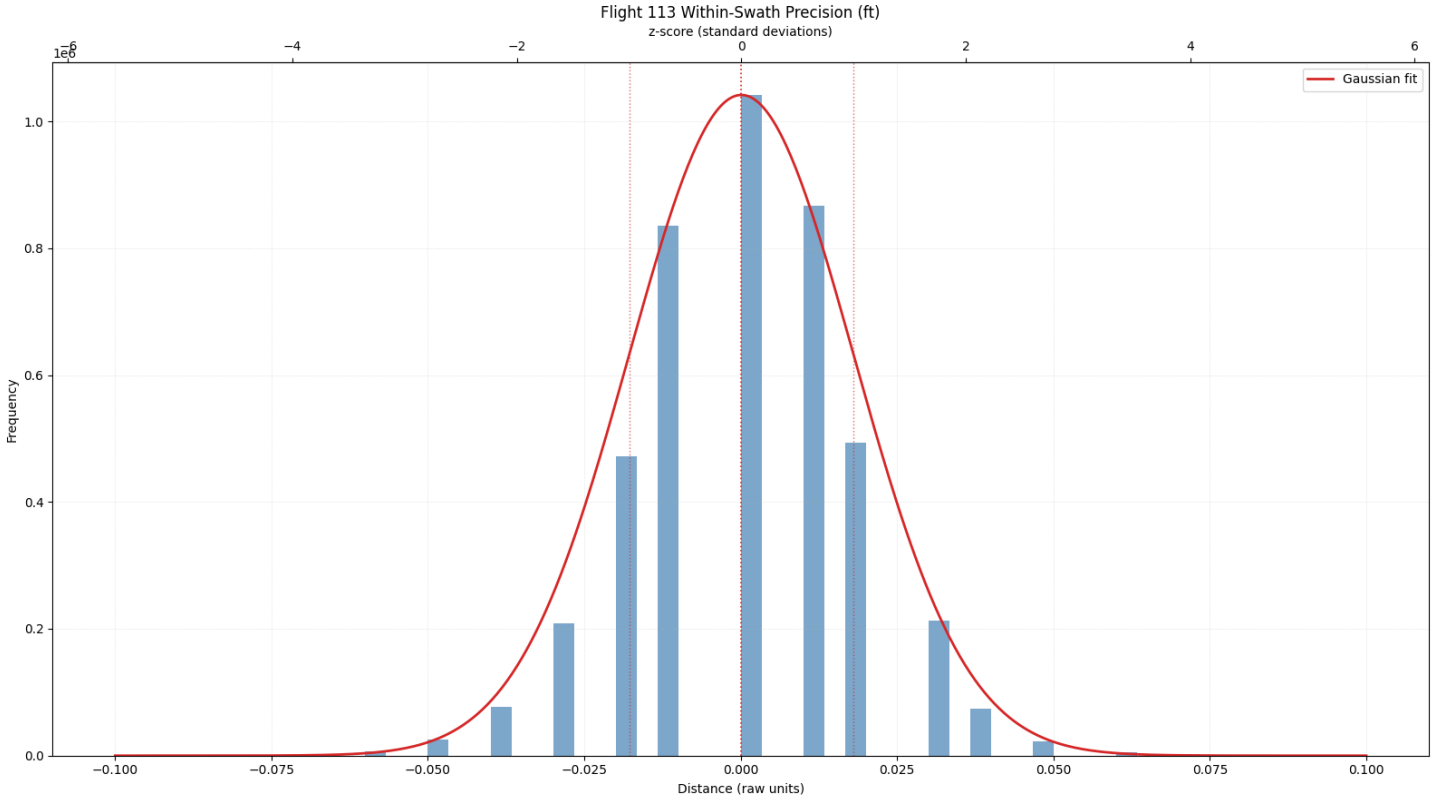
Flight 113 Within-Swath Precision (ft)
z-score (standard deviations)
−6
−4
−2
0
2
4
6
1e6
Gaussian fit
1.0
0.8
0.6
0.4
0.2
0.0
Frequency
−0.100
−0.075
−0.050
−0.025
0.000
0.025
0.050
0.075
0.100
Distance (raw units)

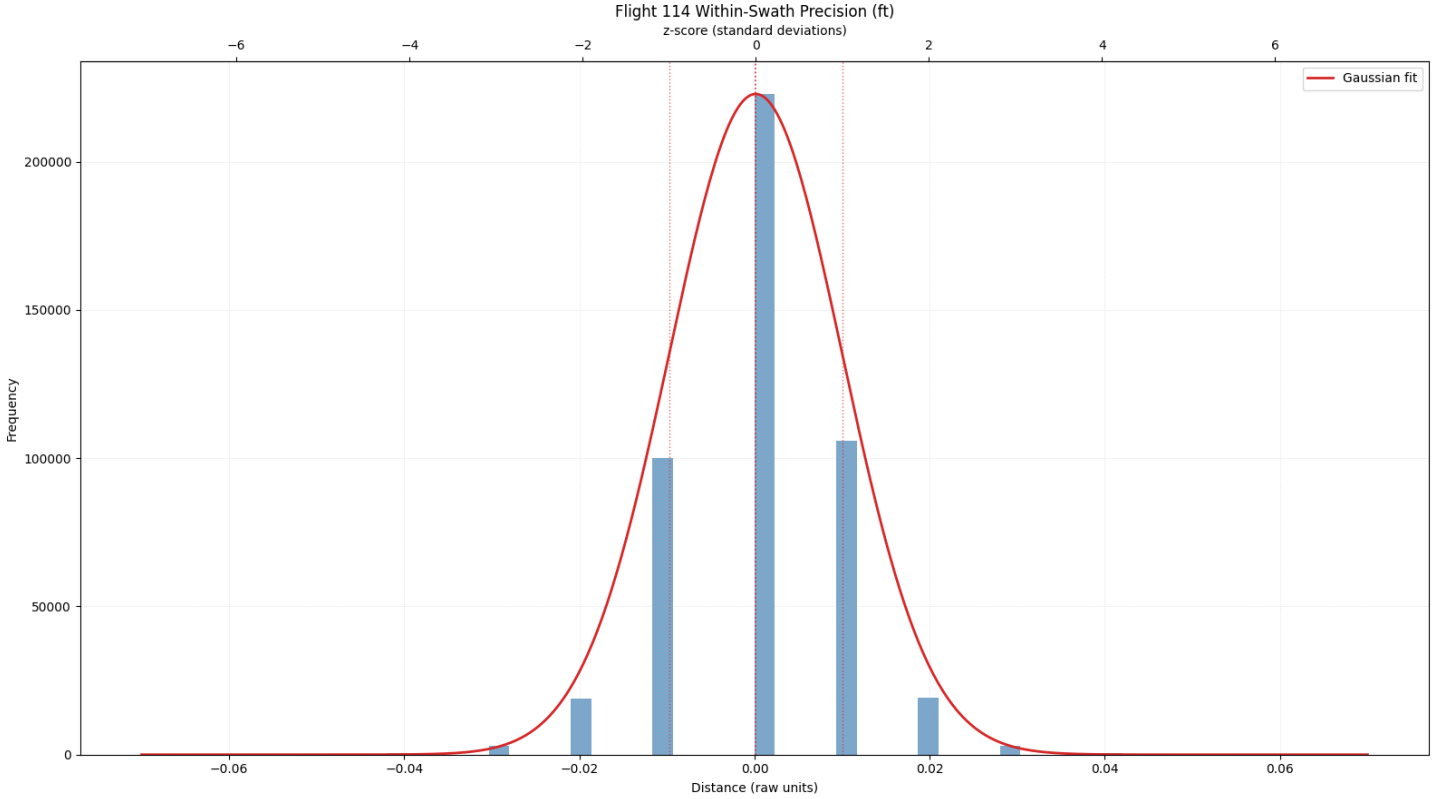
Flight 114 Within-Swath Precision (ft)
z-score (standard deviations)
−6
−4
−2
0
2
4
6
Gaussian fit
200000
150000
100000
50000
0
Frequency
−0.06
−0.04
−0.02
0.00
0.02
0.04
0.06
Distance (raw units)

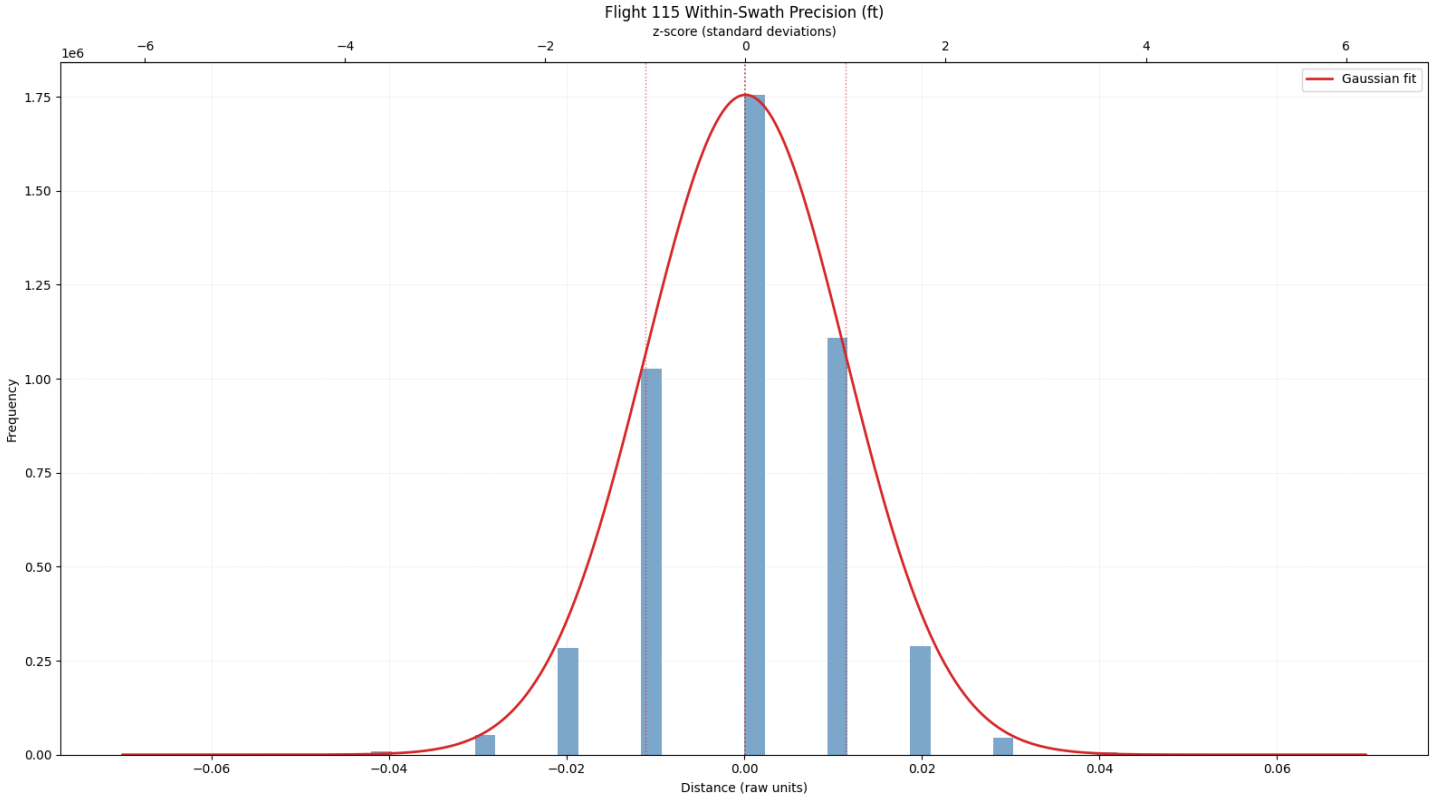
Flight 115 Within-Swath Precision (ft)
z-score (standard deviations)
−6
−4
−2
0
2
4
6
1e6
Gaussian fit
1.75
1.50
1.25
1.00
0.75
0.50
0.25
0.00
Frequency
−0.06
−0.04
−0.02
0.00
0.02
0.04
0.06
Distance (raw units)

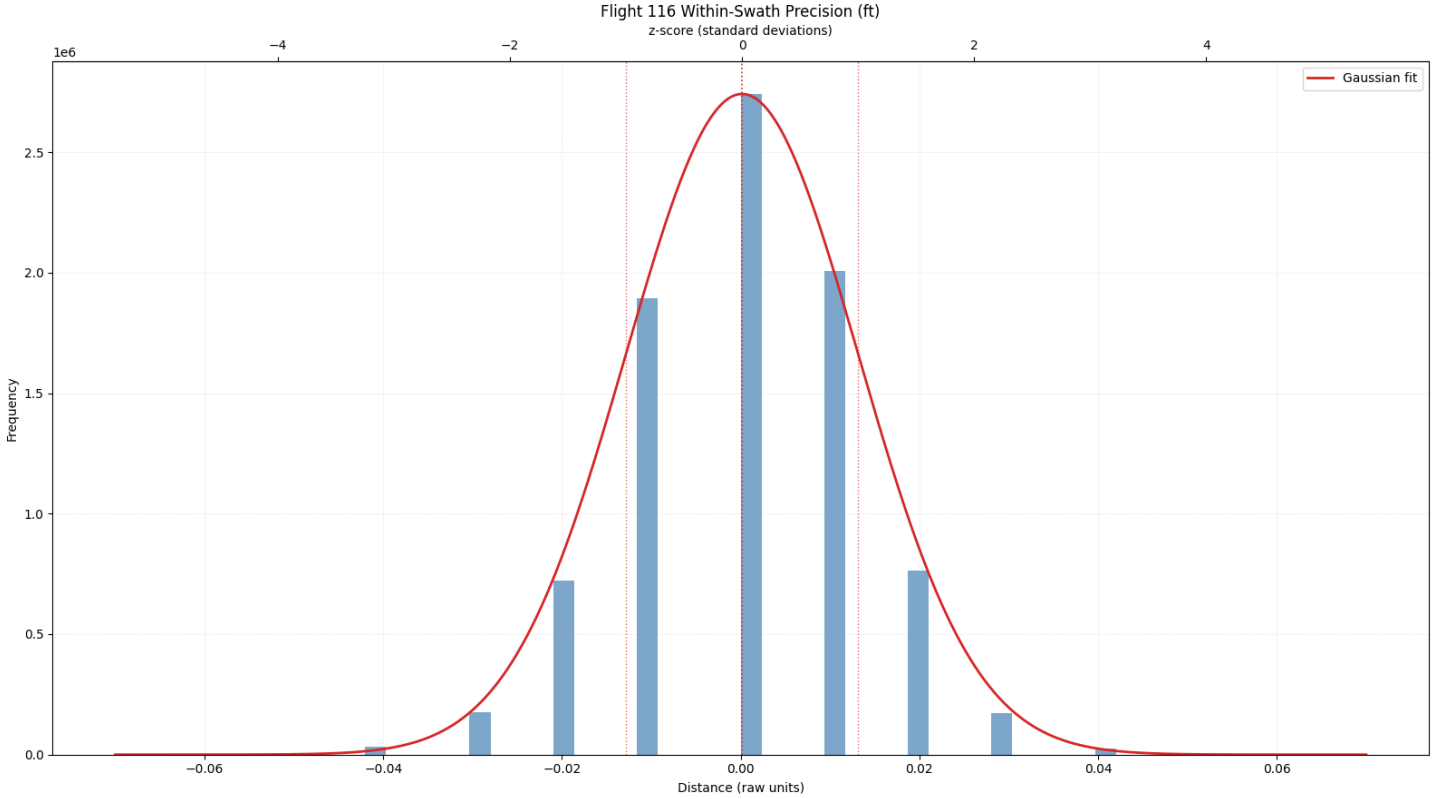
Flight 116 Within-Swath Precision (ft)
z-score (standard deviations)
−4
−2
0
2
4
1e6
2.5
2.0
1.5
1.0
0.5
0.0
Frequency
Gaussian fit
−0.06
−0.04
−0.02
0.00
0.02
0.04
0.06
Distance (raw units)

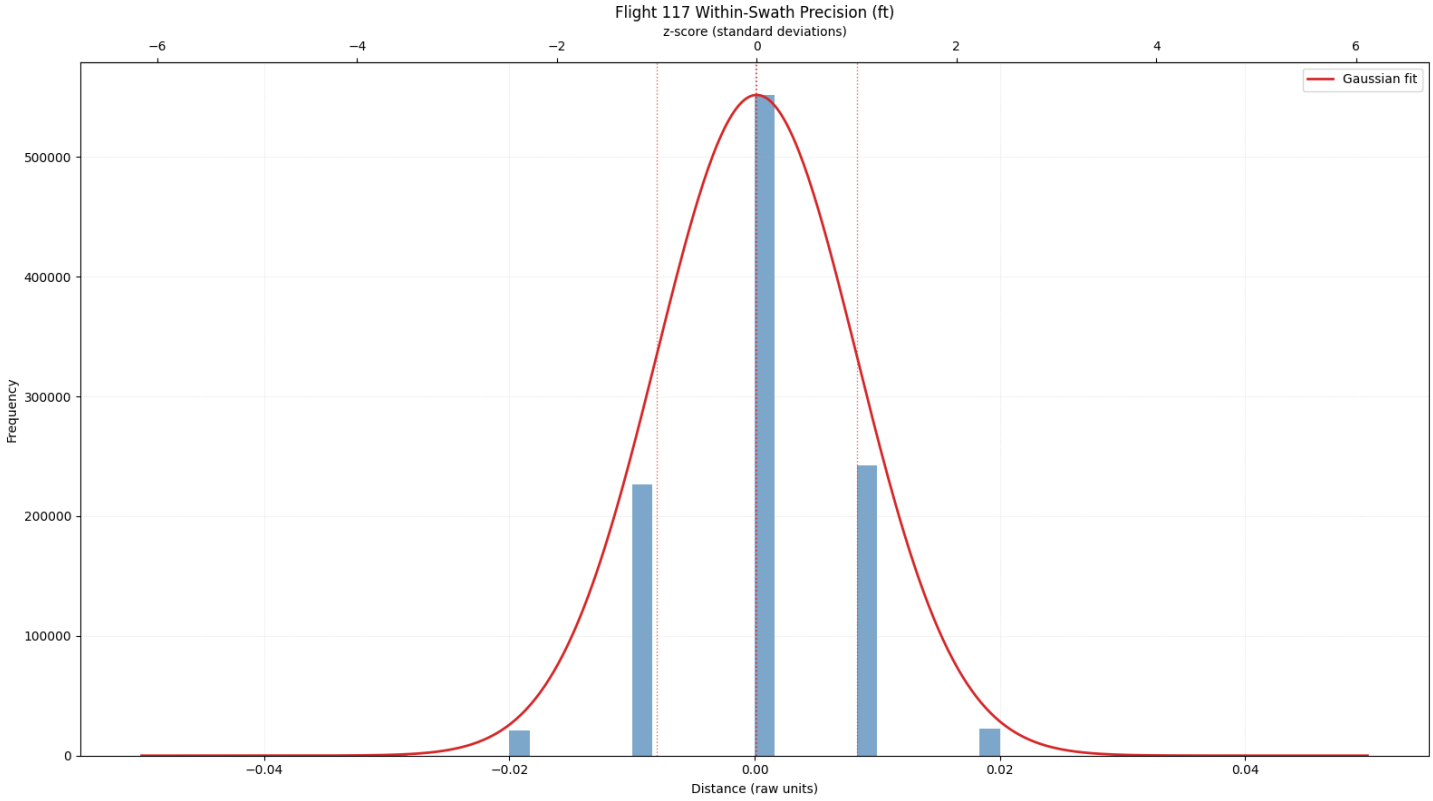
Flight 117 Within-Swath Precision (ft)
z-score (standard deviations)
−6
−4
−2
0
2
4
6
500000
400000
300000
200000
100000
0
Frequency
Gaussian fit
−0.04
−0.02
0.00
0.02
0.04
Distance (raw units)

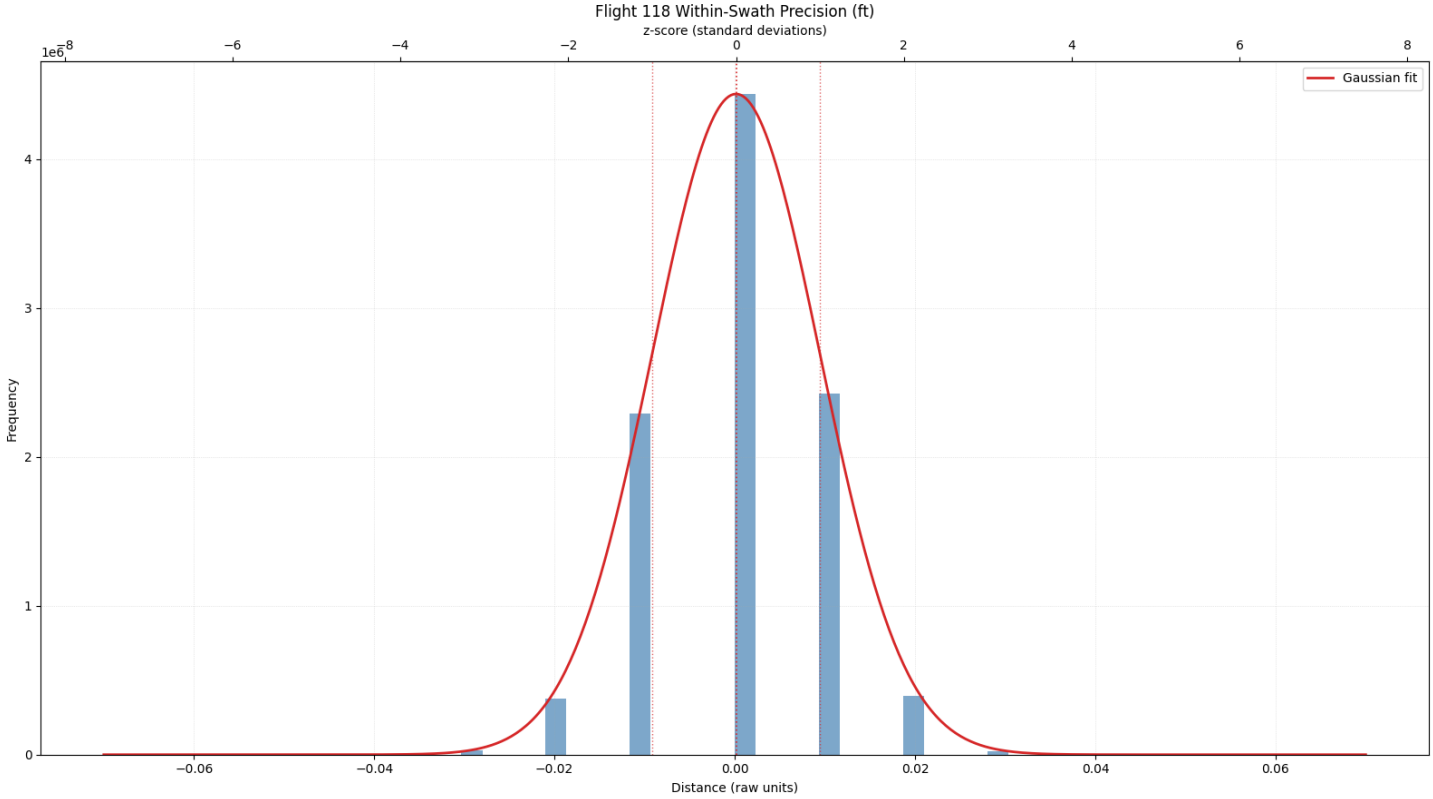
Flight 118 Within-Swath Precision (ft)
z-score (standard deviations)
−8
−6
−4
−2
0
2
4
6
8
1e6
Gaussian fit
Frequency
0
1
2
3
4
−0.06
−0.04
−0.02
0.00
0.02
0.04
0.06
Distance (raw units)

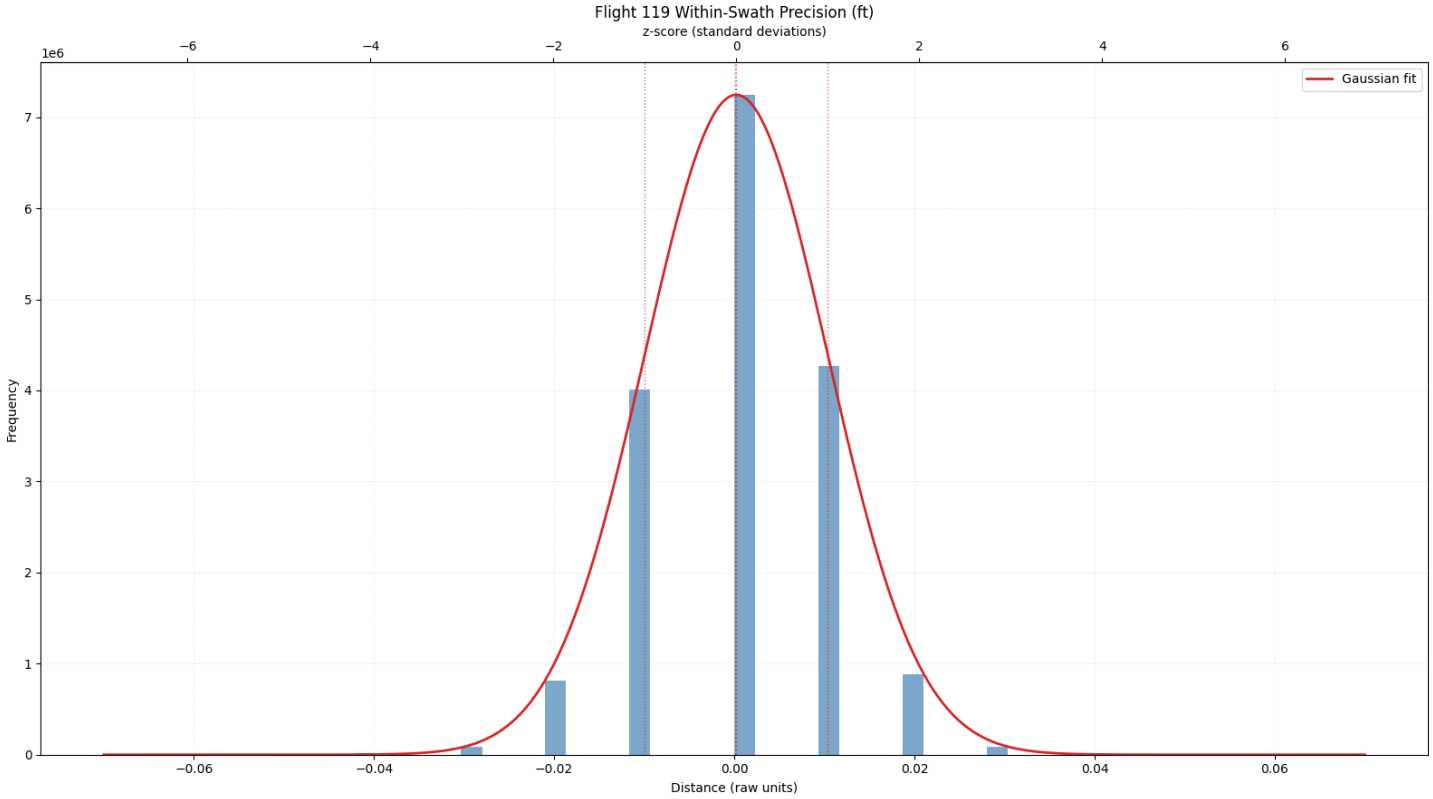
Flight 119 Within-Swath Precision (ft)
z-score (standard deviations)
−6
−4
−2
0
2
4
6
1e6
Gaussian fit
Frequency
0
1
2
3
4
5
6
7
−0.06
−0.04
−0.02
0.00
0.02
0.04
0.06
Distance (raw units)

APPENDIX D

Swath-to-Swath Histograms

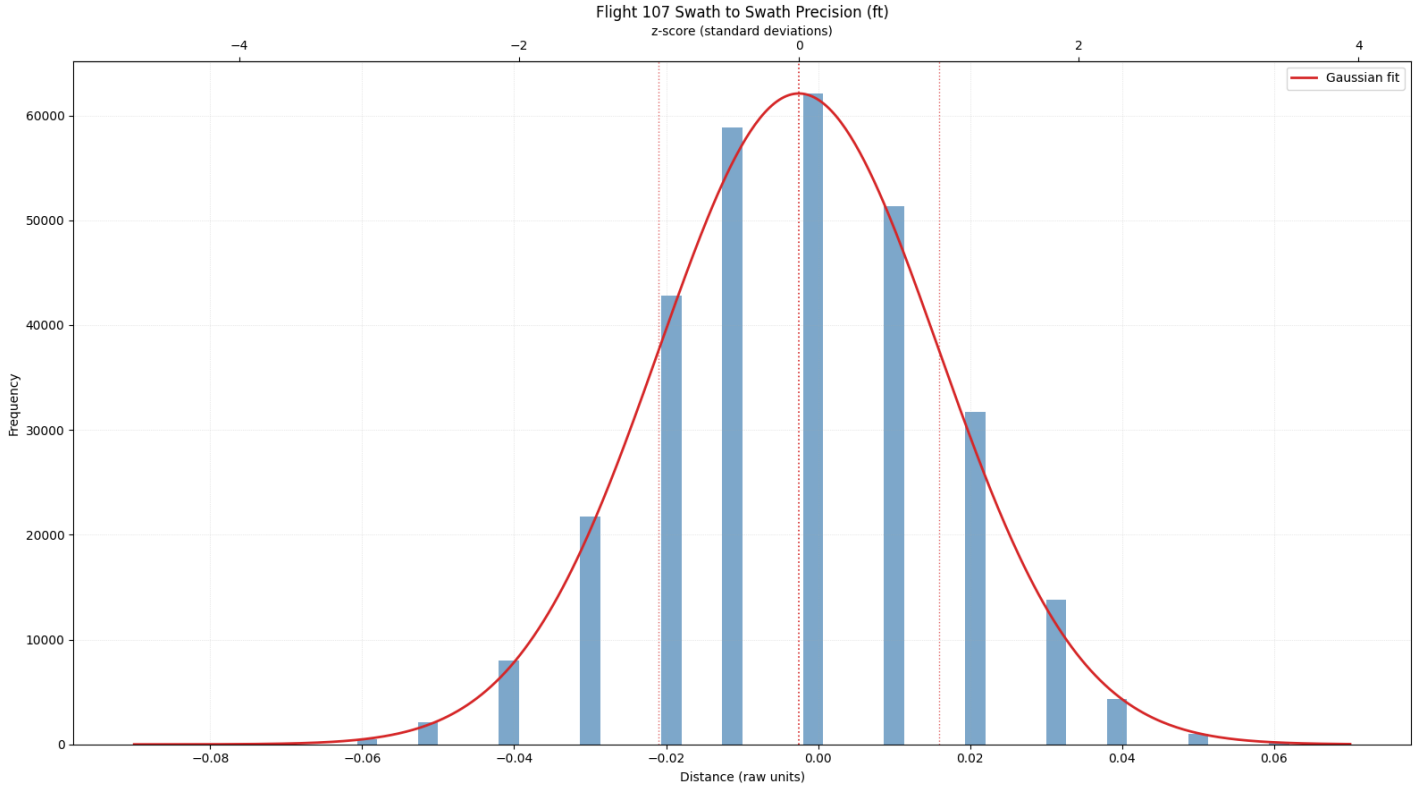
Flight 107 Swath to Swath Precision (ft)
z-score (standard deviations)
−4
−2
0
2
4
Gaussian fit
60000
50000
40000
30000
20000
10000
0
Frequency
−0.08
−0.06
−0.04
−0.02
0.00
0.02
0.04
0.06
Distance (raw units)

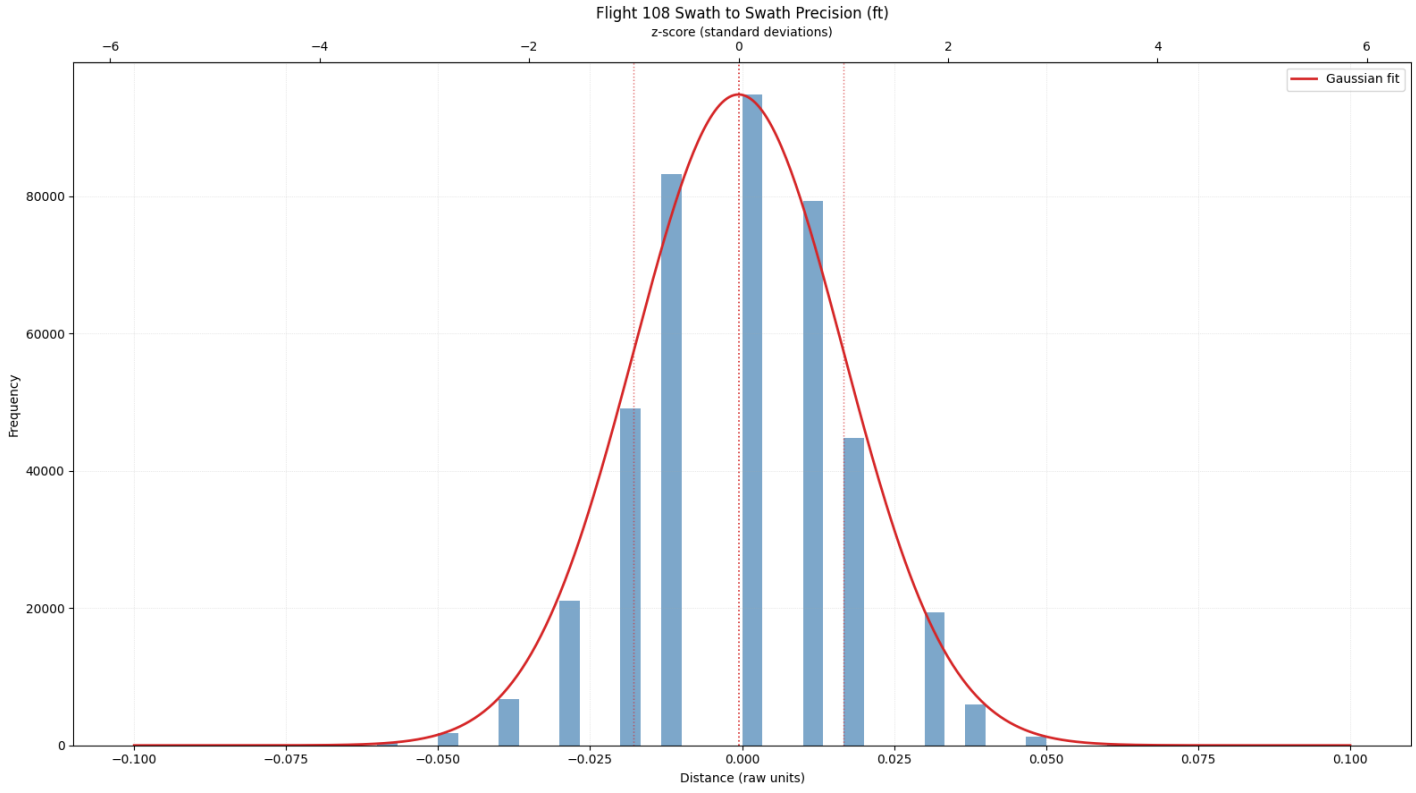
Flight 108 Swath to Swath Precision (ft)
z-score (standard deviations)
−6
−4
−2
0
2
4
6
Gaussian fit
80000
60000
40000
20000
0
Frequency
−0.100
−0.075
−0.050
−0.025
0.000
0.025
0.050
0.075
0.100
Distance (raw units)

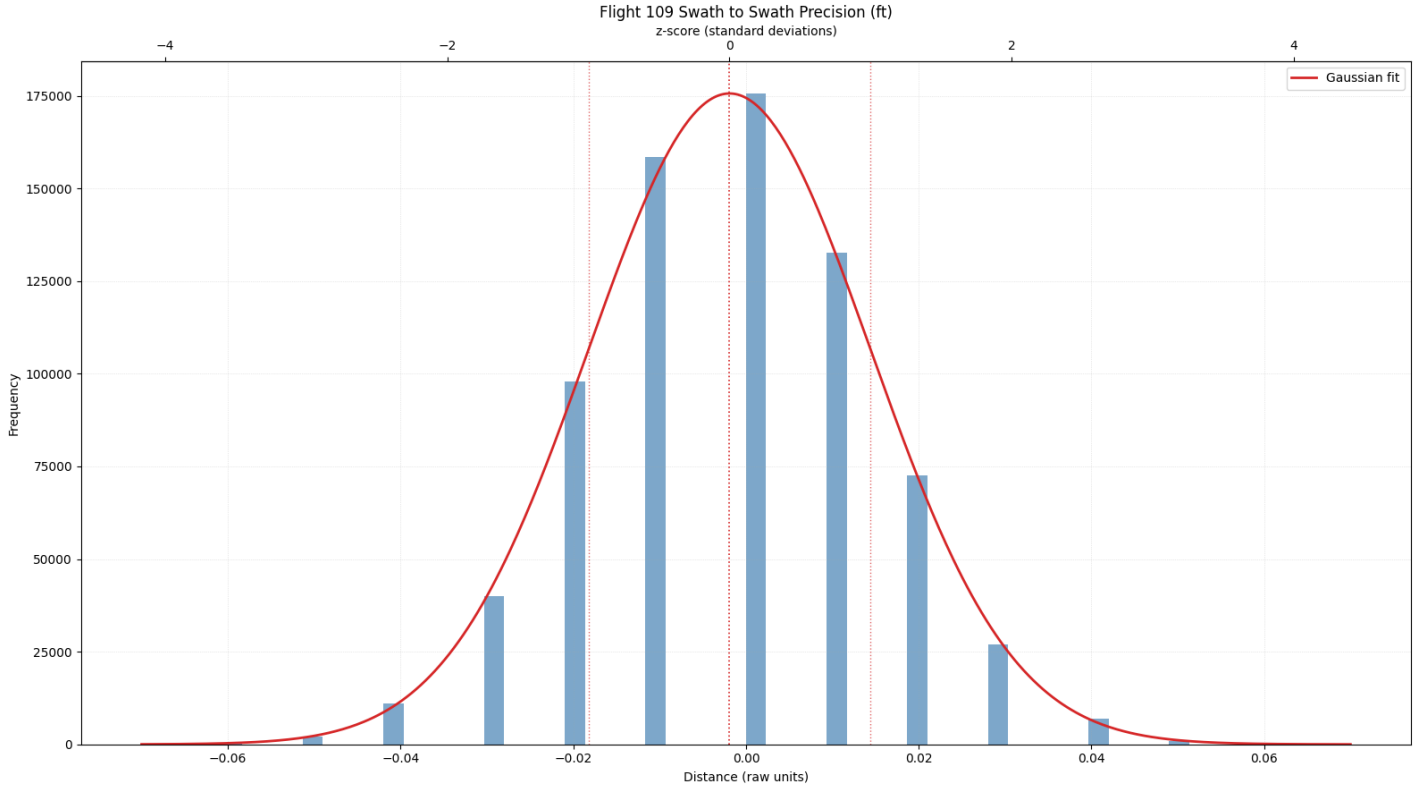
Flight 109 Swath to Swath Precision (ft)
z-score (standard deviations)
−4
−2
0
2
4
Gaussian fit
175000
150000
125000
100000
75000
50000
25000
0
Frequency
−0.06
−0.04
−0.02
0.00
0.02
0.04
0.06
Distance (raw units)

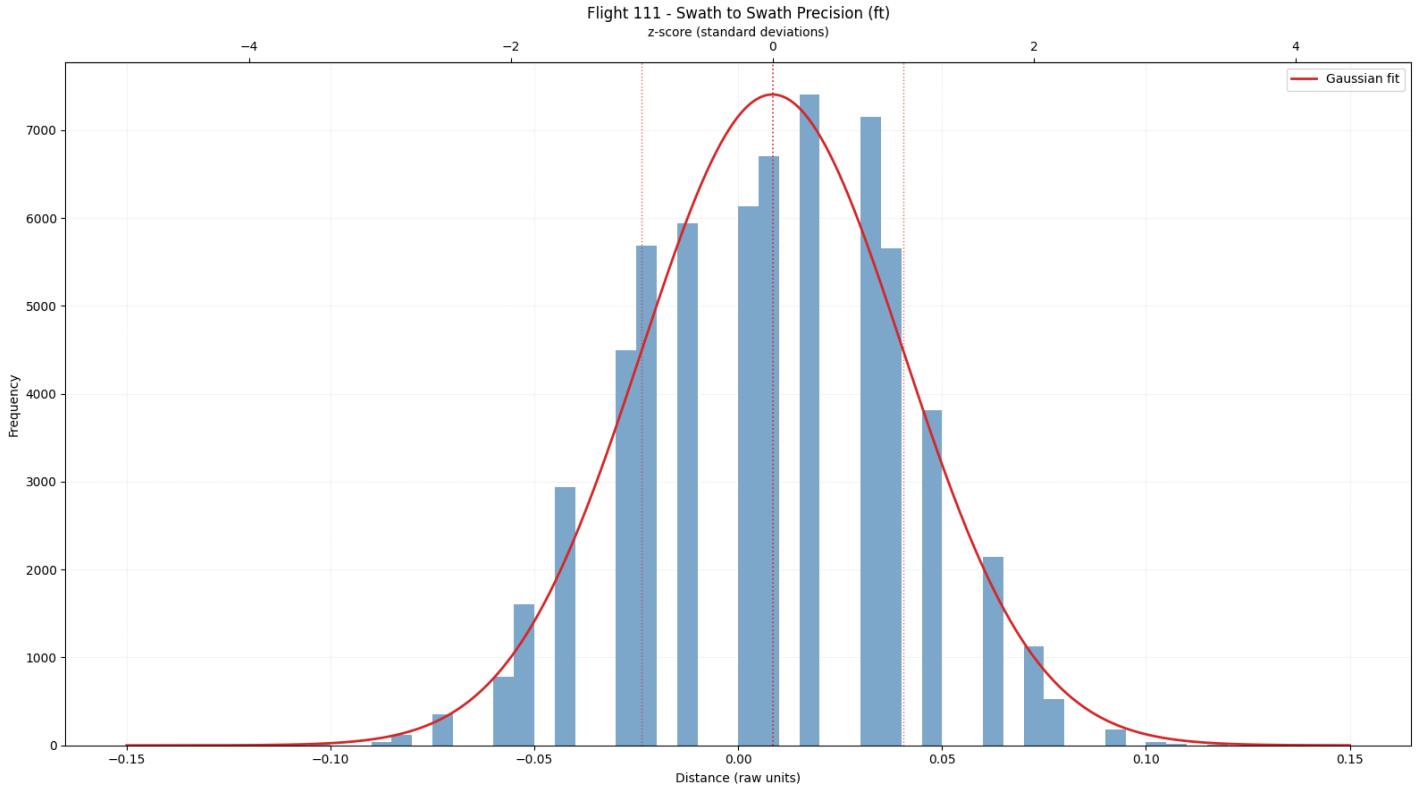
Flight 111 - Swath to Swath Precision (ft)
z-score (standard deviations)
−4
−2
0
2
4
Gaussian fit
7000
6000
5000
4000
3000
2000
1000
0
Frequency
−0.15
−0.10
−0.05
0.00
0.05
0.10
0.15
Distance (raw units)

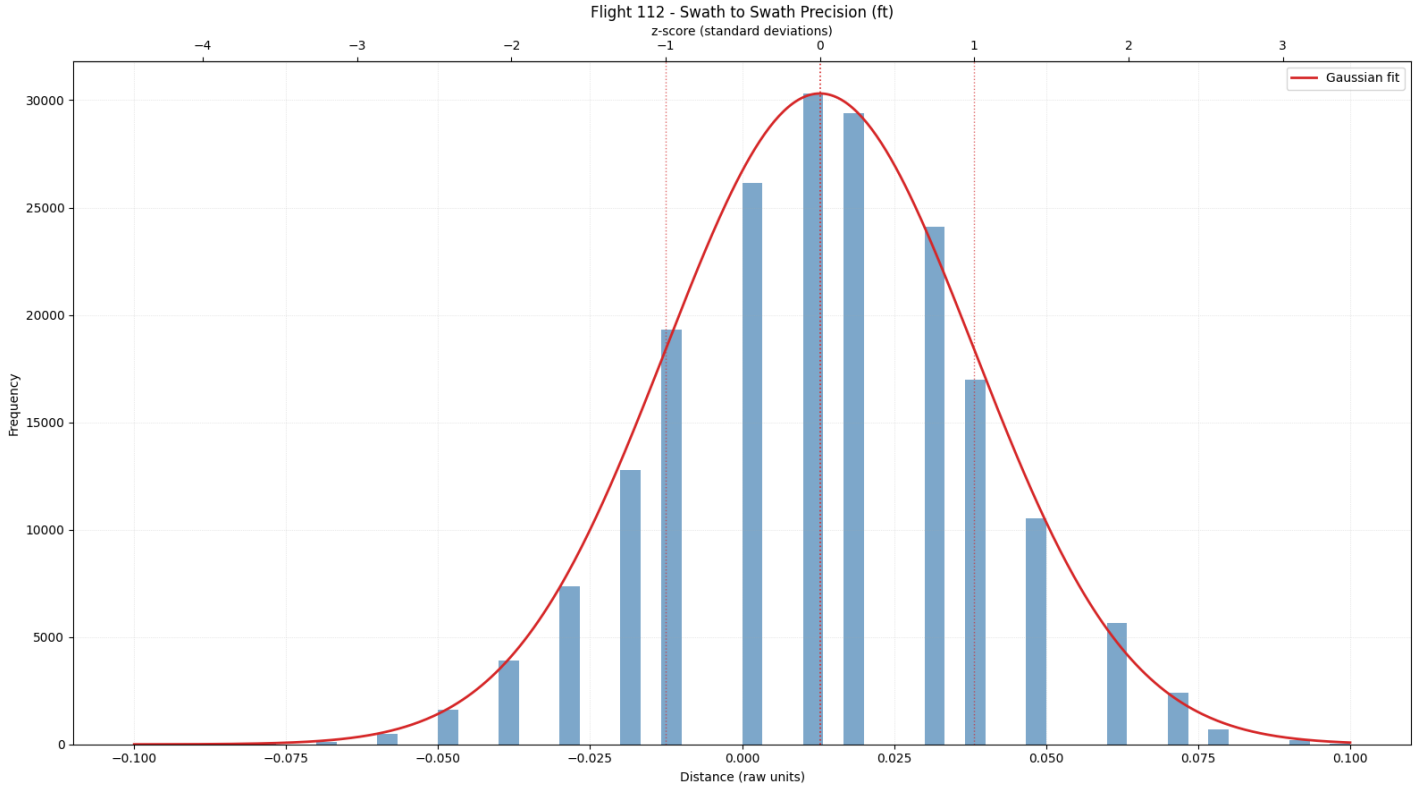
Flight 112 - Swath to Swath Precision (ft)
z-score (standard deviations)
−4
−3
−2
−1
0
1
2
3
Gaussian fit
30000
25000
20000
15000
10000
5000
0
Frequency
−0.100
−0.075
−0.050
−0.025
0.000
0.025
0.050
0.075
0.100
Distance (raw units)

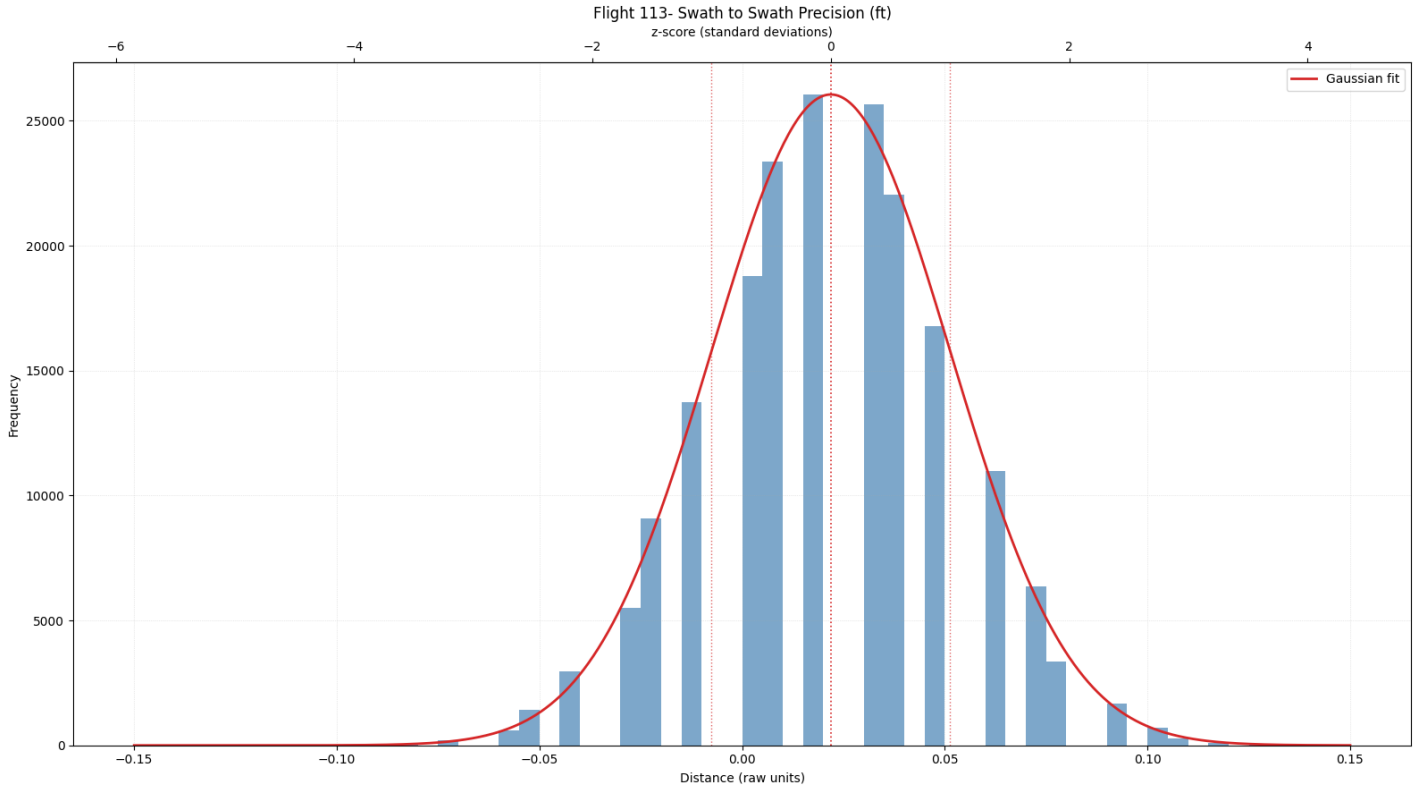
Flight 113- Swath to Swath Precision (ft)
z-score (standard deviations)
−6
−4
−2
0
2
4
Gaussian fit
25000
20000
15000
10000
5000
0
Frequency
−0.15
−0.10
−0.05
0.00
0.05
0.10
0.15
Distance (raw units)

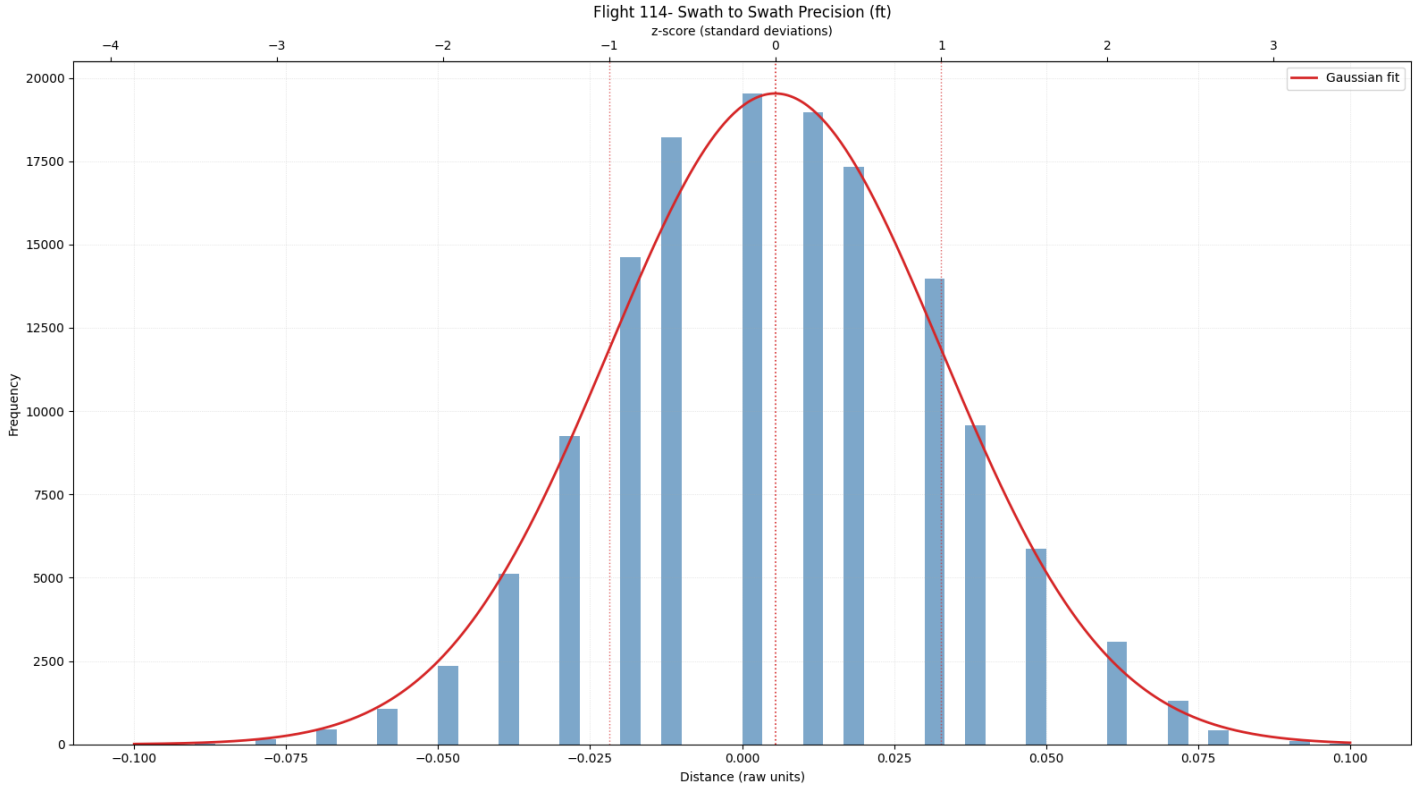
Flight 114- Swath to Swath Precision (ft)
z-score (standard deviations)
−4
−3
−2
−1
0
1
2
3
Gaussian fit
Frequency
20000
17500
15000
12500
10000
7500
5000
2500
0
−0.100
−0.075
−0.050
−0.025
0.000
0.025
0.050
0.075
0.100
Distance (raw units)

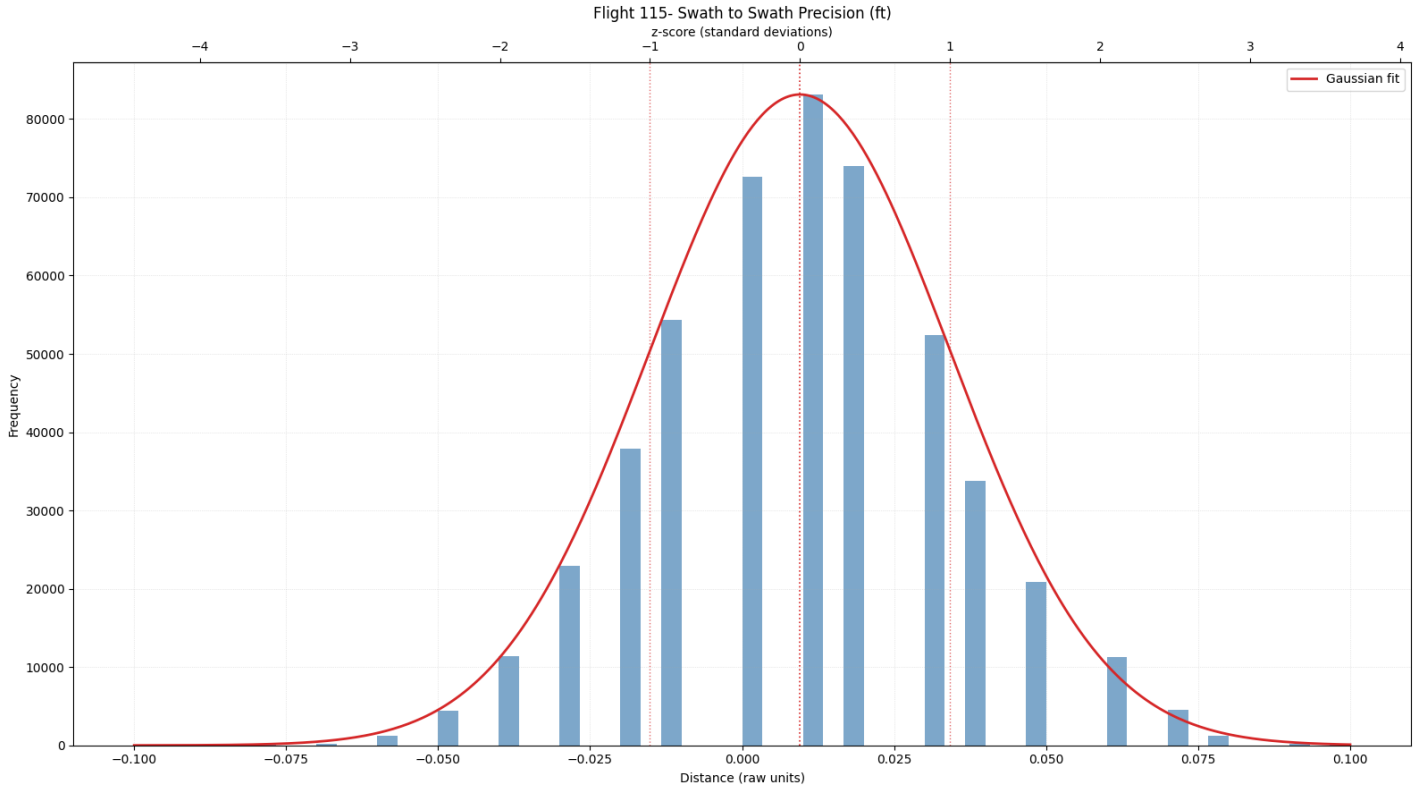
Flight 115- Swath to Swath Precision (ft)
z-score (standard deviations)
−4
−3
−2
−1
0
1
2
3
4
Gaussian fit
Frequency
80000
70000
60000
50000
40000
30000
20000
10000
0
−0.100
−0.075
−0.050
−0.025
0.000
0.025
0.050
0.075
0.100
Distance (raw units)

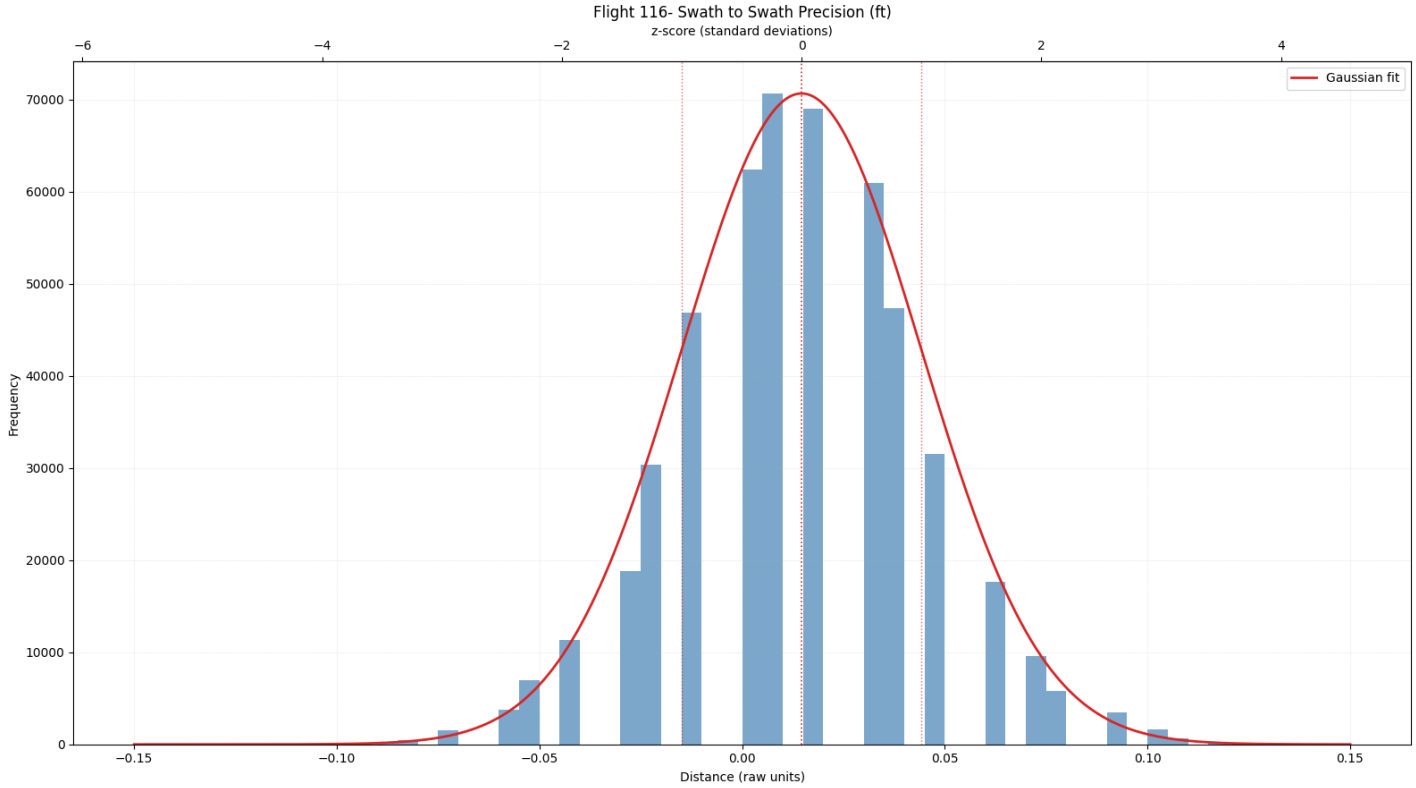
Flight 116- Swath to Swath Precision (ft)
z-score (standard deviations)
−6
−4
−2
0
2
4
Gaussian fit
70000
60000
50000
40000
30000
20000
10000
0
Frequency
−0.15
−0.10
−0.05
0.00
0.05
0.10
0.15
Distance (raw units)

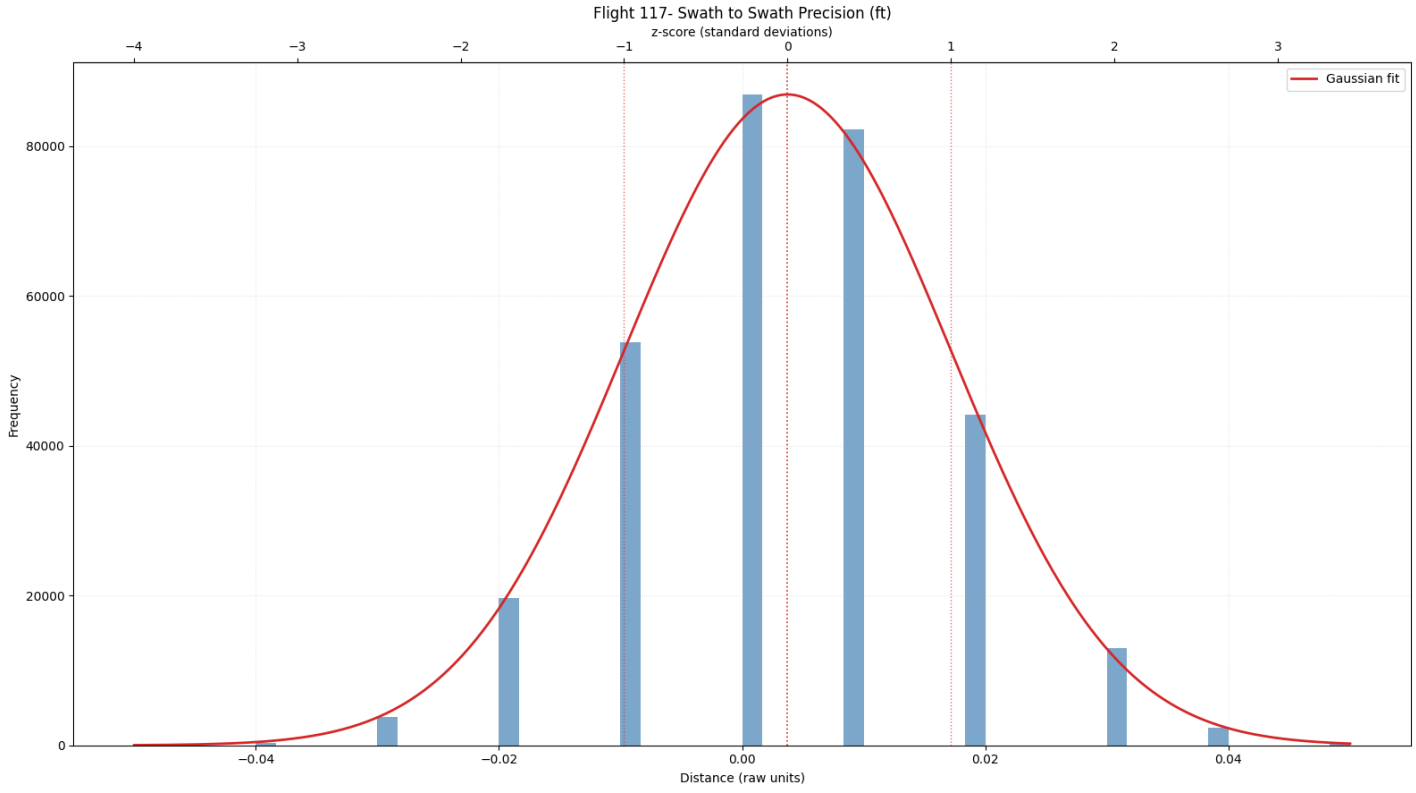
Flight 117- Swath to Swath Precision (ft)
z-score (standard deviations)
−4
−3
−2
−1
0
1
2
3
Gaussian fit
80000
60000
40000
20000
0
Frequency
−0.04
−0.02
0.00
0.02
0.04
Distance (raw units)

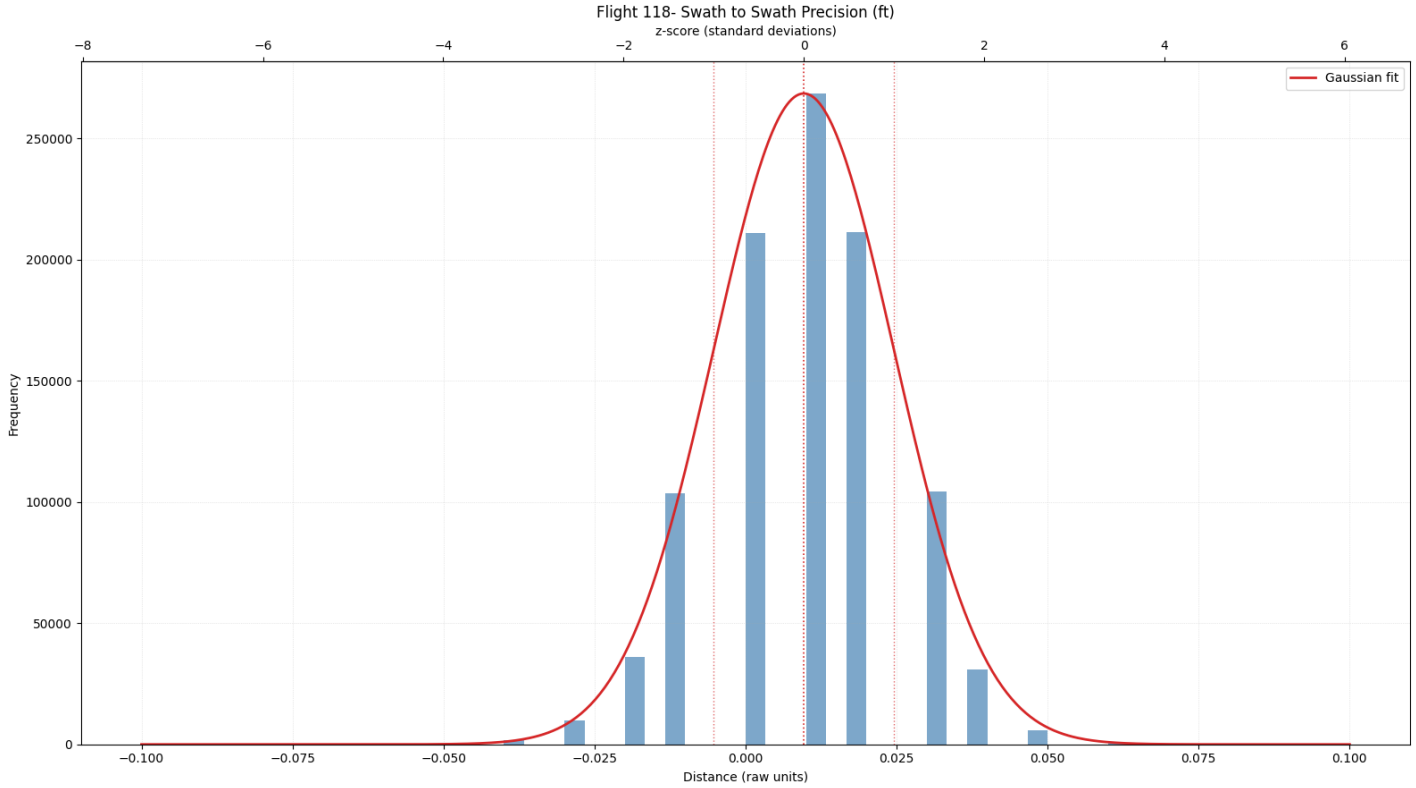
Flight 118- Swath to Swath Precision (ft)
z-score (standard deviations)
−8
−6
−4
−2
0
2
4
6
Gaussian fit
250000
200000
150000
100000
50000
0
Frequency
−0.100
−0.075
−0.050
−0.025
0.000
0.025
0.050
0.075
0.100
Distance (raw units)

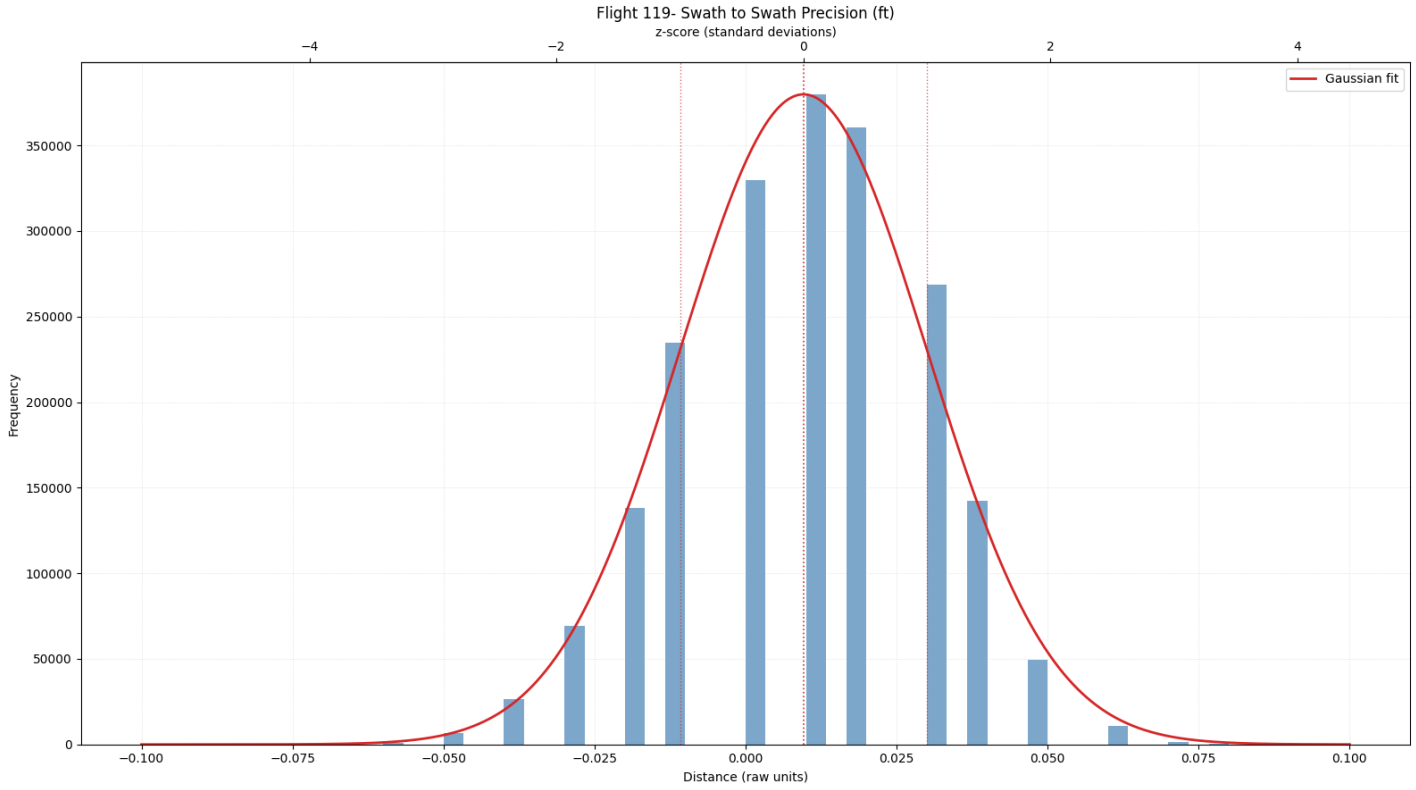
Flight 119- Swath to Swath Precision (ft)
z-score (standard deviations)
−4
−2
0
2
4
Gaussian fit
350000
300000
250000
200000
150000
100000
50000
0
Frequency
−0.100
−0.075
−0.050
−0.025
0.000
0.025
0.050
0.075
0.100
Distance (raw units)

APPENDIX E

Profile Images

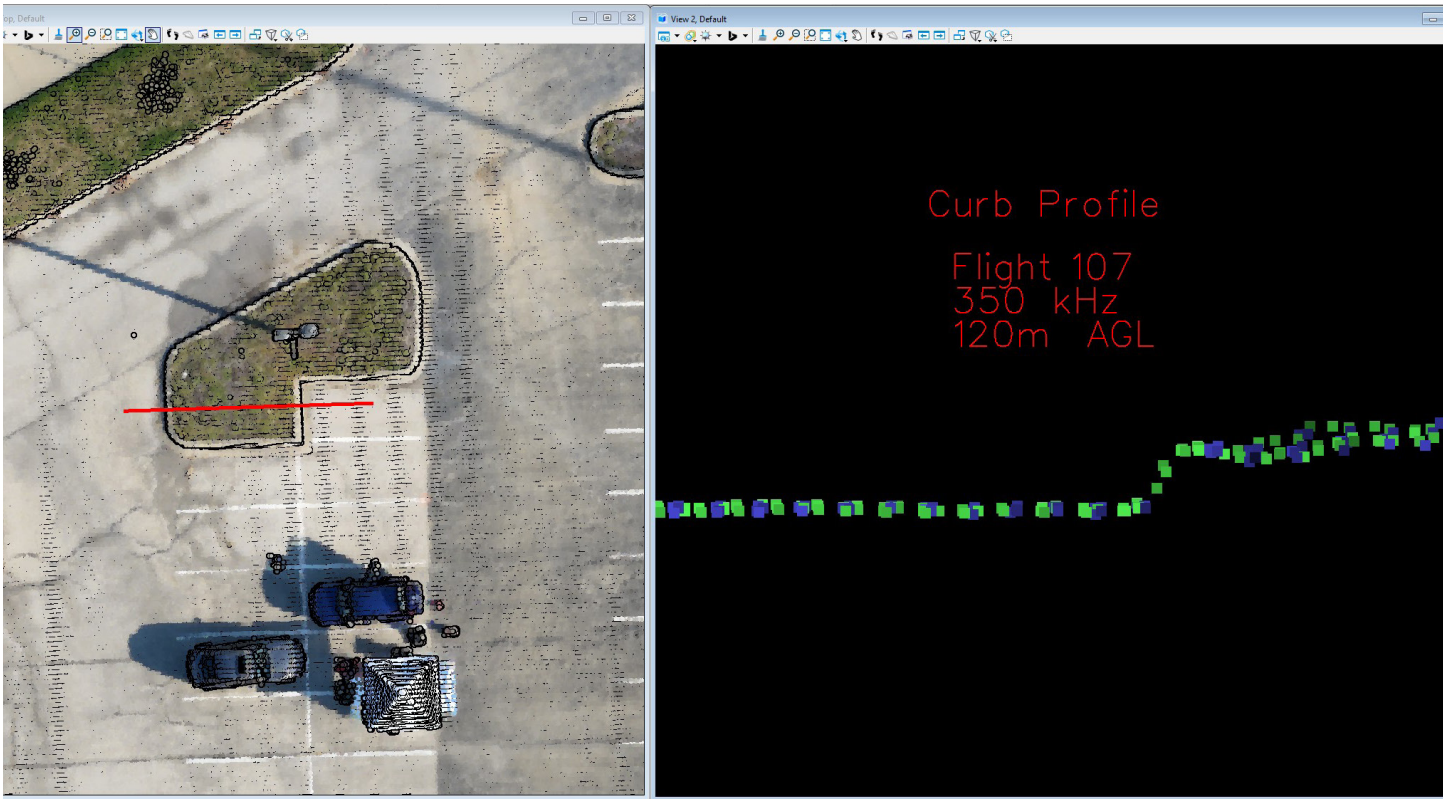
Curb Profile
Flight 107
350 kHz
120m AGL


Curb Profile
Flight 108
350 kHz
90m AGL

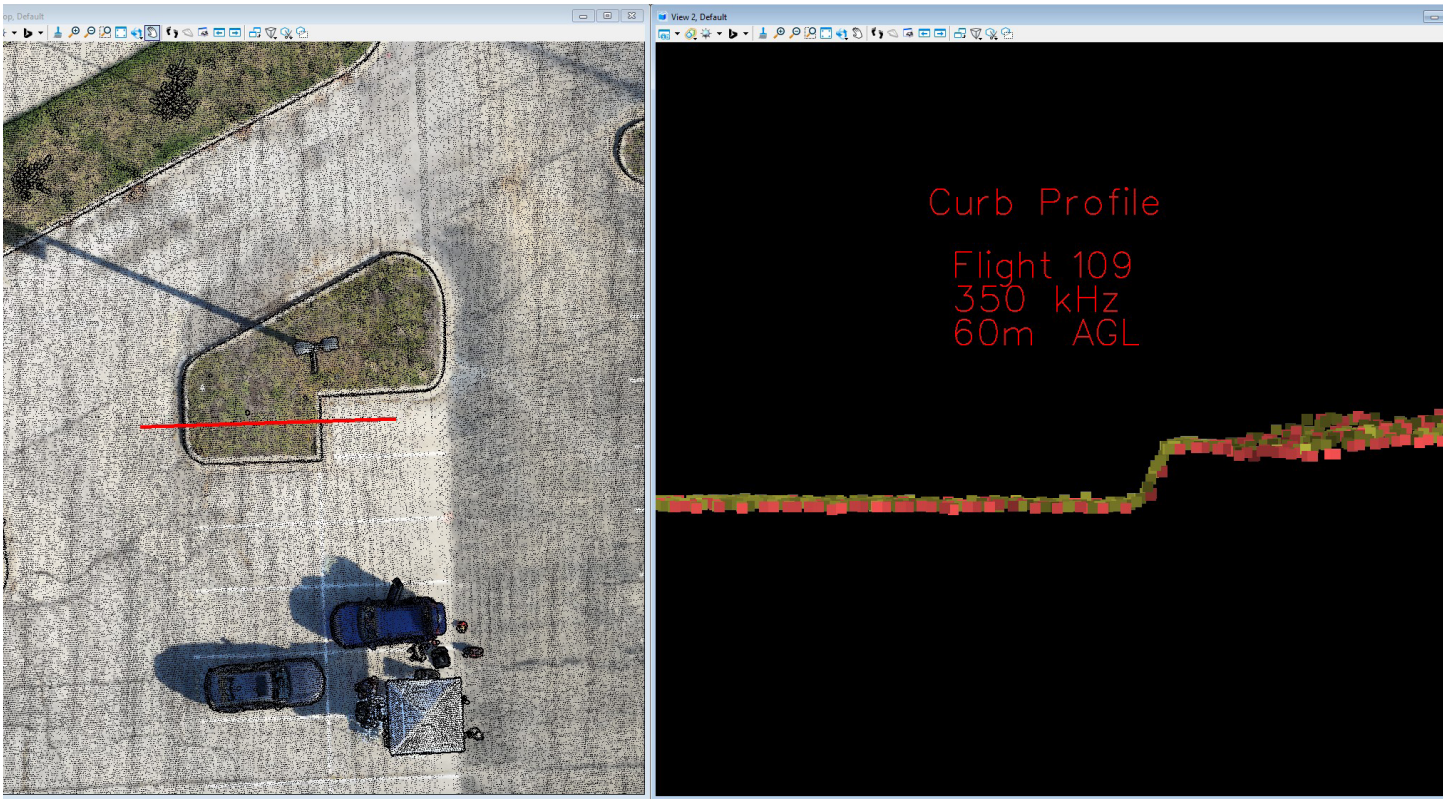
Curb Profile
Flight 109
350 kHz
60m AGL

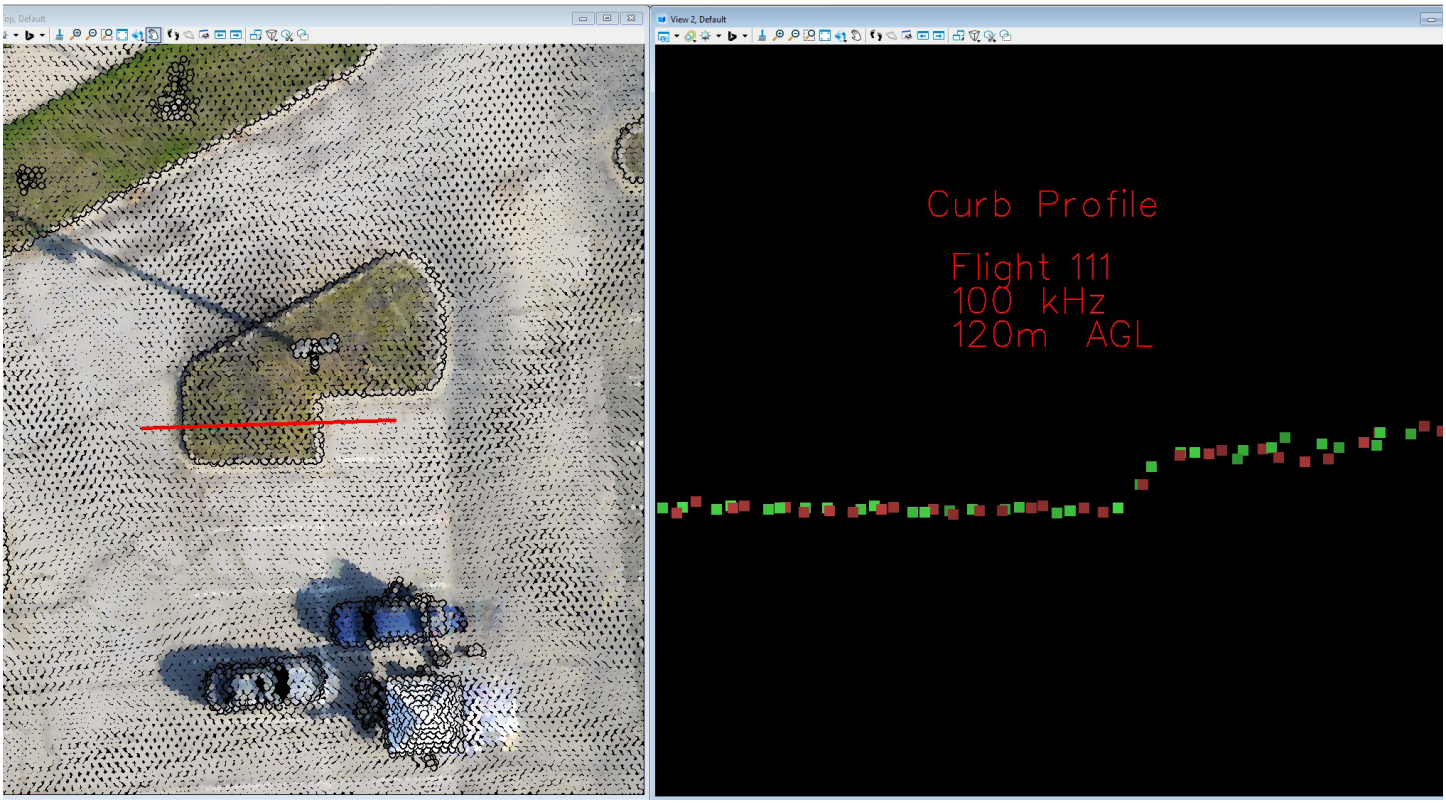
Curb Profile
Flight 111
100 kHz
120m AGL

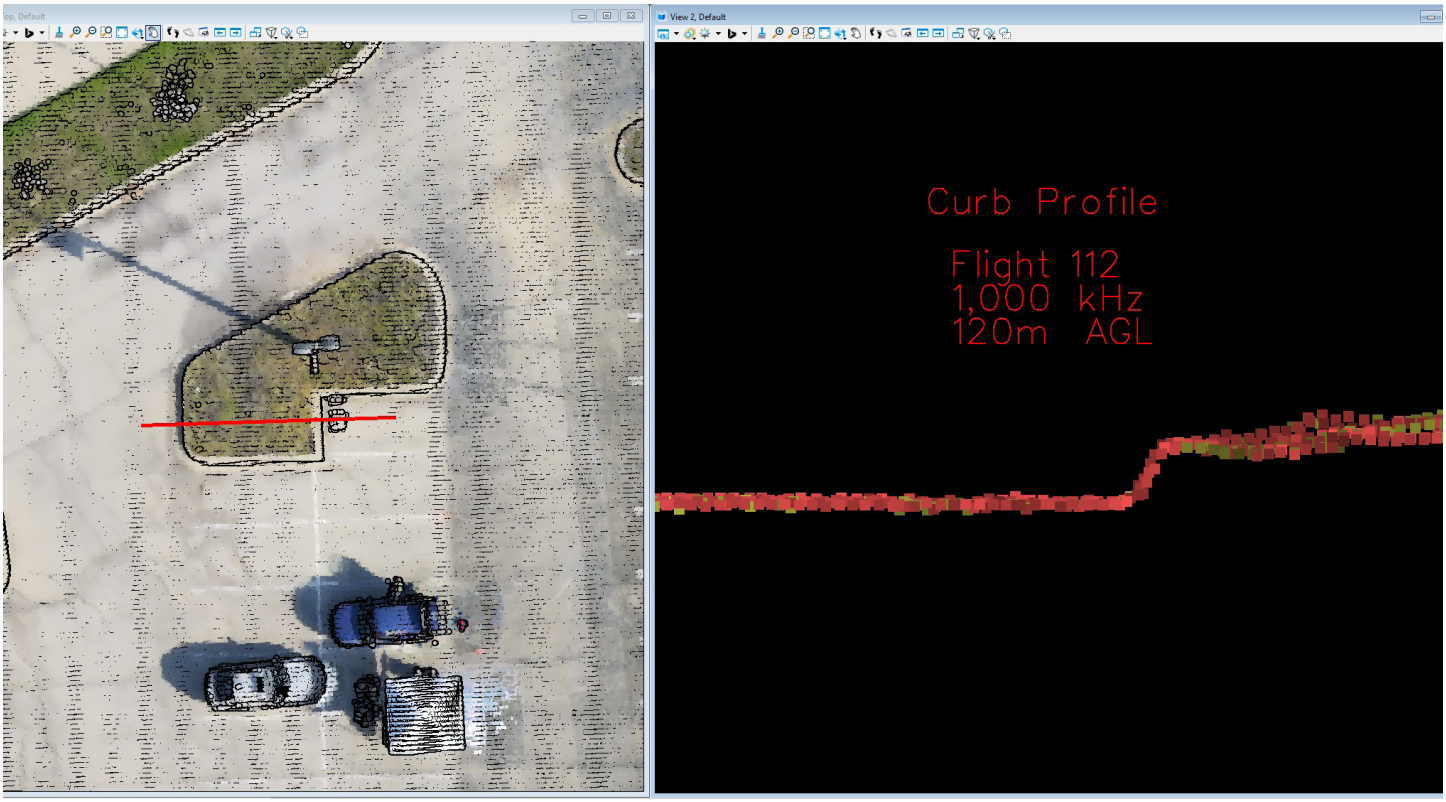
Curb Profile
Flight 112
1,000 kHz
120m AGL

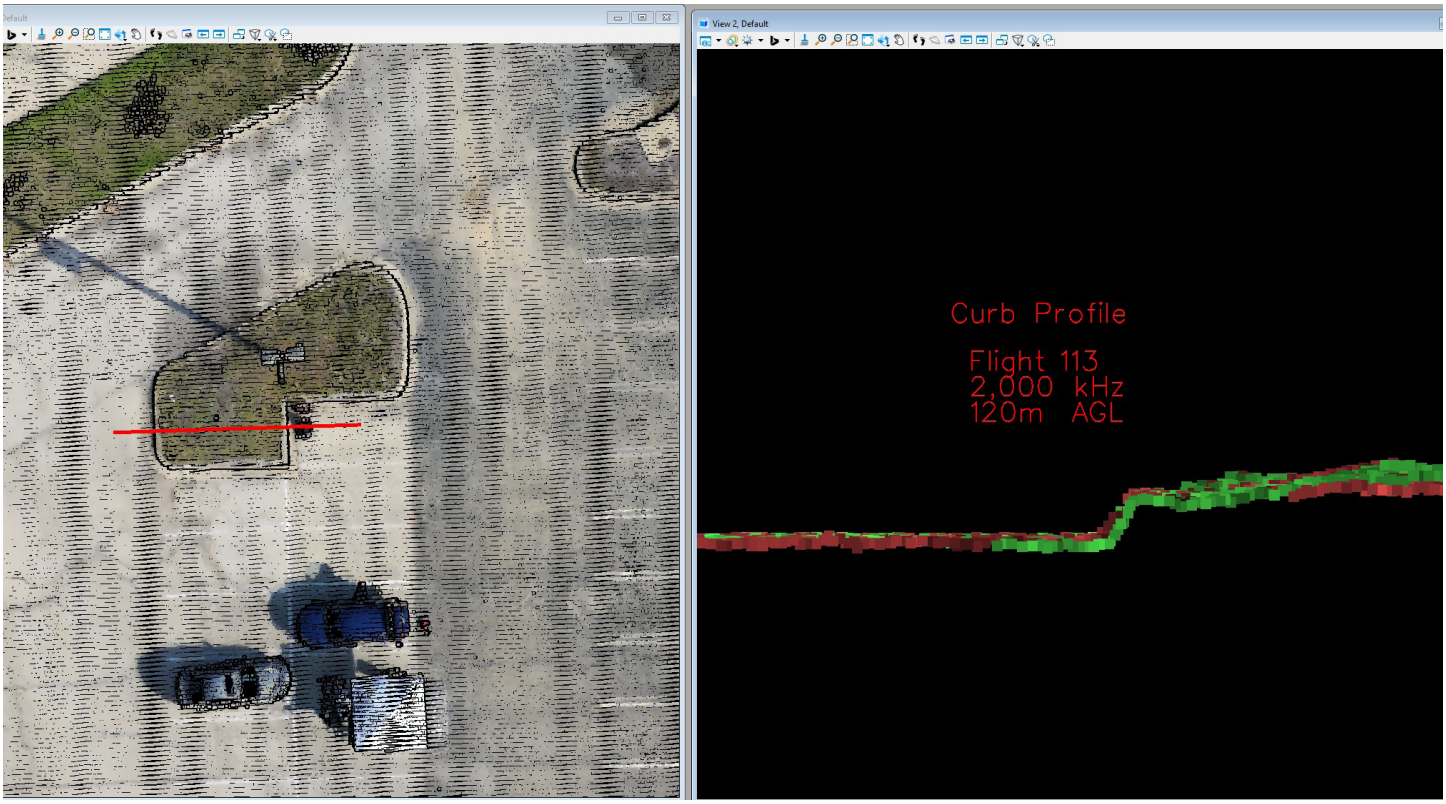
Curb Profile
Flight 113
2,000 kHz
120m AGL

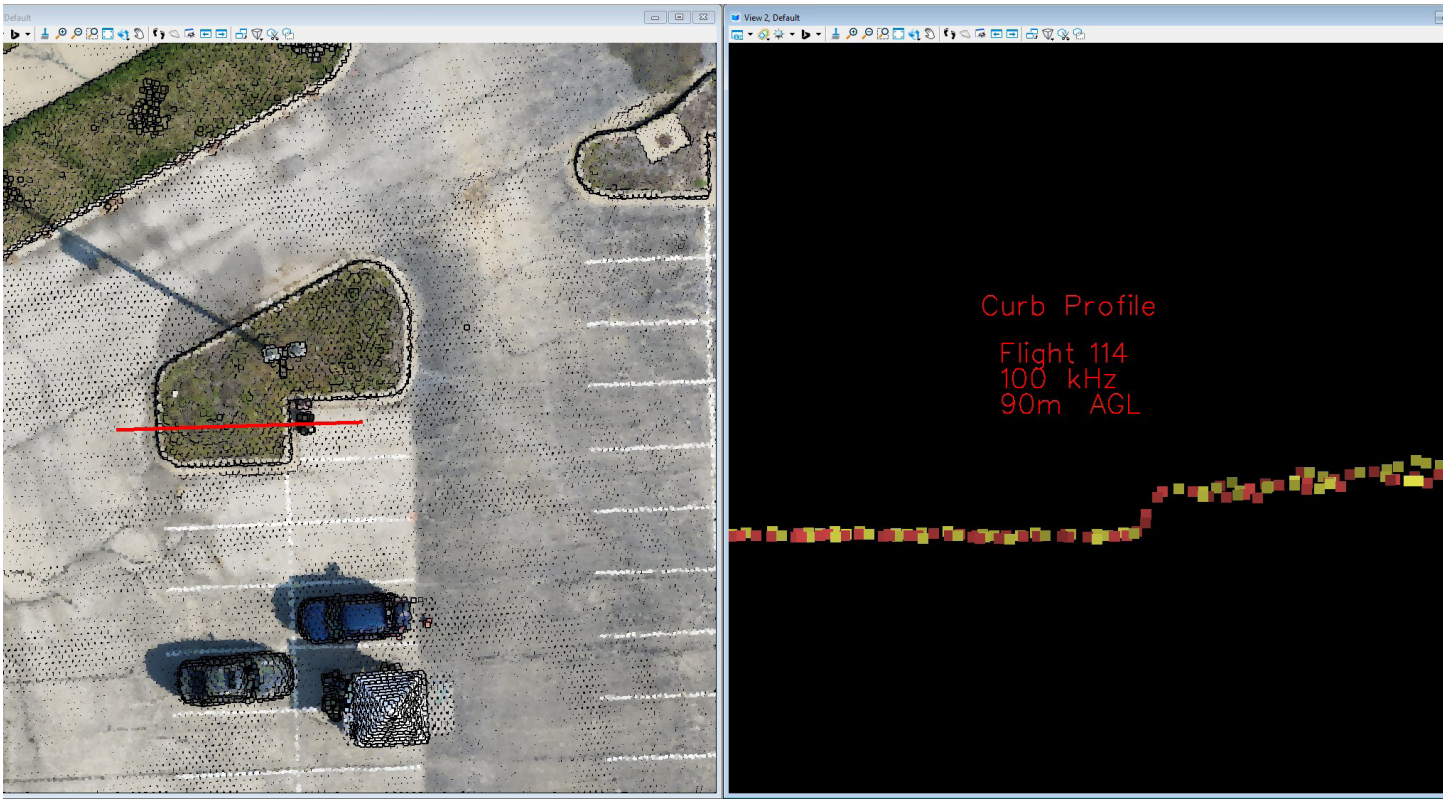
Curb Profile
Flight 114
100 kHz
90m AGL

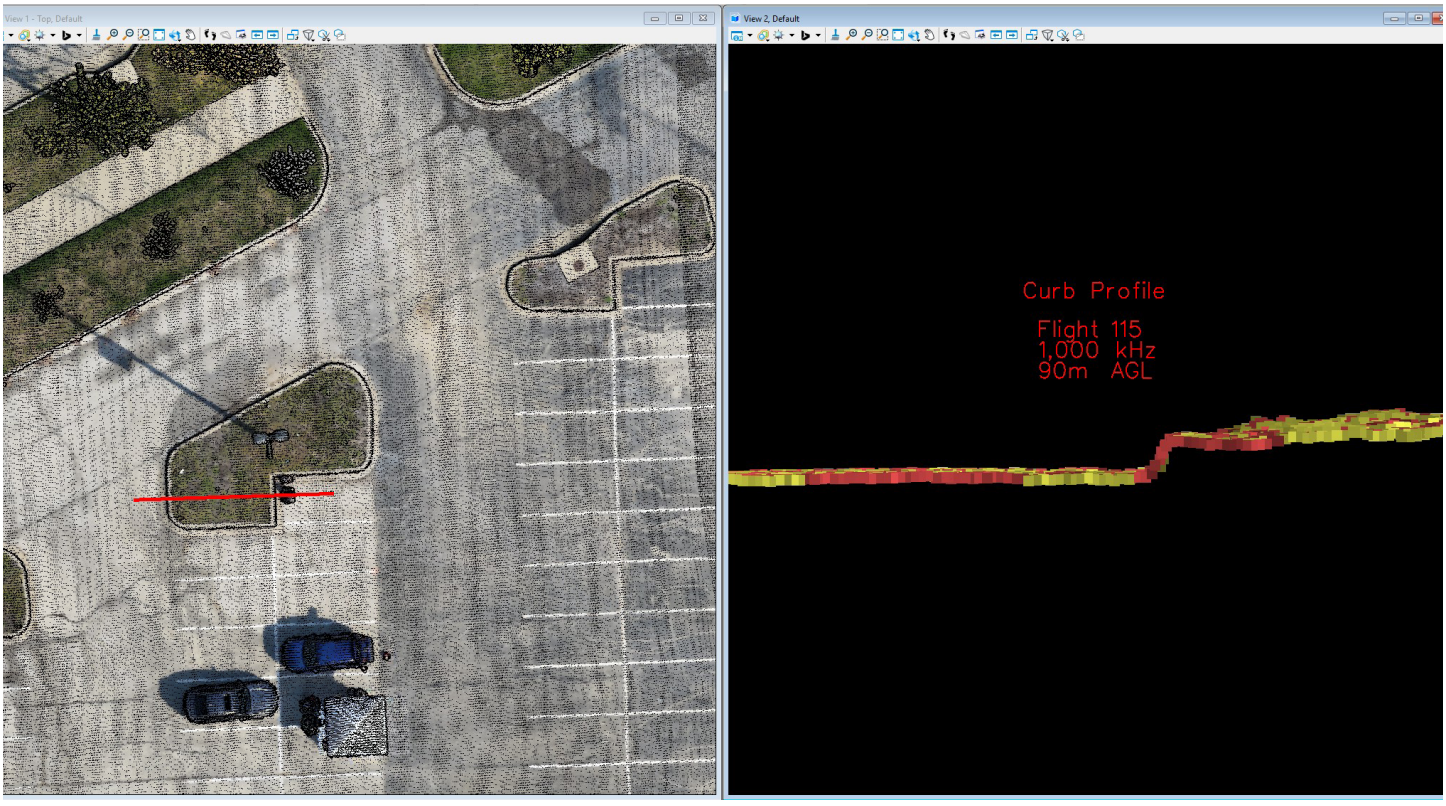
Curb Profile
Flight 115
1,000 kHz
90m AGL


Curb Profile
Flight 116
2,000 kHz
90m AGL


Curb Profile
Flight 117
100 kHz
90m AGL

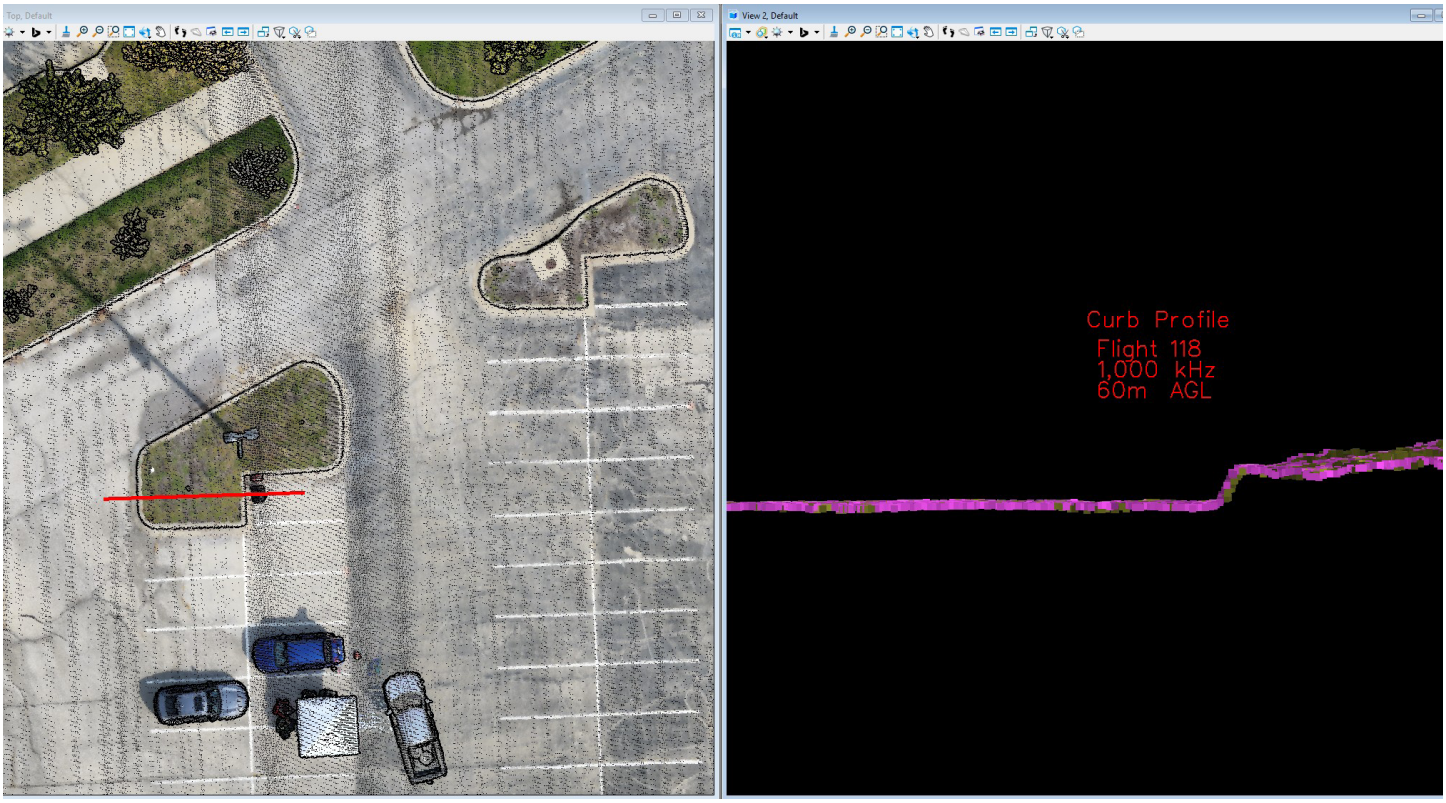
Curb Profile
Flight 118
1,000 kHz
60m AGL

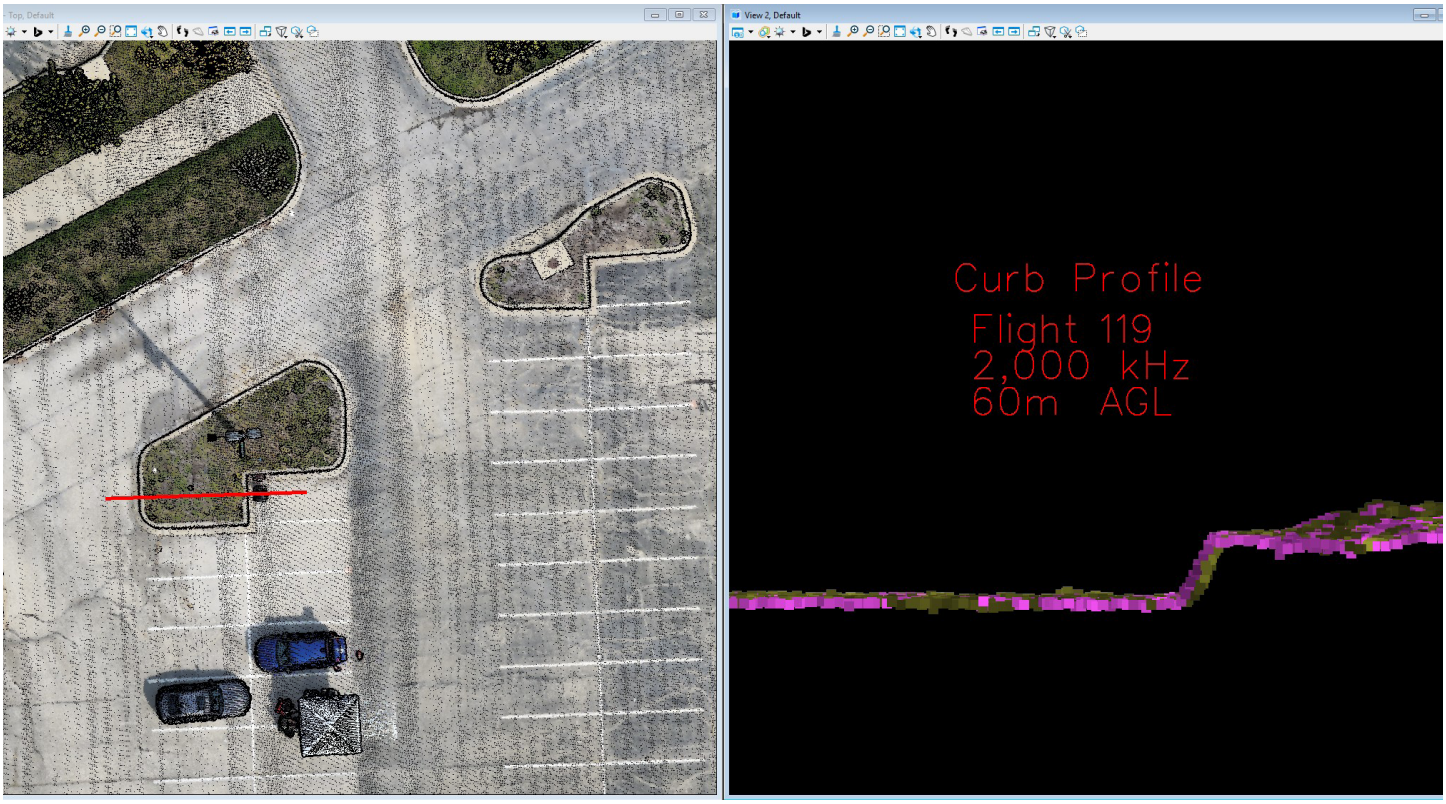
Curb Profile
Flight 119
2,000 kHz
60m AGL

APPENDIX F

Powerline Precision Histograms

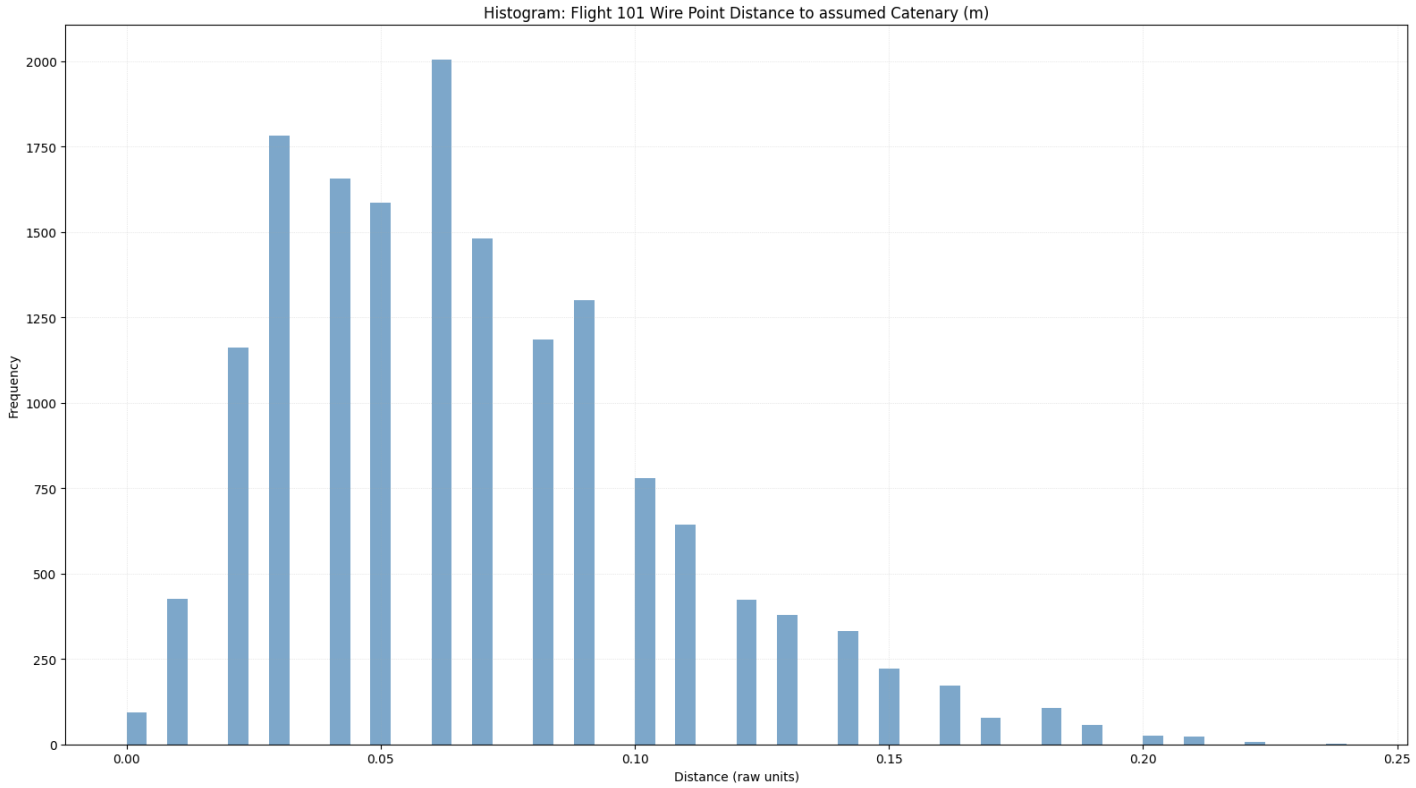
Histogram: Flight 101 Wire Point Distance to assumed Catenary (m)
Frequency
Distance (raw units)
0
250
500
750
1000
1250
1500
1750
2000
0.00
0.05
0.10
0.15
0.20
0.25

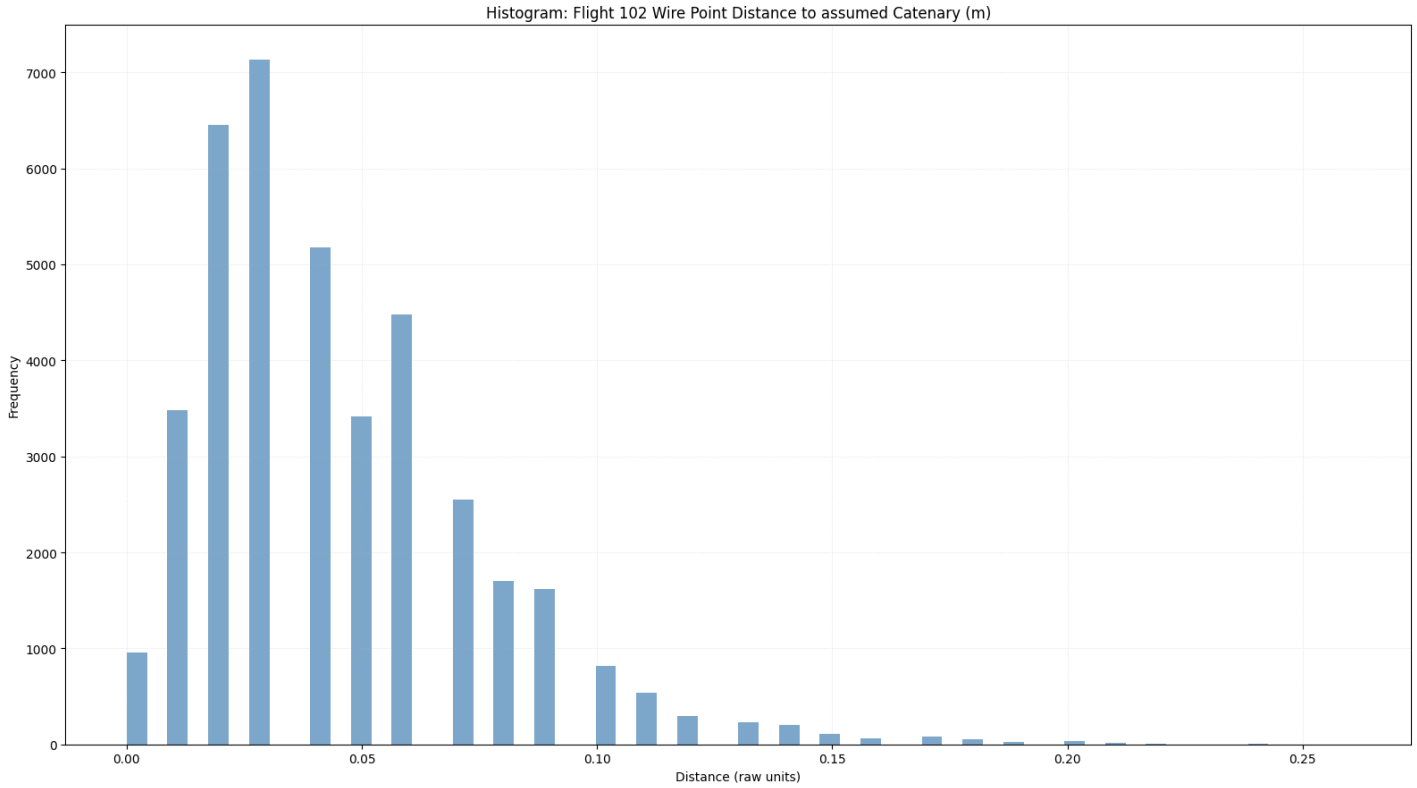
Histogram: Flight 102 Wire Point Distance to assumed Catenary (m)
Frequency
Distance (raw units)
0
1000
2000
3000
4000
5000
6000
7000
0.00
0.05
0.10
0.15
0.20
0.25

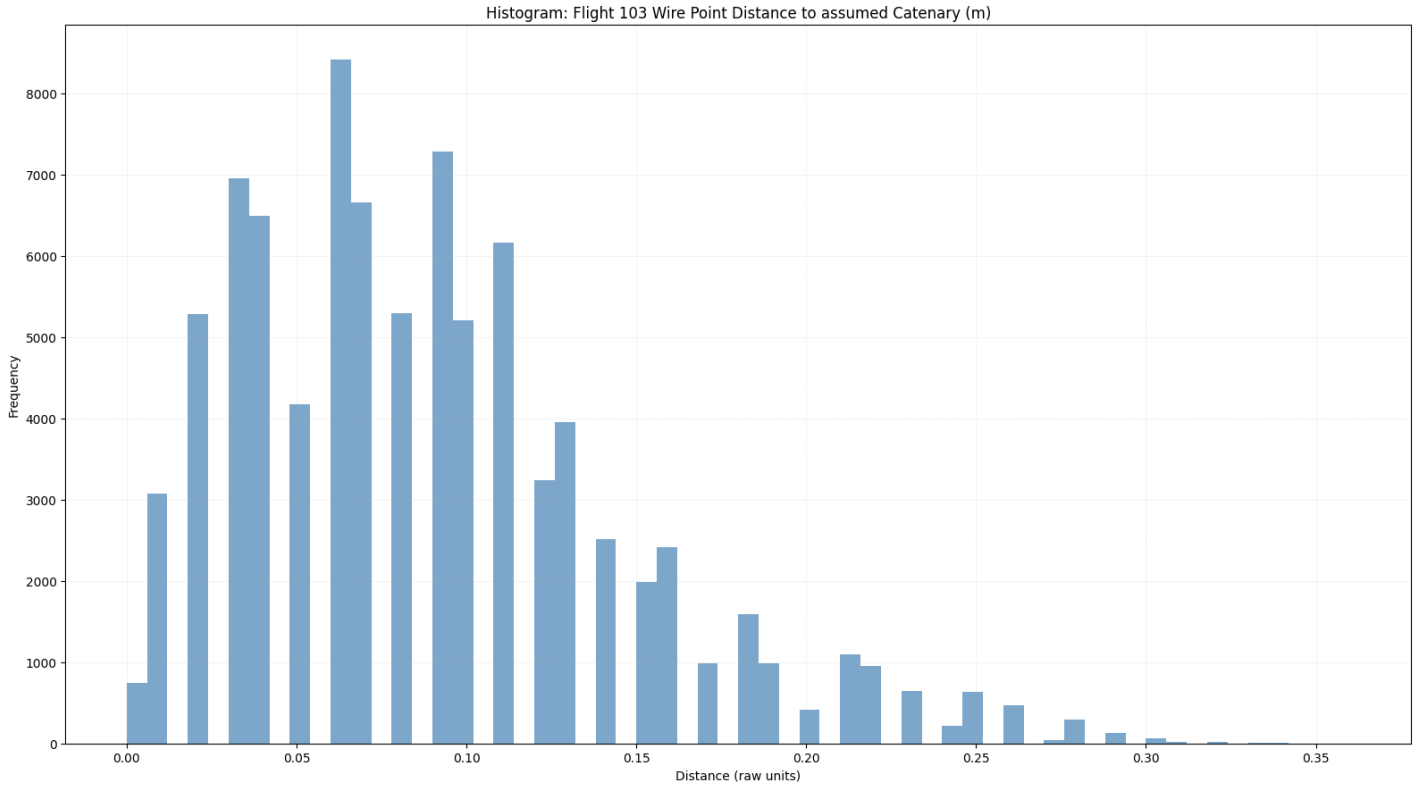
Histogram: Flight 103 Wire Point Distance to assumed Catenary (m)
Frequency
Distance (raw units)
0
1000
2000
3000
4000
5000
6000
7000
8000
0.00
0.05
0.10
0.15
0.20
0.25
0.30
0.35

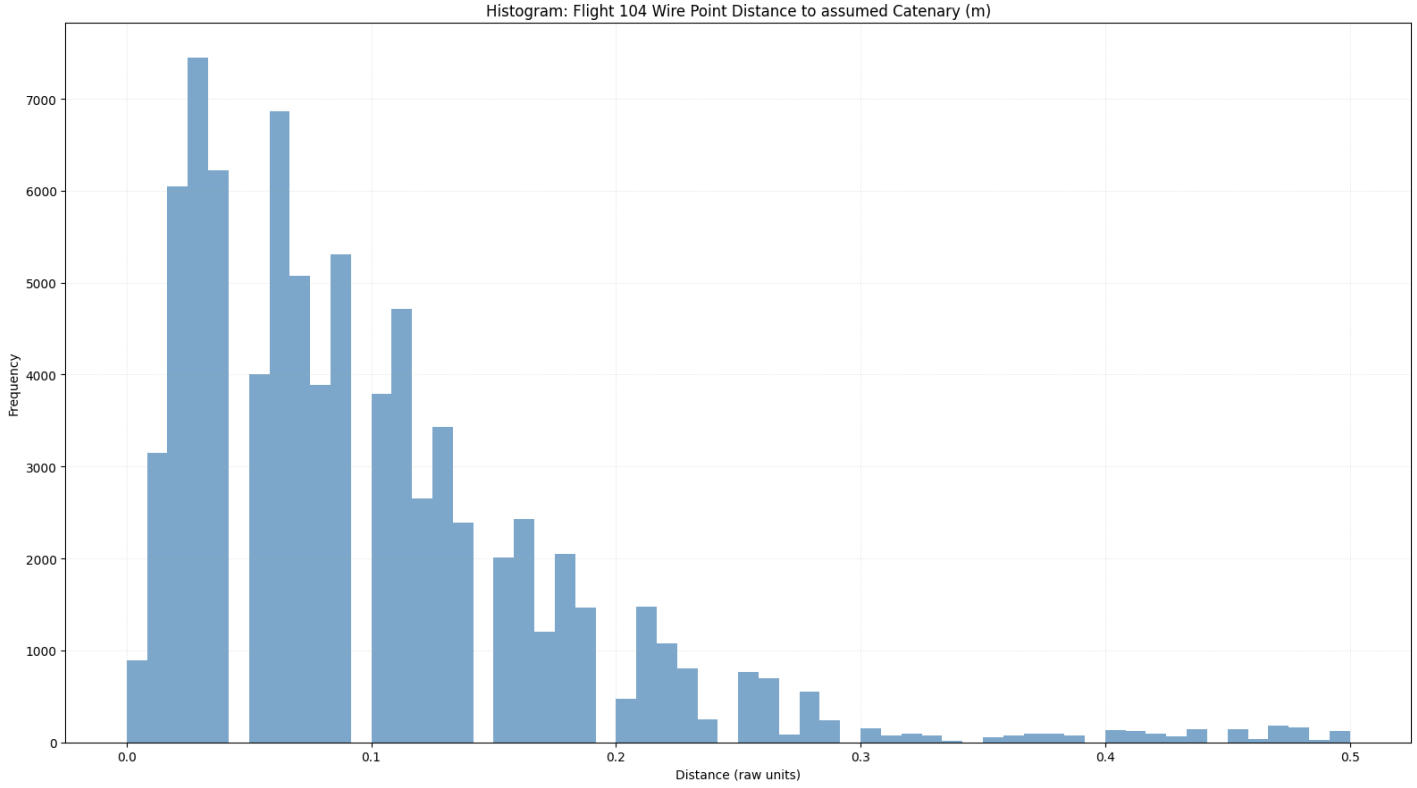
Histogram: Flight 104 Wire Point Distance to assumed Catenary (m)
Frequency
Distance (raw units)
0
1000
2000
3000
4000
5000
6000
7000
0.0
0.1
0.2
0.3
0.4
0.5

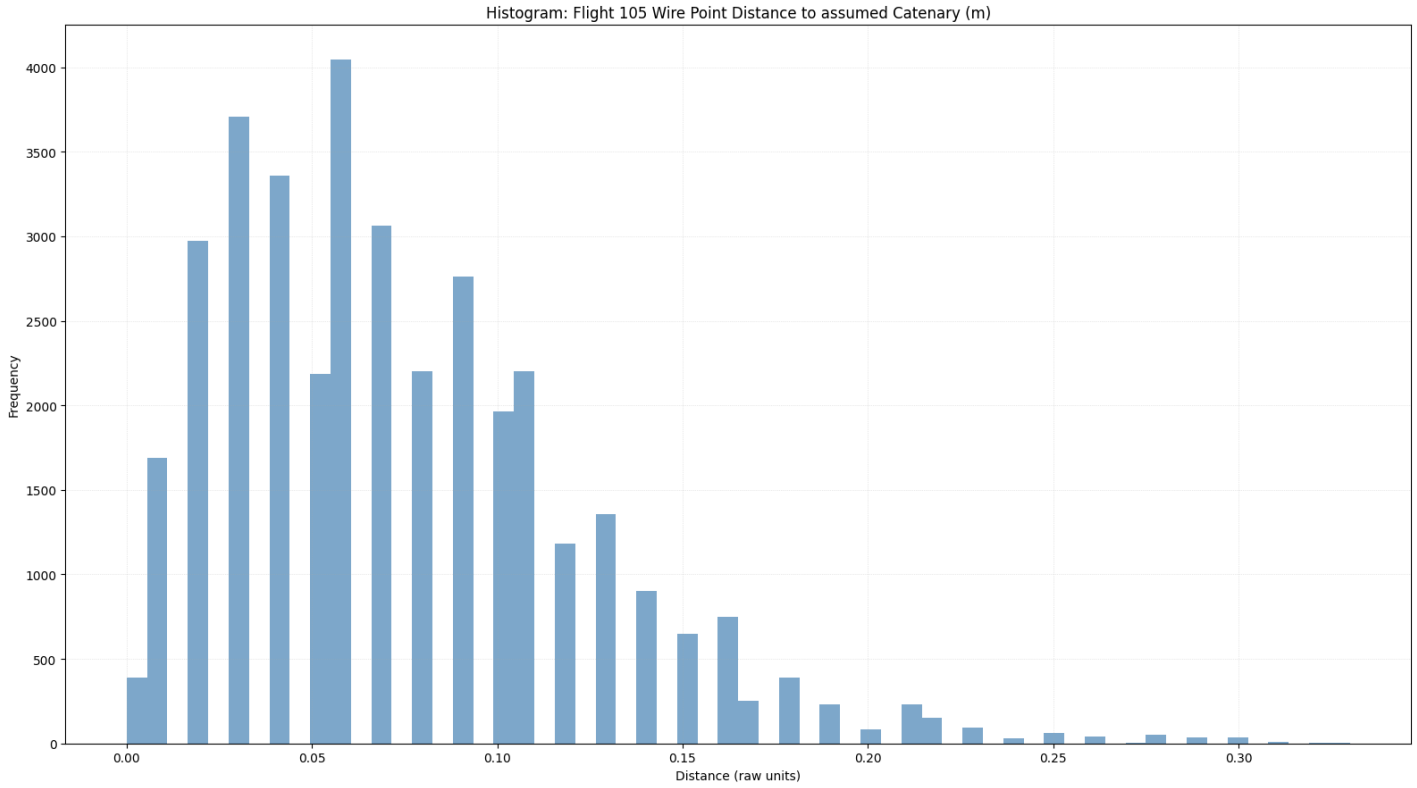
Histogram: Flight 105 Wire Point Distance to assumed Catenary (m)
Frequency
Distance (raw units)
0
500
1000
1500
2000
2500
3000
3500
4000
0.00
0.05
0.10
0.15
0.20
0.25
0.30

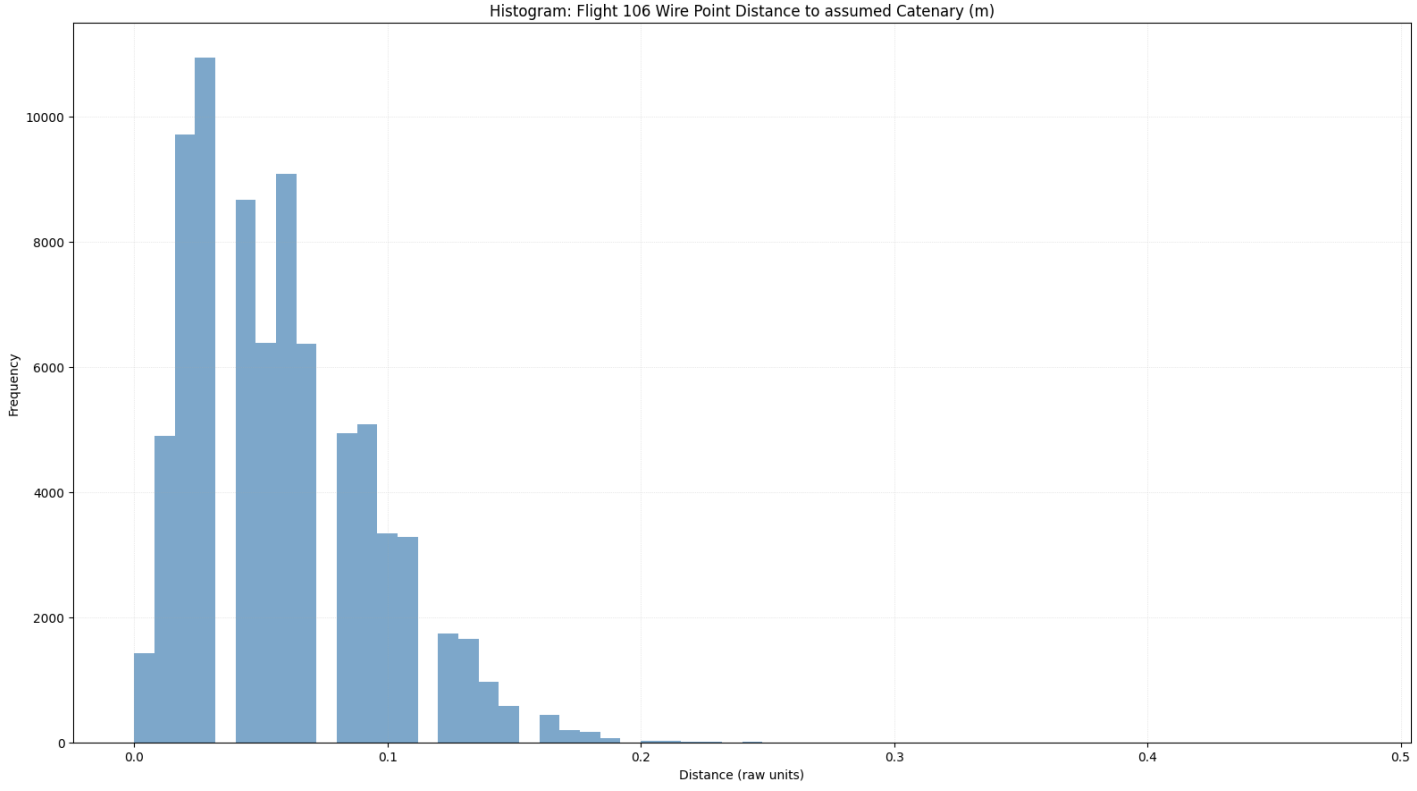
Histogram: Flight 106 Wire Point Distance to assumed Catenary (m)
Frequency
Distance (raw units)
0
2000
4000
6000
8000
10000
0.0
0.1
0.2
0.3
0.4
0.5

APPENDIX G

Powerline Profile Images

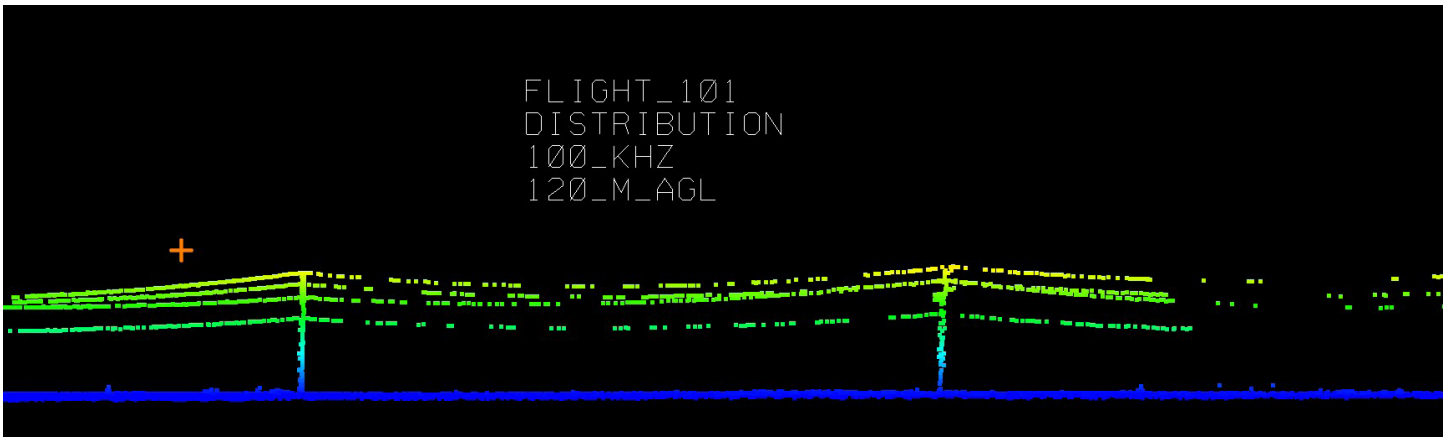
FLIGHT_101
DISTRIBUTION
100_KHZ
120_M_AGL

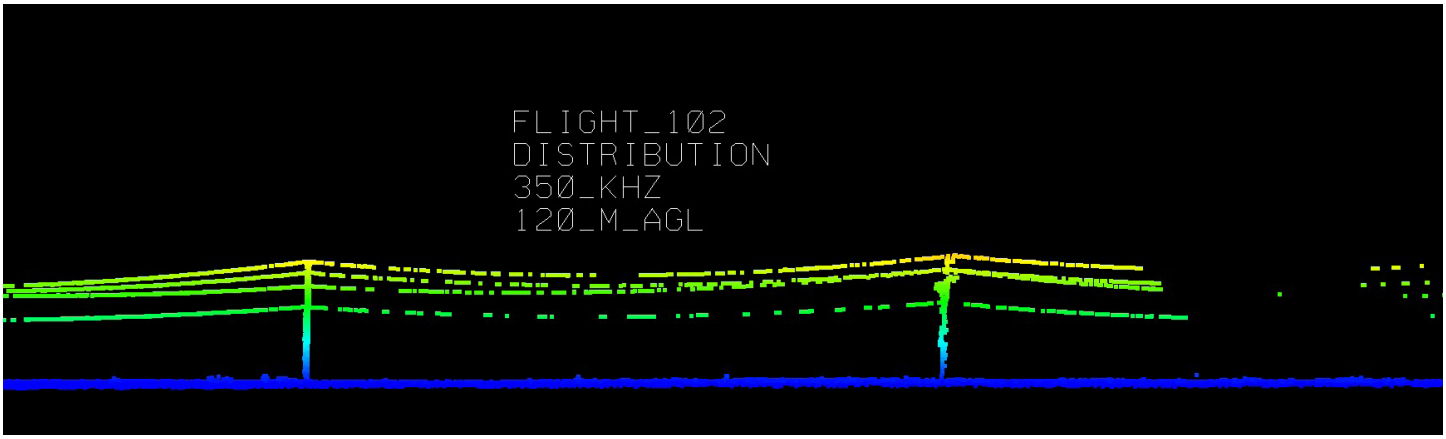
FLIGHT_102
DISTRIBUTION
350_KHZ
120_M_AGL

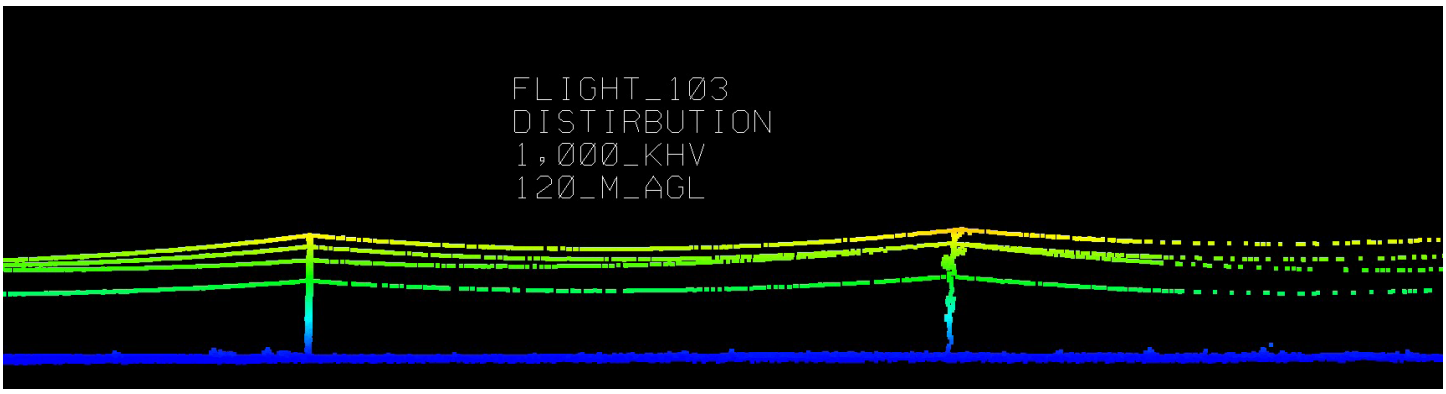
FLIGHT_103
DISTIRBUTION
1,000_KHV
120_M_AGL

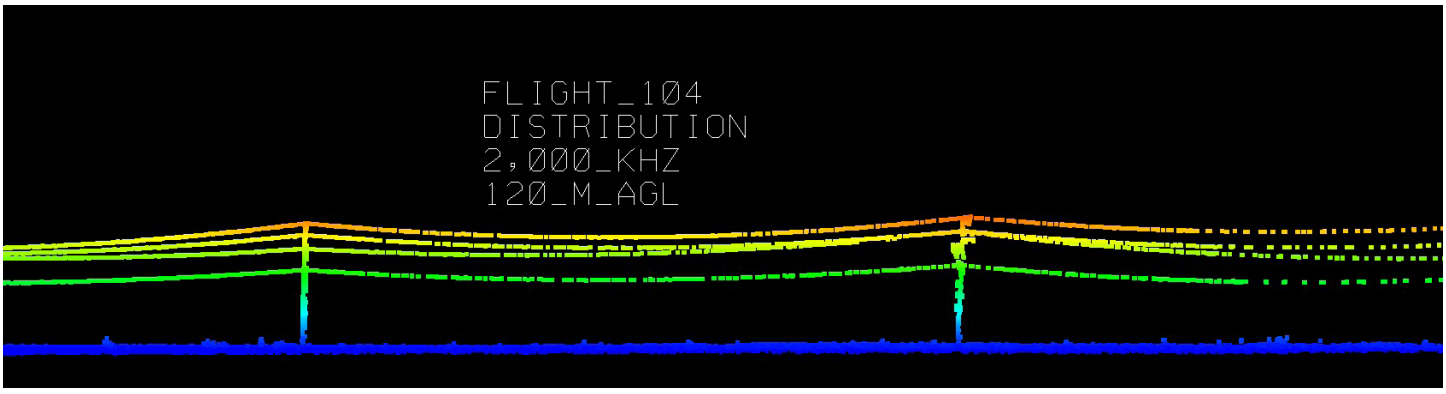
FLIGHT_104
DISTRIBUTION
2,000_KHZ
120_M_AGL

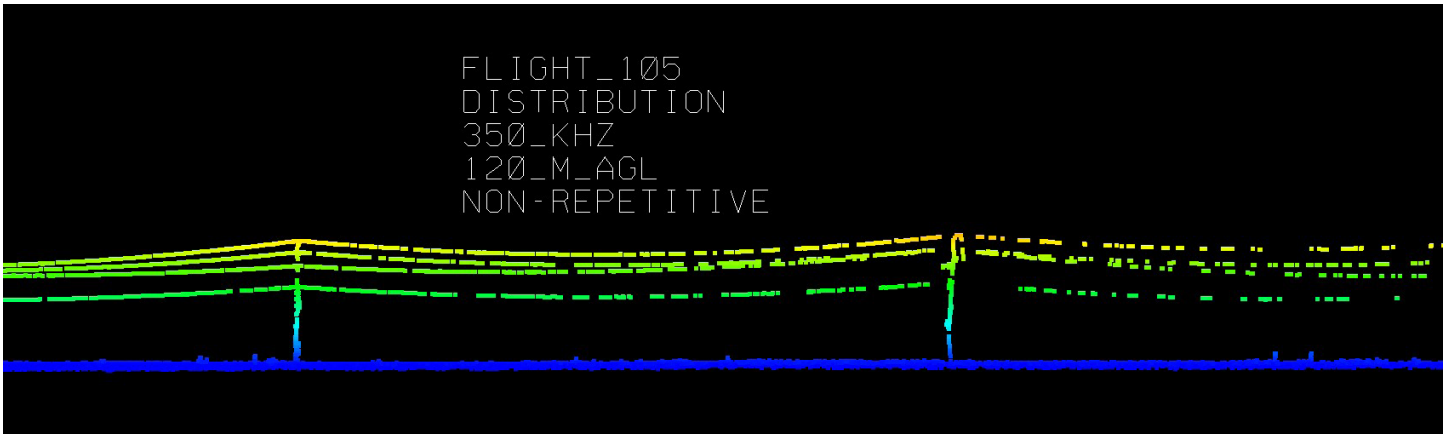
FLIGHT_105
DISTRIBUTION
350_KHZ
120_M_AGL
NON-REPETITIVE

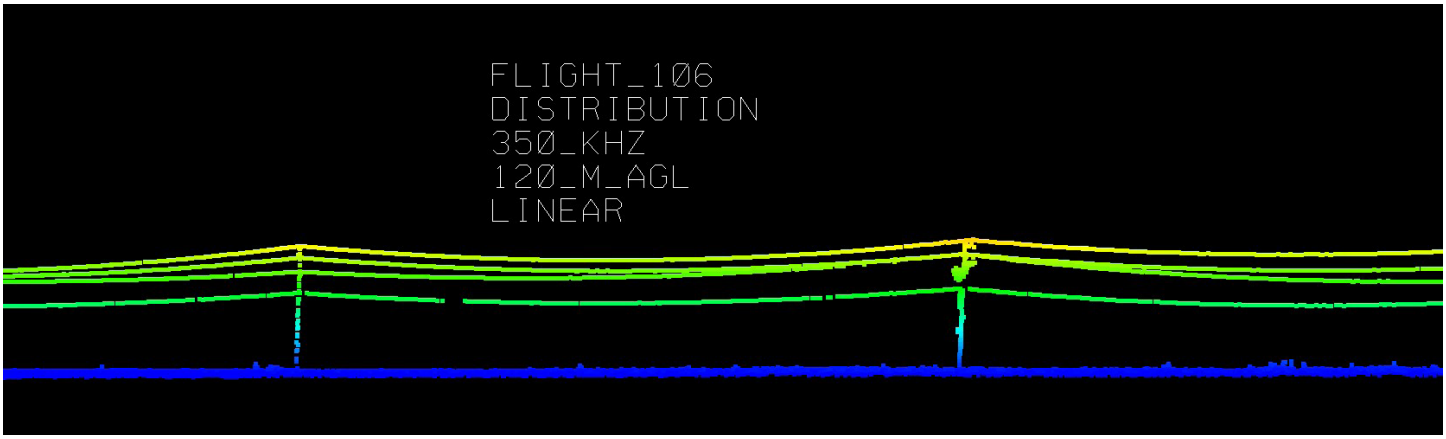
FLIGHT_106
DISTRIBUTION
350_KHZ
120_M_AGL
LINEAR

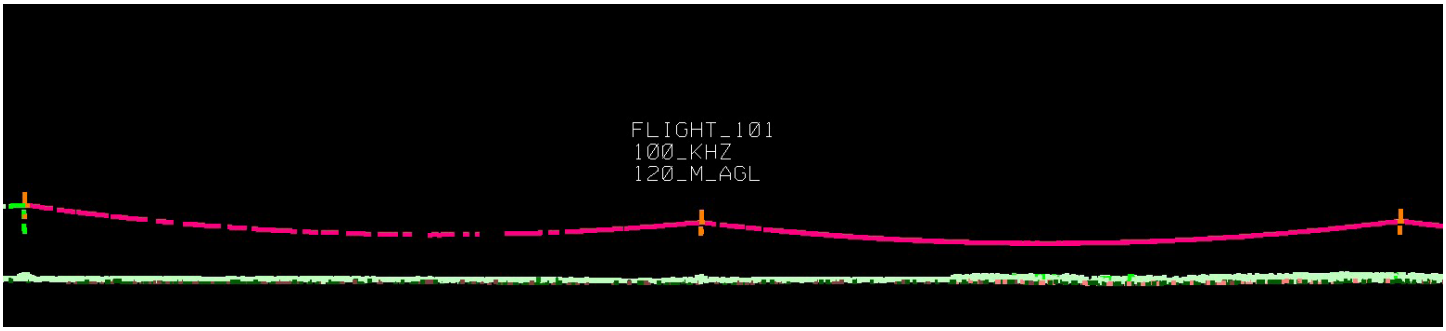
FLIGHT_101
100_KHZ
120_M_AGL

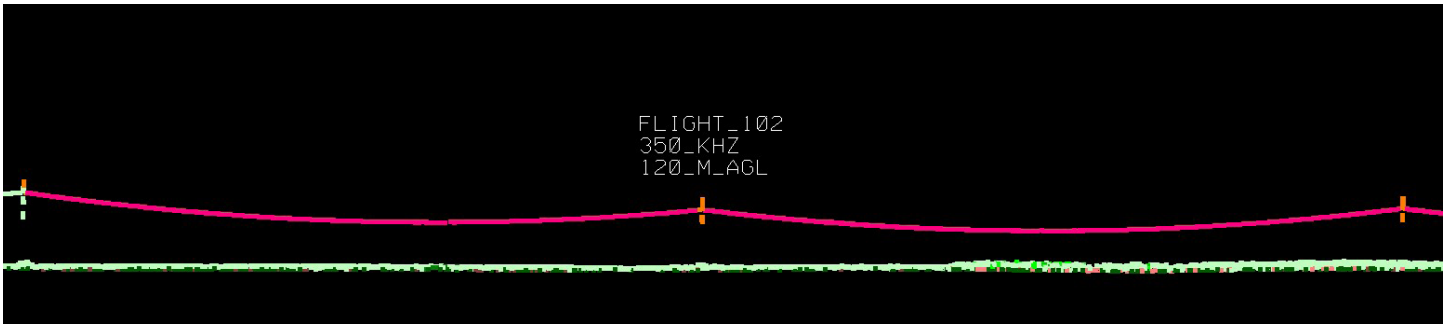
FLIGHT_102
350_KHZ
120_M_AGL

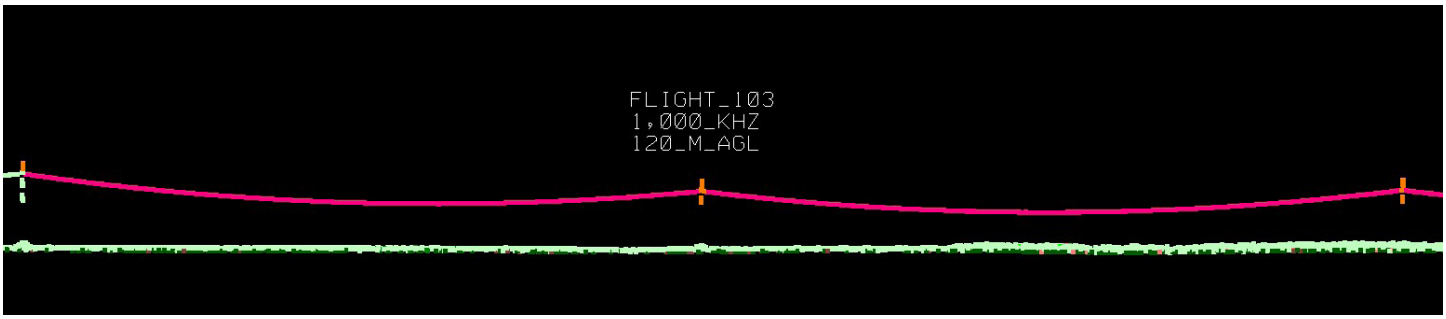
FLIGHT_103
1,000_KHZ
120_M_AGL

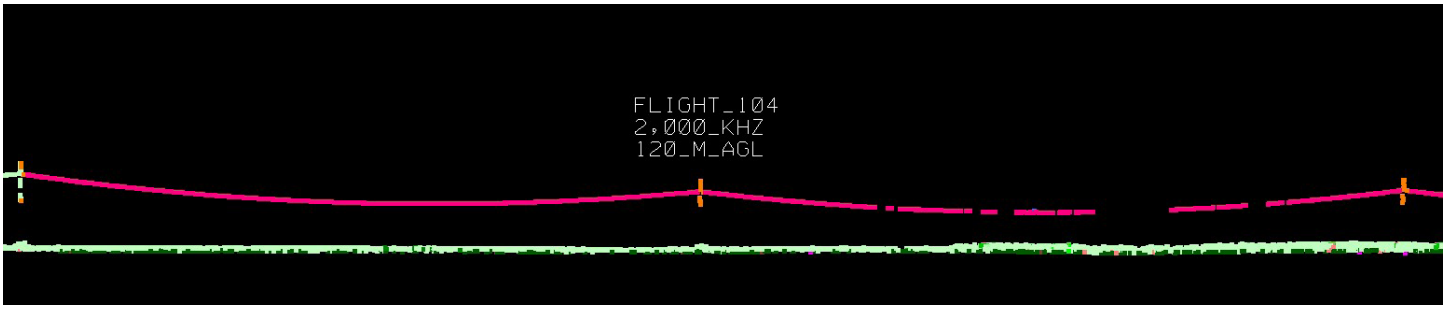
FLIGHT_104
2,000_KHZ
120_M_AGL

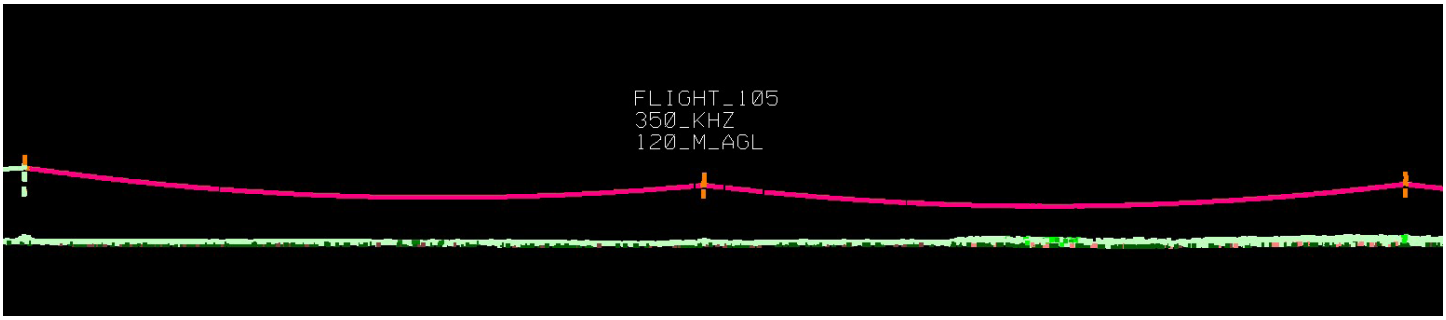
FLIGHT_105
350_KHZ
120_M_AGL

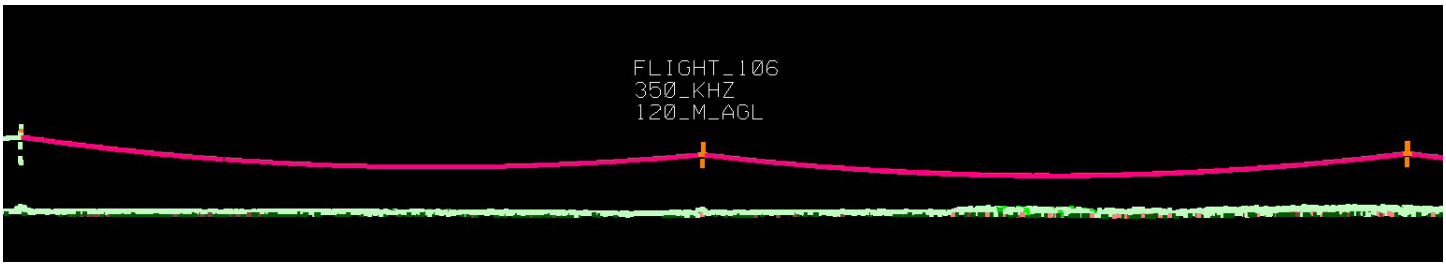
FLIGHT_106
350_KHZ
120_M_AGL